INTERNATIONAL JOURNAL FOR NUMERICAL METHODS IN ENGINEERING
Int. J. Numer. Meth. Engng 2019; **00**:1–47
Published online in Wiley Online Library (www.onlinelibrary.wiley.com). DOI: 10.1002/nme.6171

An n-sided polygonal finite element for nonlocal nonlinear analysis of plates and laminates

P. Aurojyoti[1], P. Raghu[1], A. Rajagopal[1], J. N. Reddy*[2]

[1]*Department of Civil Engineering, IIT Hyderabad, India*
[2]*Department of Mechanical Engineering, Texas A&M University, College Station, Texas, USA*

SUMMARY

In this study, a locking-free n-sided C^1 polygonal finite element is presented for nonlinear analysis of laminated plates. The plate kinematics is based on Reddy's third-order shear deformation theory (TSDT) [1, 2]. The inplane displacements are approximated using barycentric form of Lagrange shape functions. The weak-form Galerkin formulation based on the kinematics of TSDT requires the C^1 approximation of the transverse displacement over the polygonal element. This is achieved by embedding the C^0 Lagrange interpolants over a cubic Bernstein–Bezier patch defined over the n-sided polygonal element. Such an approach ensures the continuity of the derivative field at the inter-element edges. In addition, Eringen's stress-gradient nonlocal [3] constitutive equations are used in the present formulation to account for nonlocality. The effect of geometric nonlinearity is taken by considering the von Kármán' geometric nonlinearity. Examples are presented to show the effect of nonlocality, geometric nonlinearity, and the lamination scheme on the bending behavior of laminated composite plates. The results are compared with analytical solutions, conventional FEM results and with those available in the literature. Shear locking is addressed considering reduced integration and consistent interpolation techniques. The patch test is used to check the convergence of the element developed.

Received . . .

KEY WORDS: C^1 Lagrange interpolants, Polygonal Finite element, Non-local elasticity, Bezier patch, Third order shear deformation theory(TSDT), Plate bending.

1. INTRODUCTION

In last decade developing generalized finite element method based on arbitrary polygonal meshes has gained importance amongst researchers. A $n-$ sided polygonal finite element has arbitrary number of edges ($n > 3$) and is able to provide greater flexibility, suitable in complex modeling. Polygonal finite elements have been found to be of great use in finite and anisotropic elasticity [4] and modeling of micro structured materials [5]. These elements can overcome the problems associated with remeshing in standard adaptive finite elements or meshless methods which have issues with imposition of boundary conditions because of lack of Kronecker delta property in the approximation functions. The polygonal elements have many potential applications to a large variety

*Correspondence to: Email: jnreddy@tamu.edu

of problems, including: constitutive modeling in nonlinear analysis of polycrystalline materials (see [6], [7], and [8]), linear elasticity [9], analysis of cracked structures [10], vibration analysis [11], crack propagation ([12], [13]), large deformation problems (see [14], [15], and [16]), topology optimization (see [17] and [18]), hyperelastic analysis [19], contact-impact problems[20], adaptive meshing [21], plate bending problems[22], analysis of generalized elastic solids [23], and multi-material discretization and optimization (see [24] and [25]). There are other recent works on extension of polygonal finite element method for topology optimization ([26], [27]), nonlinear analysis of plates, laminates and functionally graded plates [28], and fracture problems ([29], [30]).

There have been recent works carried out by using the polygonal finite element method for analysis of plates and laminates. An assumed strain field resulting in a locking free element is considered for analysis of plates[31]. This has also been extended to the analysis of laminated composite plates using C^0-HSDT. It has been observed that there is a significant accuracy in the displacement and transverse shear stresses when the polygonal finite elements are used for the analysis[32]. In this case, shape functions were derived by following a moving least square approximation. Polygonal finite element method has also been used for analysis of laminated composite plates together with a layerwise theory [33]. This has resulted in obtaining better accuracy of inner layer shear stresses. It is to be noted that the analysis of plates and laminates based on TSDT requires C^1 continuous conformal approximants corresponding to the transverse deflection. Making proper approximations over polygonal elements with a particular degree of continuity is a challenging task. For a generic n-sided polygonal domain, there is a need to come up with a non-polynomial type approximation. Such an approximation must be locking free for plate bending problems. Polygonal finite element method thus opens up different perspective and ideas towards the study of plates and laminates, and provides a wide range of solutions to the problems that are faced by standard finite element method. For standard polygonal finite elements that have been proposed, a non-polynomial type approximation based on geometric properties of the domain such as area or distance measures of the polygon are used for the construction of C^0 continuous approximation function. Wachspress [34] has given rational polynomial using projective geometry for n-sided convex polygons. The computation of Wachspress' shape function is enhanced algebraically in [35]. Floater [36] proposed a mean value coordinate over both convex and concave shape of elements. Maximum entropy coordinates[37], piece wise linear function with sharp upper bound and lower bound [38], gradient bound for Wachspress coordinates [39], generalized barycentric coordinate [40], metric coordinates[41], Laplace coordinates ([42],[43] and [44]), moving least square coordinates [45] are among other methods to construct shape functions over polygonal elements. Warren [46] developed rational basis function for arbitrary convex polytopes. It is observed that, C^0 type approximants are quite common over polygonal elements and there has been some attempts to achieve C^1 type approximants [47].

The other challenging task has been on numerical evaluation of integrals over polygonal domains. For numerical integration over a polygonal domain, partitioning the physical or canonical element to n sub-triangles and applying Gauss quadrature rules on each triangular subdomain [43] is commonly being used. Although quadrature rules for polygons have been developed [48], due to the non-polynomial nature of basis functions, higher quadrature rules are required to obtain accurate results. Higher order quadrature in two and higher dimensions have been proposed recently [49]. In some works, moment fitting equations have been used to get quadrature schemes in polygons and polyhedrons [50]. It involves the integration of monomial basis function and use of Lasserres method (see [51],[52] and [53] for details). This approach excludes the need of dividing polygons into different sub domains. Alternate methods have been proposed, for instance, instead of dividing the regular n-gon into sub-triangles in the second step of mapping, it is mapped to a unit disk by conformal mapping. After mapping to the unit disk, various cubature rule may be applied. This method retains the length and angle measures [54]. This method was extended to find the optimum number of integration points in the disk based on Frobenius norm and infinity norm [55]. However, such mapping procedures are computationally very expensive and require special tools to map from rectangle in Cartesian real space to a disk in complex space and vice versa. The results obtained

from this are also sometimes found to be erroneous. Eight-node quadrilateral spline finite element has been used for numerical integration over polygons [56].

Three nodal integration schemes are available for numerical integration (a) nodal strain method (b) stabilized conforming nodal integration (SCNI) scheme [57], (c) nodal averaging techniques. These methods address the issues related to the stability of solution[58]. The inherent errors arising in numerical integration of various schemes has been addressed in [59]. From this prospective, alternative methods of numerical integration over polytopic meshes are discussed in [60], where the requirement of quadrature points and weights are excluded. Herein, the numerical integration has been made to solely depends on the integrand and its derivatives values on the vertices of the polytope. Other methods, such as naturally stabilized nodal integration scheme (NSNI) have also been devised as alternative approaches, that consider integration at the nodes[61]. For analysis of thin plates, different procedures are developed to avoid integration errors, especially when FSDT is used. Stabilization techniques with one point integration [62], discrete shear gap procedure [63], hybrid stress approach [64], discrete Kirchhoff Mindlin quadrilateral technique (DKMQ) [65] are methods to address some of these problems. In case of isoparametric mapping, it has been shown that, the convergence of the solution are further improved by dividing the *n*-gon into quadrilaterals instead of triangles. In this case, the background cells will have more Gauss points towards the edges of the polygonal element. It has been shown recently that, use of polynomial projection technique and subsequent adaptivity helps in ensuring convergence in L^2 norm of the solution [66]. Ensuring a consistency in approximation also ensures convergence of the solution [67],[68]. In some works, this polynomial consistency is achieved indirectly, by assuming some approximations for the gradients in displacement field [69].

Analysis of thick plates and laminates have been made over a period of time using higher order shear deformation theories. Higher order theories like TSDT [1], HSDT [70] and [71], exponential deformation theories (ESDT), trigonometric shear deformation theories(TrSDT) [72] have been proposed by researchers to overcome the challenges faced by CLPT and FSDT. Most of these theories are in a sense variants of the Reddys third order shear deformation theory (TSDT). Kim et al.[73] used third-order theory which includes vonKármán' nonlinearity and coupled stress effects in bending analysis of plates. The weak formulation of TSDT has transverse displacement and their gradient involved, hence requires C^1 continuity of the primary variable (Generalized displacements)[74].

In this work we use TSDT for the nonlinear analysis of plates and laminates. In this work C^0 and C^1 Lagrange shape functions over a $n-$ sided polygonal finite element are derived. The barycentric form of Lagrange approximants are based on distance measures associated with the polygon. C^1 approximants are achieved by embedding a Bezier patch over the polygon and using a de Boors algorithm[75] to transform C^0 approximants to C^1 approximants. Another issue of concern is the shear locking phenomenon observed in thin plate limits. In order to address this issue, many approaches have been introduced and assessed for triangular and quadrilateral elements including reduced integration, selective reduced integration, assumed natural strains, the discrete Kirchhoff methods. In the present study , we explore the viability of both reduced integration and consistent interpolation technique to alleviate shear and membrane locking. There have been recent needs for analysis of micro or nanostructural devices which are essentially of laminated plate structures. At these smaller length scales in every material, in homogeneity exists which causes material instability and nonlinear behavior at macroscopic scales. Classical continuum theories do not incorporate internal material length scales in material description. Nonlocal continuum models can be improved by incorporating a length scale parameter. In this study, we use Eringen's stress-gradient model (a diffusion model) in the polygonal finite element approach.

The primary focus of the present study is to present a C^1 polygonal finite element formulation of Reddy's third-order theory [1, 2] to analyze laminated plates while accounting for geometric nonlinearity and Eringen's nonlocal model [3]. The inplane displacements are approximated using the C^0 shape functions. The weak-form Galerkin formulation of the TSDT requires C^1 approximation over a polygonal element for transverse displacement. This is achieved by embedding the C^0 Lagrange interpolants over a cubic Bernstein–Bezier patch defined over the n-sided

polygonal element. Using a standard de Boors algorithm[75], the continuity of the approximation is enhanced from C^0 to C^1. Such an approach ensures the continuity of the derivative field at the inter element edges. Eringen's nonlocal [3] constitutive equations are used in the present formulation. The effect of geometric nonlinearity is taken by considering von Kármán' type strains. The remainder of the paper is organized as follows. A detailed explanation of barycentric form of Lagrange shape function, Bernstein-Bezier patch and the derivation of C^1 Laplace shape function for n-sided polygon is given in section 2 and section 3. Numerical integration procedure adopted in the present work is described in section 4. Section 5 and section 6 presents nonlocal elasticity and TSDT theory. Shear locking and its remedy is described in section 7. Numerical examples using the proposed element are presented in Section 8 to showcase the novelty of the proposed element and at last, some concluding remarks are given in section 9.

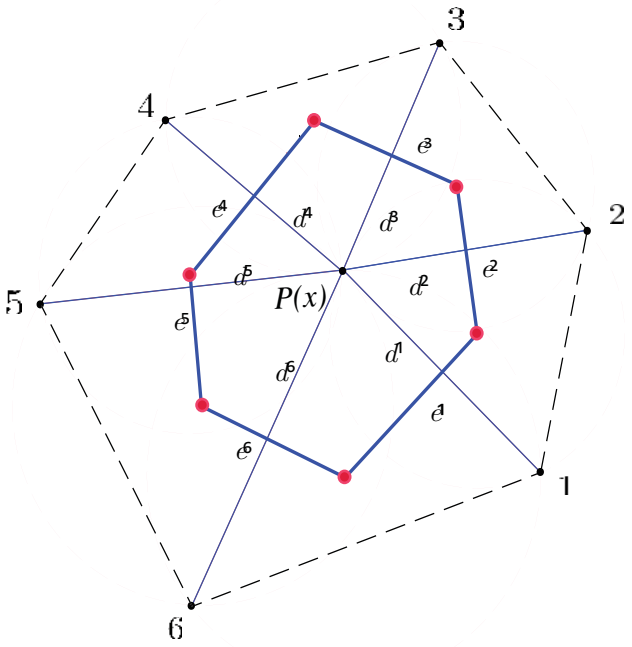

Figure 1. Voronoi diagram of a point $\boldsymbol{P}(\boldsymbol{x})$ which has six natural neighbors. The distance measures are $e_j(\boldsymbol{x})$ and $d_j(\boldsymbol{x})$.

2. INTERPOLATION OVER AN ARBITRARY n-GON

For an arbitrary convex n-gon, the barycentric form of C^0 Lagrange interpolants based on the distance measure associated with the Voronoi is constructed as discussed here. Let $\boldsymbol{P}(\boldsymbol{x})$ be any point inside the polygon. The point has n natural neighbors (see Figure 1). The circumcenter of the circle, that is formed by circumscribing the triangle obtained by any two consecutive natural neighbors and $\boldsymbol{P}(\boldsymbol{x})$ is shown in red. if $e_j(x)$ is the Voronoi edge length associated to point $\boldsymbol{P}(\boldsymbol{x})$ and node $\boldsymbol{j}$ and, $d_j(\boldsymbol{x})$ is the distance between point $\boldsymbol{P}(\boldsymbol{x})$ and $\boldsymbol{j}$, then the weight related to these two distance measures about the point $\boldsymbol{P}(\boldsymbol{x})$ is given by

$$\alpha_j(\boldsymbol{x}) = \frac{e_j(\boldsymbol{x})}{d_j(\boldsymbol{x})}, \quad \boldsymbol{x} \in \mathbb{R}^2 \tag{1}$$

and the Lagrange interpolation function $\phi_i^L(\boldsymbol{x})$ is defined as

$$\phi_i^L(\boldsymbol{x}) = \frac{\alpha_i(\boldsymbol{x})}{\sum_{j=1}^{n} \alpha_j(\boldsymbol{x})}, \quad \boldsymbol{x} \in \mathbb{R}^2 \tag{2}$$

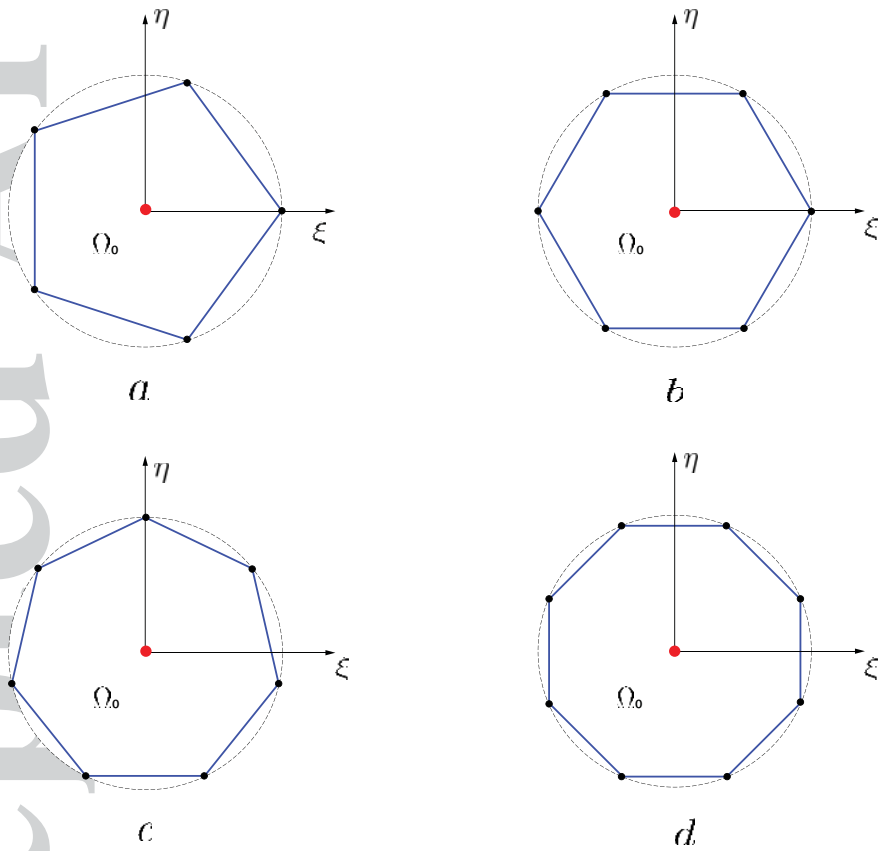

Figure 2. Canonical element for (a) pentagon (b) Hexagon (c) Heptagon (d)Octagon

Shape functions are computed over a canonical element, as it facilitates numerical integration and makes the computation of integrals easy. Canonical elements for different n-gons are shown in Figure 2, where *n*-gons are inscribed in a unit circle. This is analogous to the natural coordinate system for quadrilateral elements [76]. Let us define $\mathbf{J} = \frac{\partial x}{\partial \xi}$ as the Jacobian matrix from physical element to canonical element, (see Figure 2). The derivatives of the shape function in the physical space is given by the relation $\nabla \phi_i^L = \mathbf{J^{-1}} \nabla_\xi \phi_i^L$, where ∇_ξ is the gradient in the natural coordinate system. Double derivatives in the physical coordinates are also calculated in the same fashion, where the transformation matrix elements are functions of previous Jacobian matrix elements [76]. Here we relate every physical polygon to their respective canonical form, which facilitates the computation of the Lagrange shape function in barycentric form at every point on the polygon. The second derivatives of the basis functions in the physical coordinate system (x, y) are related to

the local coordinates (ξ, η) as follows

$$\left\{ \begin{array}{c} \frac{\partial^2 \psi_i^e}{\partial x^2} \\ \\ \frac{\partial^2 \psi_i^e}{\partial y^2} \\ \\ \frac{\partial^2 \psi_i^e}{\partial x \partial y} \end{array} \right\} = \boldsymbol{A}.\boldsymbol{B}$$

where

$$\boldsymbol{A} = \left[\begin{array}{ccc} (\frac{\partial x_e}{\partial \xi})^2 & (\frac{\partial y_e}{\partial \xi})^2 & 2\frac{\partial x_e}{\partial \xi}\frac{\partial y_e}{\partial \xi} \\ (\frac{\partial x_e}{\partial \eta})^2 & (\frac{\partial y_e}{\partial \eta})^2 & 2\frac{\partial x_e}{\partial \eta}\frac{\partial y_e}{\partial \eta} \\ \frac{\partial x_e}{\partial \xi}\frac{\partial x_e}{\partial \eta} & \frac{\partial y_e}{\partial \xi}\frac{\partial y_e}{\partial \eta} & \frac{\partial x_e}{\partial \eta}\frac{\partial y_e}{\partial \xi} + \frac{\partial x_e}{\partial \xi}\frac{\partial y_e}{\partial \eta} \end{array} \right]^{-1}, \quad \boldsymbol{B} = \left\{ \begin{array}{c} \frac{\partial^2 \psi_i^e}{\partial \xi^2} \\ \\ \frac{\partial^2 \psi_i^e}{\partial \eta^2} \\ \\ \frac{\partial^2 \psi_i^e}{\partial \xi \partial \eta} \end{array} \right\} - \left[\begin{array}{cc} \frac{\partial^2 x_e}{\partial \xi^2} & \frac{\partial y_e}{\partial \xi} \\ \\ \frac{\partial^2 x_e}{\partial \eta^2} & \frac{\partial^2 y_e}{\partial \eta^2} \\ \\ \frac{\partial^2 x_e}{\partial \xi \partial \eta} & \frac{\partial^2 y_e}{\partial \xi \partial \eta} \end{array} \right] \left\{ \begin{array}{c} \frac{\partial \psi_i^e}{\partial x} \\ \\ \frac{\partial \psi_i^e}{\partial y} \end{array} \right\}$$

where x_e and y_e are the coordinates in the physical space and are given by
$x_e = \sum_{i=1}^{n} \phi_i^e x_i$ and $y_e = \sum_{i=1}^{n} \phi_i^e y_i$

ϕ_i^e and ψ_i^e are the C^0 and C^1 shape functions respectively in (ξ, η) coordinate.

3. C^1 INTERPOLANTS OVER AN n-SIDED POLYGONAL FINITE ELEMENT

Galerkin weak form of the laminated plate bending governing equations (see 21-25), based on nonlocal nonlinear TSDT, contains the transverse displacement and their higher order derivatives. So, the basis function we use for the formulation must have C^1 continuity between the edges of the elements. The C^0 Lagrange basis functions obtained in the previous section would be used for deriving C^1 Laplace basis function by embedding it in Bernstein-Bezier patch, following a degree elevation algorithm as given by de Boor algorithm[77]. An m^{th} degree Berstein-Bezier surface over the simplex is represented as

$$c(\boldsymbol{\xi}) = \sum_{|\boldsymbol{i}|=m} C_i^m(\boldsymbol{\xi}) c_i \tag{3}$$

where, c_i is the Bezier ordinate corresponding to control point i/m. The control points over an n-sided polygons are shown in Figure 3(a) and Figure 3(b).

$C_i^m(\boldsymbol{\xi})$ are Bernstein polynomials in n-variables.

$$C_i^m(\boldsymbol{\xi}) = \binom{m}{\boldsymbol{i}} (\xi_1)^{i_1} (\xi_2)^{i_2} ... (\xi_n)^{i_n} \tag{4}$$

where,

$$\binom{m}{\boldsymbol{i}} = \frac{m!}{i_1! i_2! ... i_n!} \tag{5}$$

ξ_1,ξ_2... ξ_n are the barycentric coordinates and satisfy the property $\sum_i \xi_i = 1$.

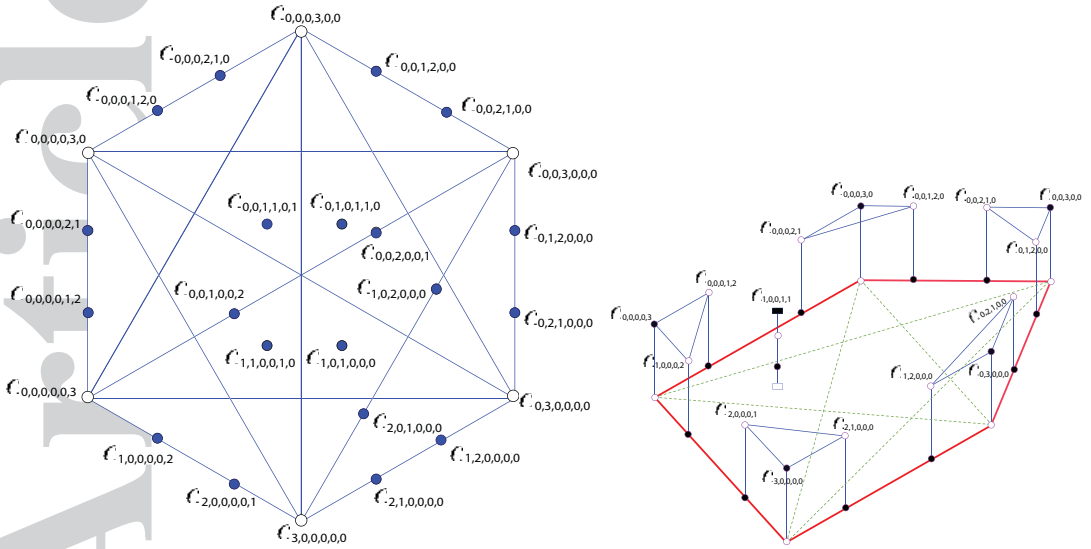

Figure 3. Control points in a Bezier patch (a) Bezier patch ordinates defined on a regular hexagon (b) 3D Bezier ordinates defined on a pentagon.

If $\phi(x,y) = (\phi_1(x,y), \phi_2(x,y)...\phi_n(x,y))$ are the C^0 interpolants in 2-D, and we use $\phi(x,y)$ in the place of $\xi_n, (n = 1,2,3...n)$ in equation (4), it degree elevates and forms Bezier surface accordingly. There are (n^2)+$\binom{n}{k}$ points in the surface which are called as tangent and central control points, except the n nodal points. The central ordinates depend upon the average value of the nodal ordinates and tangent ordinates. Such a procedure is helpful to ensure the continuity of derivatives at the control points and along the edges of the n-gon. This results in C^1 interpolants at the corner nodes of the polygon. The Bezier ordinates are shown in Figure 3. Empty circles at each node of the polygon are known as nodal ordinates and the filled circles in between any two node represent tangent ordinates whereas, others represent central ordinates. For cubic Bernstein Bezier patch, we will select $m = 3$. Here the C^0 shape functions are raised to the power of the degree of the simplex considered and are elevated via de Boor's algorithm (see equation (4)). Hence for cubic simplex with $m = 3$, equation (4) becomes

$$w^3(\boldsymbol{\phi}) = \sum_{|\boldsymbol{i}|=3} C_{\boldsymbol{i}}^3(\boldsymbol{\phi}) c_{\boldsymbol{i}} \tag{6}$$

$w^3(\phi)$ gives us the C^1 shape function. It is continuously differentiable as the C^0 shape functions are raised to the third degree. It satisfies the property of quadratic completeness, in turn, gives double derivative as a constant curvature for the fourth order partial differential equations. In a particular line connecting node $'i'$ to any other $(n-1)$ nodes, tangent Bezier ordinates are dependent on the nodal values and its gradients (w.r.t x and y). The vertex ordinates are same as the nodal values at that particular node. Let the transverse displacement is $w(x,y)$, the directional derivatives along d at $(x,y)_I$ and along $\hat{d}$ at $(x,y)_J$ can be written as follows

$\frac{\partial w(x,y)_I}{\partial d} = \nabla w(x,y).\mathbf{d} = \frac{\partial w(x,y)}{\partial x}(x_J - x_I) + \frac{\partial w(x,y)}{\partial y}(y_J - y_I) = \theta_{Ix}(x_J - x_I) + \theta_{Iy}(y_J - y_I)$

$\frac{\partial w(x,y)_J}{\partial \hat{d}} = \nabla w(x,y).\hat{\mathbf{d}} = -(\frac{\partial w(x,y)}{\partial x}(x_j - x_i) + \frac{\partial w(x,y)}{\partial y}(y_j - y_i)) = -(\theta_{jx}(x_j - x_i) + \theta_{jy}(y_j - y_i))$

The gradients are related to Bezier ordinates as follows,

$$\frac{\partial w(x,y)_I}{\partial d} = 3(c_i - c_j), i = 2e_I + e_J, j = 3e_I$$

$$\frac{\partial w(x,y)_J}{\partial \hat{d}} = 3(c_i - c_j), i = 2e_J + e_I, j = 3e_J$$

$$b_{2e_Ie_J} = \frac{1}{3}(\theta_{Ix}(x_J - x_I) + \theta_{Iy}(y_J - y_I)) + w(x,y)_I \tag{7}$$

$$b_{e_I2e_J} = \frac{1}{3}(\theta_{Jx}(x_J - x_I) + \theta_{Jy}(y_J - y_I)) + w(x,y)_J \tag{8}$$

From the above, tangent ordinates relate to the nodal values and gradient values. Similarly, the center ordinates are related to the all other ordinates which in turn gives the idea of a transformation matrix $[\boldsymbol{T}]$ that relates the nodal values to the tangent ordinates as given below

$$w^3(\boldsymbol{\phi}) = \{\boldsymbol{C}(\boldsymbol{\phi})\}^T\{\boldsymbol{c}\} = \{\boldsymbol{C}(\boldsymbol{\phi})\}^T[\boldsymbol{T}]\{\boldsymbol{w}\} = \{\boldsymbol{\Psi}(\boldsymbol{\phi})\}^T\{\boldsymbol{w}\} \tag{9}$$

where $\{\boldsymbol{c}\} = [\boldsymbol{T}]\{\boldsymbol{w}\}$, $\{\boldsymbol{\Psi}(\boldsymbol{\phi})\}^T = \{\boldsymbol{C}(\boldsymbol{\phi})\}^T[\boldsymbol{T}]$ and $\{\boldsymbol{\Psi}(\boldsymbol{\phi})\}$ are the C^1 interpolation functions obtained. The construction of $[\boldsymbol{T}]$ matrix has similar procedure for different n-sided n-gon. The transformation matrix has $3n$ columns, n rows for nodal ordinates, $(n^2 - n)$ rows for tangent ordinates and $\binom{n}{3}$ rows for center ordinates. The plot of C^0 Laplace shape functions is shown in Figure 4. The plot of C^1 shape functions and its derivatives are given in Figure 5, 6 and 7 respectively. The distribution of various other types of C^0 shape functions over polygonal domain as discussed in detail in [78] are shown in Figure 8.

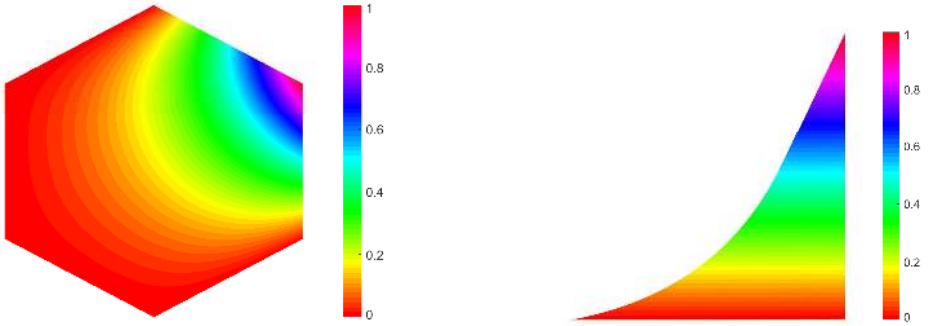

Figure 4. C^0 Lagrange shape function for an hexagonal element.

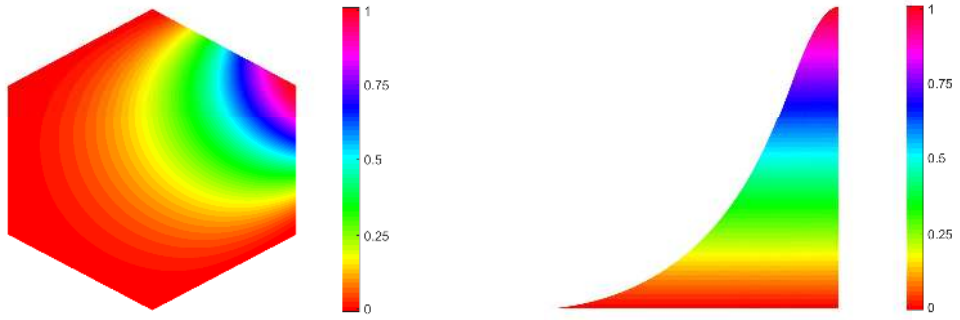

Figure 5. C^1 Lagrange shape function for an hexagonal element.

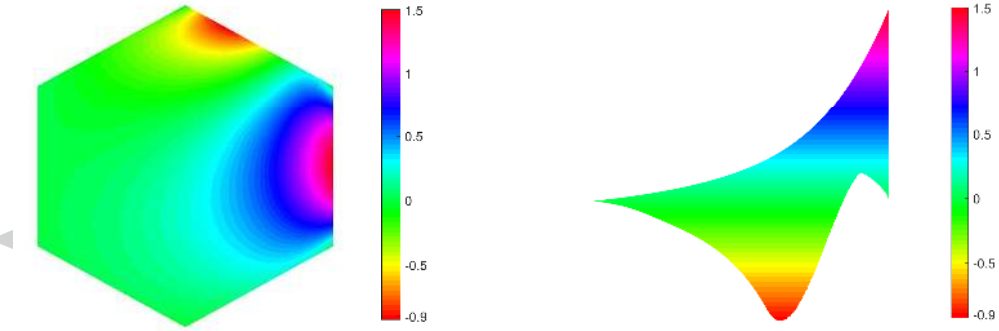

Figure 6. Derivative of C^1 Lagrange shape function with respect to y.

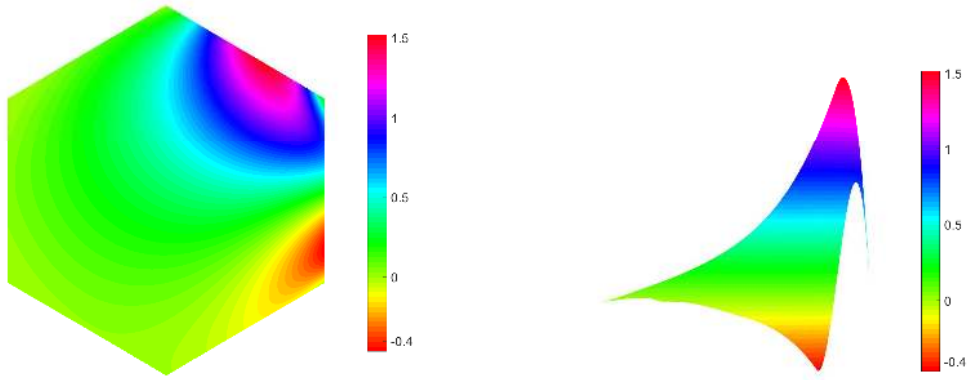

Figure 7. Derivative of C^1 shape function with respect to x.

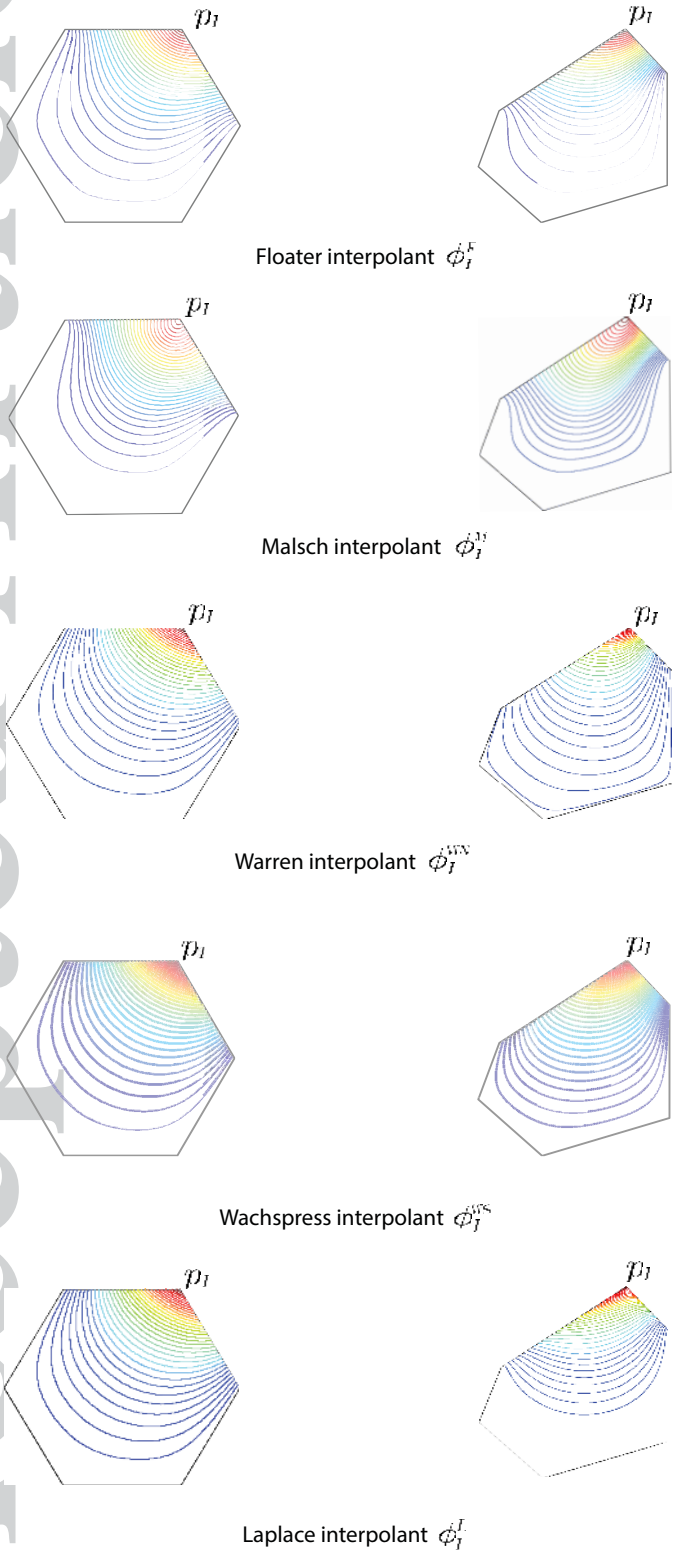

Figure 8. Comparison of the presented interpolants ϕ_I^*: isoline plots for a canonical polygonal domain Ω_0 (left column) and a physical polygonal domain Ω (right column).

For generation of polygonal meshes, we use a simple method to generate polygonal elements from any arbitrary domain, using information about domain geometry and centroidal Voronoi tessellation (CVT) concept (see [66] and [19]). Lloyd's algorithm ensures optimal distribution of points throughout the domain and hence gives high-quality mesh. More number of iteration can be taken to get a regularized mesh. The method is similar to polymesher [79]. Balaji et al.[66] used this method for different geometries and applied region wise adaptive strategy to obtain graded polygonal meshes for plane elasticity problems. In this work we have used this method to generate the polygonal meshes.

4. NUMERICAL INTEGRATION OVER $n-$ SIDED POLYGONAL ELEMENT

To integrate the stiffness terms (as given in Appendix-3) over polygons, various methods has been discussed in section 1. Among them, the method of partitioning of the canonical element into n number of sub-triangles is used in this study where n is the number of sides of the polygon. Canonical element for different polygons is given in Figure 2. Gauss points are obtained from the background triangular subdomains by dividing the canonical element to n sub-triangles. 3, 6, 13, 25 number of integration points can be taken in each sub-triangle. Figure 9 illustrates this procedure. The position of different Gauss points are shown in Figure 10. Mathematically,

$$\begin{aligned}\int_{\Omega}\psi d\Omega &= \sum_{N}\int_{\bar{\Omega}}\psi d\bar{\Omega}\\ &= \sum_{N}\int_{\bar{\Omega}_0}\psi|\boldsymbol{J}|d\bar{\Omega}_0\\ &= \sum_{N}\int_{\bar{\Omega}_\triangleleft}\psi|\boldsymbol{J}||\boldsymbol{J}_\triangleleft|d\bar{\eta}d\bar{\xi}\end{aligned}$$

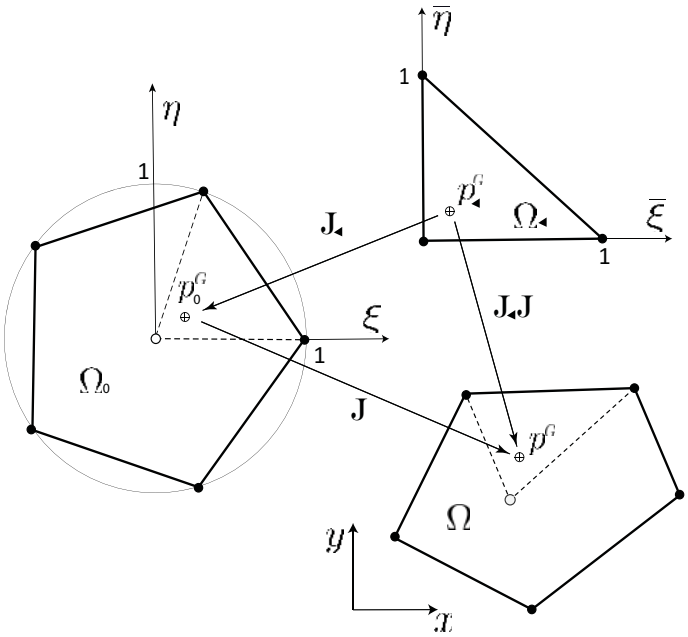

Figure 9. Partition of pentagonal element in to n sub triangles and mapping of quadrature points.

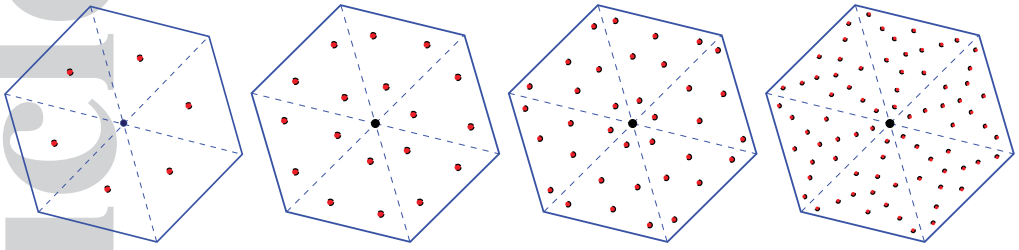

Figure 10. Illustration of Gauss point locations in an hexagonal element (a) One point Gauss rule (b) 3 point Gauss rule (c) 6 point Gauss rule (d) 13 point Gauss rule.

where n is the number of Gauss points considered. Gauss points in the canonical element are obtained from the background triangle by following a two step transformation as shown in Figure 9.

$$\xi = \sum_{j=1}^{j=3} N_j \xi_j, \eta = \sum_{j=1}^{j=3} N_j \eta_j$$

where ξ_j, η_j are the coordinates of Gauss points in the background triangle element, (see Figure 9). In the following section we discuss on how the proposed polygonal finite element is used for a nonlocal nonlinear formulation for analysis of thick plates and laminates using the TSDT.

5. NONLOCAL ELASTICITY

In the standard continuum theory, the material is assumed to be continuous at the macro scale and the behavior of the material is characterized by local constitutive laws in which the stress at a point depends on the strain at that point only. The effect of the neighborhood is neglected in the classical continuum theory. Since the macroscopic behavior depends on the material behavior at lower length scales, it is important to capture the underlying mechanisms that are happening at that smaller length scales. To capture such behavior, it is required to use continuum theories that are regularized, in a sense that, local character of the stress-strain relation is abandoned and the constitutive equations become nonlocal. The effect of nonlocality can be introduced by spatial averages of stress or strain in the constitutive models. The idea of nonlocality is first attributed to the works of Eringen[80] and Kröner [81]. These models are also found to capture the size effects observed in experiments, by capturing the interatomic and intermolecular forces.

Nonlocal stress tensor $\boldsymbol{\sigma}^{nl}$ at point $\boldsymbol{x}$ as per Eringen [82] is given by:

$$\boldsymbol{\sigma}^{nl}(\boldsymbol{x}) = \int \chi(|\boldsymbol{x'} - \boldsymbol{x}|, \kappa)\boldsymbol{\sigma}(\boldsymbol{x'})\, dv' \tag{10}$$

where $\chi(|\boldsymbol{x'} - \boldsymbol{x}|, \kappa)$ is the Kernel function and $\boldsymbol{\sigma}(\boldsymbol{x'})$ is known as macroscopic stress tensor at $\boldsymbol{x'}$. τ is the material parameter which is a function of internal and external characteristic lengths. Kernel function in 2D can be written as follows,

$$\chi(|\boldsymbol{x}|, \kappa) = (\pi\tau l^2)^{-1} exp(-\boldsymbol{x}.\boldsymbol{x}/l^2\kappa) \tag{11}$$

Equation (10) can also be written in differential form as

$$\left(1 - \kappa^2 l^2 \nabla^2\right) \boldsymbol{\sigma}^{nl} = \boldsymbol{\sigma} \tag{12}$$

where a and l are the internal and external characteristic lengths, respectively (see [3]),$\kappa = \frac{(e_0 a)^2}{l^2}$, e_0 is a material constant. μ is the nonlocal parameter having value $\kappa^2 l^2$.

6. THIRD ORDER SHEAR DEFORMATION THEORY

The in-plane displacements of the Reddy third-order shear deformation theory (see [1, 2]) are expanded up to cubic in thickness ordinate, while the transverse displacement is assumed to be independent of the thickness coordinate (i.e., transverse normals are inextensible). This leads to the quadratic variation of the transverse shear strains and shear stresses. Thus, the theory avoids introduction of any shear correction factors, unlike in first-order shear deformation theory (FSDT).

Displacement field

Kinematics of TSDT can be written as

$$\begin{aligned} u(x,y,z) &= u_0(x,y) + z\phi_x - \frac{4z^3}{3h^2}\left(\phi_x + \frac{\partial w_0}{\partial x}\right) \\ v(x,y,z) &= v_0(x,y) + z\phi_y - \frac{4z^3}{3h^2}\left(\phi_y + \frac{\partial w_0}{\partial y}\right) \\ w(x,y,z) &= w_0(x,y) \end{aligned} \tag{13}$$

where (u_0, v_0, w_0) are the displacements of the point on the mid plane in the in-plane directions. (i.e., $z = 0$). ϕ_x and ϕ_y represent the rotations of a transverse normal line at the mid-plane ($\phi_x = \frac{\partial u}{\partial z}$ and $\phi_y = \frac{\partial v}{\partial z}$). h is the total thickness of the plate. Strain displacement relationships for TSDT are given in Appendix-1 and lamina constitutive relationships are given in Appendix-2.

Governing equations

Following the principle of virtual displacements, the equilibrium equations of TSDT are obtained as follows (the nonlocality in the nonlinear terms is neglected)

$$\frac{\partial N_{xx}^{nl}}{\partial x} + \frac{\partial N_{xy}^{nl}}{\partial y} = 0 \tag{14}$$

$$\frac{\partial N_{xy}^{nl}}{\partial x} + \frac{\partial N_{yy}^{nl}}{\partial y} = 0 \tag{15}$$

$$\begin{aligned} &\frac{\partial \bar{Q}_x^{nl}}{\partial x} + \frac{\partial \bar{Q}_y^{nl}}{\partial y} + \frac{\partial}{\partial x}\left(N_{xx}^{nl}\frac{\partial w_0}{\partial x} + N_{yy}^{nl}\frac{\partial w_0}{\partial y}\right) + \frac{\partial}{\partial y}\left(N_{xy}^{nl}\frac{\partial w_0}{\partial x} + N_{yy}^{nl}\frac{\partial w_0}{\partial y}\right) \\ &+ c_1\left(\frac{\partial^2 P_{xx}^{nl}}{\partial x^2} + 2\frac{\partial^2 P_{xy}^{nl}}{\partial x\,\partial y} + \frac{\partial^2 P_{yy}^{nl}}{\partial y^2}\right) + q = 0 \end{aligned} \tag{16}$$

$$\frac{\partial \bar{M}_{xx}^{nl}}{\partial x} + \frac{\partial \bar{M}_{xy}^{nl}}{\partial y} - \bar{Q}_x^{nl} = 0 \tag{17}$$

$$\frac{\partial \bar{M}_{xy}^{nl}}{\partial x} + \frac{\partial \bar{M}_{yy}^{nl}}{\partial y} - \bar{Q}_y^{nl} = 0 \tag{18}$$

where $c_1 = \frac{4}{3h^2}$ and

$$\bar{M}_{\alpha\beta}^{nl} = M_{\alpha\beta}^{nl} - c_1 P_{\alpha\beta}^{nl}, \quad \bar{Q}_\alpha^{nl} = Q_\alpha^{nl} - c_2 R_\alpha^{nl}, c_2 = 3c_1$$

Local and nonlocal stress resultants are related as:

$$\mathcal{L}(N_{\alpha\beta}^{nl}) = N_{\alpha\beta}, \quad \mathcal{L}(M_{\alpha\beta}^{nl}) = M_{\alpha\beta}, \quad \mathcal{L}(P_{\alpha\beta}^{nl}) = P_{\alpha\beta} \quad \mathcal{L}(Q_\alpha^{nl}) = Q_\alpha, \quad \mathcal{L}(R_\alpha^{nl}) = R_\alpha \tag{19}$$

Where,

$$\left\{\begin{array}{c} N_{\alpha\beta} \\ M_{\alpha\beta} \\ P_{\alpha\beta} \end{array}\right\} = \int_{-\frac{h}{2}}^{\frac{h}{2}} \sigma_{\alpha\beta} \left\{\begin{array}{c} 1 \\ z \\ z^3 \end{array}\right\} dz, \left\{\begin{array}{c} Q_\alpha \\ R_\alpha \end{array}\right\} = \int_{-\frac{h}{2}}^{\frac{h}{2}} \sigma_{\alpha z} \left\{\begin{array}{c} 1 \\ z^2 \end{array}\right\} dz, \mathcal{L} = (1 - \mu\nabla^2) \tag{20}$$

where x and y are replaced by $\alpha \; and \; \beta$. q is the transverse load. Definition of stress resultants and subsequent constitutive equations are presented in Appendix-4.

Finite element model

The weak forms of nonlocal governing equations ((104)) - ((108)) given in Appendix-4 are:

$$\int_{\Omega^e} \left[N_{xx}\delta u_{0,x} + N_{xy}\delta u_{0,y}\right] dxdy - \oint_{\Gamma^e} (\hat{n}_x N_{xx}\delta u_0 + \hat{n}_y N_{xy}\delta u_0) ds = 0 \tag{21}$$

$$\int_{\Omega^e} \left[N_{xy}\delta v_{0,x} + N_{yy}\delta v_{0,y}\right] dxdy - \oint_{\Gamma^e} (\hat{n}_x N_{xy}\delta v_0 + \hat{n}_y N_{yy}\delta v_0) ds = 0 \tag{22}$$

$$\begin{aligned}
&\int_{\Omega^e} \Big\{ \bar{Q}_x \delta w_{0,x} + \bar{Q}_y \delta w_{0,y} + (N_{xx}\frac{\partial w_0}{\partial x} + N_{xy}\frac{\partial w_0}{\partial y})\delta w_{0,x} + (N_{xy}\frac{\partial w_0}{\partial x} + N_{yy}\frac{\partial w_0}{\partial y})\delta w_{0,y} \\
&- c_1(P_{xx}\delta w_{0,xx} + P_{yy}\delta w_{0,yy} + 2P_{xy}\delta w_{0,xy}) - [1 - \mu\nabla^2] q\delta w_0 \Big\} dxdy \\
&- \oint_\Gamma \Big\{ (\bar{Q}_x \hat{n}_x + \bar{Q}_y \hat{n}_y)\delta w_0 + (N_{xx}\frac{\partial w_0}{\partial x} + N_{xy}\frac{\partial w_0}{\partial y})\hat{n}_x \delta w_0 + (N_{xy}\frac{\partial w_0}{\partial x} + N_{yy}\frac{\partial w_0}{\partial y})\hat{n}_y \delta w_0 \\
&+ c_1 \Big[\frac{\partial P_{xx}}{\partial x}\hat{n}_x + \frac{\partial P_{yy}}{\partial y}\hat{n}_y + (\frac{\partial P_{xy}}{\partial x}\hat{n}_y + \frac{\partial P_{xy}}{\partial y}\hat{n}_x) \Big] \delta w_0 ds \\
&- c_1 \Big[P_{xx}\frac{\partial \delta w_0}{\partial x}\hat{n}_x + P_{yy}\frac{\partial \delta w_0}{\partial y}\hat{n}_y + (P_{xy}\frac{\partial \delta w_0}{\partial x}\hat{n}_y + P_{xy}\frac{\partial \delta w_0}{\partial y}\hat{n}_x) \Big] \Big\} ds = 0
\end{aligned} \tag{23}$$

$$\int_{\Omega^e} \left(\bar{Q}_x \delta\phi_x + \bar{M}_x \delta\phi_{x,x} + \bar{M}_{xy}\delta\phi_{x,y} \right) dxdy - \oint_{\Gamma^e} \left(M_{xx}\hat{n}_x\delta\phi_x + M_{xy}\hat{n}_y\delta\phi_y \right) ds = 0 \tag{24}$$

$$\int_{\Omega^e} \left(\bar{Q}_y \delta\phi_y + \bar{M}_y \delta\phi_{y,y} + \bar{M}_{xy}\delta\phi_{y,x} \right) dxdy - \oint_{\Gamma^e} \left(M_{yy}\hat{n}_y\delta\phi_y + M_{xy}\hat{n}_x\delta\phi_x \right) ds = 0 \tag{25}$$

Finite element approximations

Observation of the weak forms results in the following primary variables,

$$\left\{ u,\; v,\; w,\; \frac{\partial w}{\partial x},\; \frac{\partial w}{\partial y}\; \frac{\partial^2 w}{\partial x \partial y},\; \phi_x,\; \phi_y \right\}$$

The weak form requires C^0 approximation for, $(u, v, \phi_x \; and \; \phi_y)$ and C^1 approximation for w. Herein, we use C^0 and C^1 Laplace shape functions for $u, v, \phi_x \; , \; \phi_y$ and w respectively. The approximations are given as

$$u(x,y) \approx \sum_{j=1}^{m} U_j \psi_j^{(1)}(x,y) \tag{26}$$

$$v(x,y) \approx \sum_{j=1}^{m} V_j \psi_j^{(1)}(x,y) \tag{27}$$

$$w(x,y) \approx \sum_{j=1}^{n} \bar{\Delta}_j \varphi_j(x,y) \tag{28}$$

$$\phi_x(x,y) \approx \sum_{j=1}^{n} \mathcal{X}_j \psi_j^{(2)}(x,y) \tag{29}$$

$$\phi_y(x,y) \approx \sum_{j=1}^{n} \mathcal{Y}_j \psi_j^{(2)}(x,y) \tag{30}$$

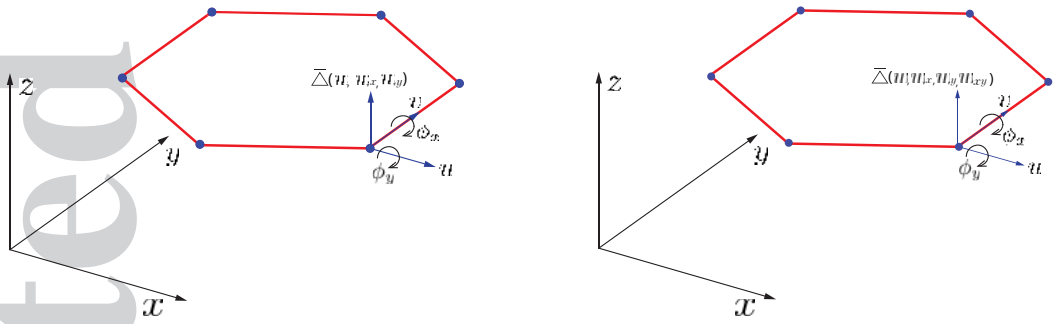

(a) (b)

Figure 11. $n-$ sided polygonal finite element (a) non-conforming element (b) conforming element.

Where $\psi_j^{(1)}(x,y)$ and $\psi_j^{(2)}(x,y)$ are C^0 continuous Laplace interpolants. $\varphi_j(x,y)$ are C^1 continuous Laplace interpolants. The finite element equations are obtained by substituting the approximations given in equations (26)–(30) into the weak forms in equations (21)–(25). The degrees of freedoms are shown in Figure 11 for a conforming and nonconforming polygonal element. The final form of equation can be written as follows.

$$\mathbf{K\Delta} = \mathbf{F} \tag{31}$$

$$\begin{bmatrix} \mathbf{K}^{11} & \mathbf{K}^{12} & \mathbf{K}^{13} & \mathbf{K}^{14} & \mathbf{K}^{15} \\ \mathbf{K}^{21} & \mathbf{K}^{22} & \mathbf{K}^{23} & \mathbf{K}^{24} & \mathbf{K}^{25} \\ \mathbf{K}^{31} & \mathbf{K}^{32} & \mathbf{K}^{33} & \mathbf{K}^{34} & \mathbf{K}^{35} \\ \mathbf{K}^{41} & \mathbf{K}^{42} & \mathbf{K}^{43} & \mathbf{K}^{44} & \mathbf{K}^{45} \\ \mathbf{K}^{51} & \mathbf{K}^{52} & \mathbf{K}^{53} & \mathbf{K}^{54} & \mathbf{K}^{55} \end{bmatrix} \begin{Bmatrix} \mathbf{U} \\ \mathbf{V} \\ \bar{\mathbf{\Delta}} \\ \mathcal{X} \\ \mathcal{Y} \end{Bmatrix} = \begin{Bmatrix} \mathbf{F}^1 \\ \mathbf{F}^2 \\ \mathbf{F}^3 \\ \mathbf{F}^4 \\ \mathbf{F}^5 \end{Bmatrix}$$

The values of stiffness matrix coefficients and force vector terms are defined in Appendix-3. Newton Raphson method is invoked to solve the nonlinear equations. Algorithm for the same is presented in the Appendix-3.

7. SHEAR LOCKING

When an element is subjected to bending, it suppose to represent the curvature for it. The strain profile in any element is dependent on the approximation function used for it. With linear approximations for transverse displacement, it results in constant strain, which is undesirable if the element is subjected to bending. As a result, the energy corresponding to bending becomes zero and it becomes resistant to any bending. Here, the rotation is becoming inconsistent with what is predicted by transverse displacement. In this case, member reaches equilibrium faster than it would in reality. This phenomena happens when the member is thin. In thick members, the effect is negligible as the transverse shear stresses is not equal to zero. In the mathematical perspective, when both continuity and completeness in the approximation for the primary variable are satisfied, some elements do not represent the transverse shear strains correctly. In other words, for the chosen approximation function, strain profile is inconsistent with the bending energy expression. This results in additional shear stress which is actually not present in the member. This is known as shear locking. This phenomena is predominant in numerical analysis of bending problems in plate and beams. In this context, the transverse shear energy expression for TSDT is analyzed (see equation 32). In thin plate limits, the value of a/h becomes very large and the contribution of shear terms to the stiffness has to be zero. This puts a constraint on the two terms (see equation 34) inside the equation (33) to be zero, which represents the transverse shear energy term for HSDT.

$$\frac{1}{2}\int_{\Omega_e}(\bar{Q}_{44}\gamma_{yz}^2+\bar{Q}_{45}\gamma_{yz}\gamma_{xz})dxdy+\frac{1}{2}\int_{\Omega_e}(\bar{Q}_{55}\gamma_{xz}^2+\bar{Q}_{45}\gamma_{yz}\gamma_{xz})dxdy \tag{32}$$

$$\frac{1}{2}\int_{\Omega_e}(1-c_2)^2[\bar{Q}_{44}(\frac{\partial w}{\partial y}+\phi_y)^2+2\bar{Q}_{45}(\frac{\partial w}{\partial y}+\phi_y)(\frac{\partial w}{\partial x}+\phi_x)+\bar{Q}_{55}(\frac{\partial w}{\partial x}+\phi_x)^2]dxdy \tag{33}$$

$$\frac{\partial w}{\partial x}+\phi_x=0,\ \ \frac{\partial w}{\partial y}+\phi_y=0 \tag{34}$$

But equation (34) does not satisfy in a discretized sense. In other words, when we calculate numerically, it does not satisfy the shear terms to get vanished. Hence we say that locking occurs. As a result, the element exhibits additional stiffness against bending. This issue has been addressed in earlier works (see [83] and [84]). For Mindlin plates formulation, the bending and shear terms can be separated to avoid locking [85]. This was also studied in the context of meshless methods for the same Mindlin formulation [86]. This is extended for laminated composites [87], shear deformable shell elements for composite structures [88] and for triangular plate elements [89]. Two methods i.e., reduced integration and consistent interpolation technique are used in the present work to get rid of locking in elements and explained below.

1. *Reduced integration*: This method treats $\frac{\partial w}{\partial x}$, $\frac{\partial w}{\partial y}$, ϕ_x and ϕ_y terms in equation (33) with same degree of approximation. This is achieved by taking lesser number of integration points to calculate the shear energy term. By doing this, it is ensured that the terms in shear energy expression gives lesser contribution to the stiffness. The method is known as reduced integration. Phan et al.[74] used reduced integration and found the result to be the same when full integration is used for TSDT, hence ensuring that locking is not present. In this study, the proposed polygonal plate bending element has been tested for thin plate limits with reduced integration. Results for this method has been discussed in the numerical example (section 8).

2. *Consistent interpolation*: This procedure is based on taking the degree of approximation for ϕ, $\frac{\partial w}{\partial x}$ and $\frac{\partial w}{\partial y}$ to be same in the shear energy term. By doing this, it is ensured that, both shear energy and bending energy terms gets integrated correctly for any number of Gauss points. This method is known as consistent interpolation. Here, the approximation for ϕ_x and ϕ_y is taken as the derivative

of C^1 shape function which are quadratic in nature. Hence they are consistent with $\frac{\partial w}{\partial x}$ and $\frac{\partial w}{\partial y}$, because w is cubic. This allows the terms to get integrated as per their degree of approximation hence the element captures kinematics of deformation. A parametric study has been conducted to demonstrate the effect of this method and presented in numerical examples section 8.

8. NUMERICAL RESULTS AND DISCUSSIONS

In this section we present numerical examples to demonstrate the efficiency of the proposed polygonal finite element. First we demonstrate through a linear analysis example that the polygonal elements give relatively more accurate solutions than the conventional elements and closer to analytical solutions. As a second case we perform a displacement patch test to show the convergence of the solution. The effect of numerical integration scheme on shear locking is studied in next example. We finally compare the results obtained with various nonlocal parameters to demonstrate the effect of nonlocality and nonlinearity on the bending behavior of laminated composite plates. Different boundary conditions and lamination schemes are considered. The discretization of the domain is made using the proposed n-sided polygonal element. The analysis is performed for various values of nonlocal parameters. Each node has 5 degrees of freedom (Figure 11). Simply supported boundary conditions of SS-1 (Figure 15) and SS-3 (Figure 14) type are considered. The effect of lamination scheme is also considered as a parameter in this study. Plots for stresses and maximum deflection are shown. Different value of a/h is taken to study the effect of it on the deflection value. The dimensionless center deflection considered in the analysis is given by

$$\bar{w} = \frac{w\left(\frac{a}{2}, \frac{b}{2}, 0\right) E_2 h^3}{q_0 a^4} \tag{35}$$

where a, b, h are the length, breadth, and thickness of the plate respectively and q_0 is the intensity of the transverse distributed load.

8.1. Example 1

A square cross-ply symmetric (0°/90°/90°/0°) (see Figure 13(b)) laminated plate of length a=5 units is considered for analysis. The laminate made of equal thickness layers each of 0.125 units. The a/h ratio of the plate is taken as 10. The plate is subjected to a distributed load of maximum amplitude of 1 unit varying sinusoidally. Simply supported boundary condition of SS-3 type as shown in Figure 14 is considered. The domain is discretized using polygonal elements as shown in Figure 13(a). The nonlocal parameter is taken as 0 and 1 and the results are compared with those obtained from FEM [90]. Material properties considered are given below:

$$E_1/E_2 = 25,\ G_{12}/E_2 = 0.5,\ G_{23}/E_2 = 0.2,\ G_{12} = G_{13},\ \nu_{12} = 0.25,\ \nu_{12} = \nu_{13}$$

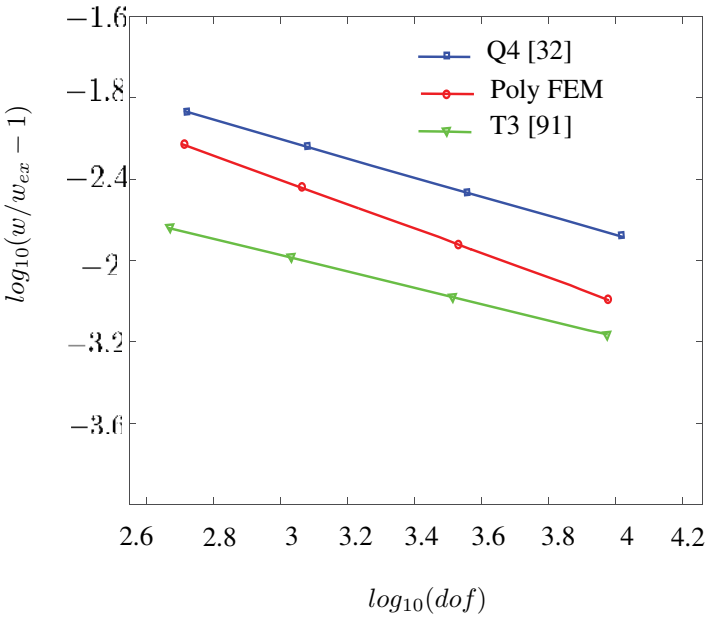

(a)

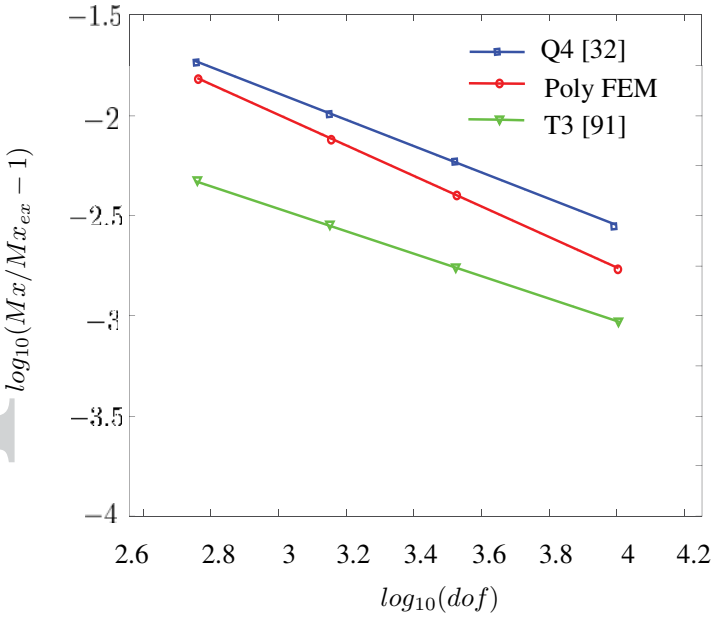

(b)

Figure 12. Convergence test (a) Convergence in the transverse displacement (w). (b) Convergence in the central moment (M).

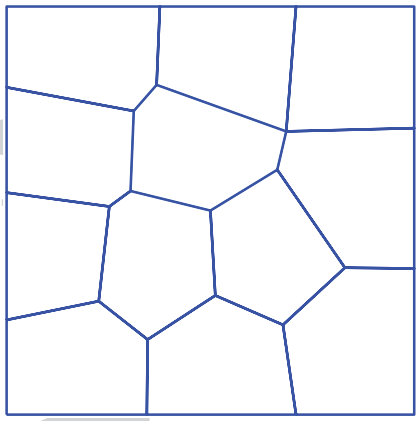

(a)

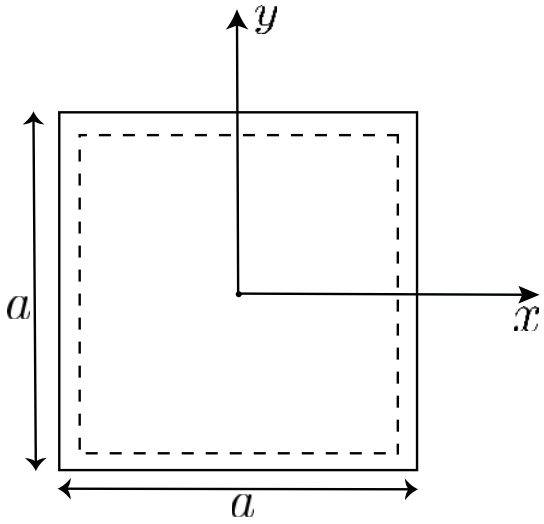

(b)

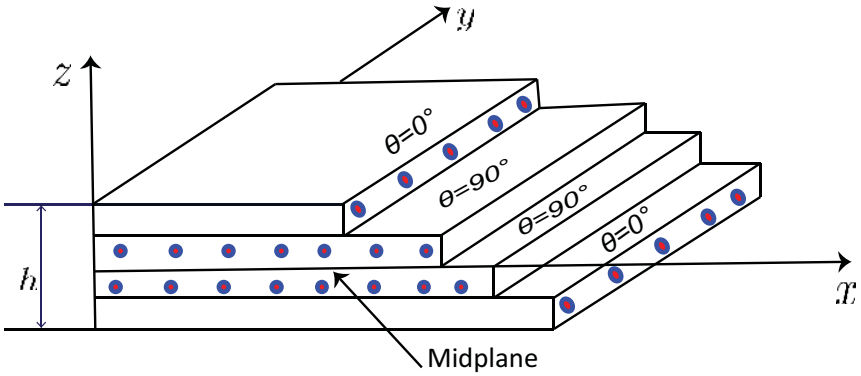

(c)

Figure 13. (a) Polygonal mesh discretization of square plate with 12 elements. (b) Boundary condition of the plate. (c) Geometry of 4 layer cross-ply (0°/90°/90°/0°) laminate.

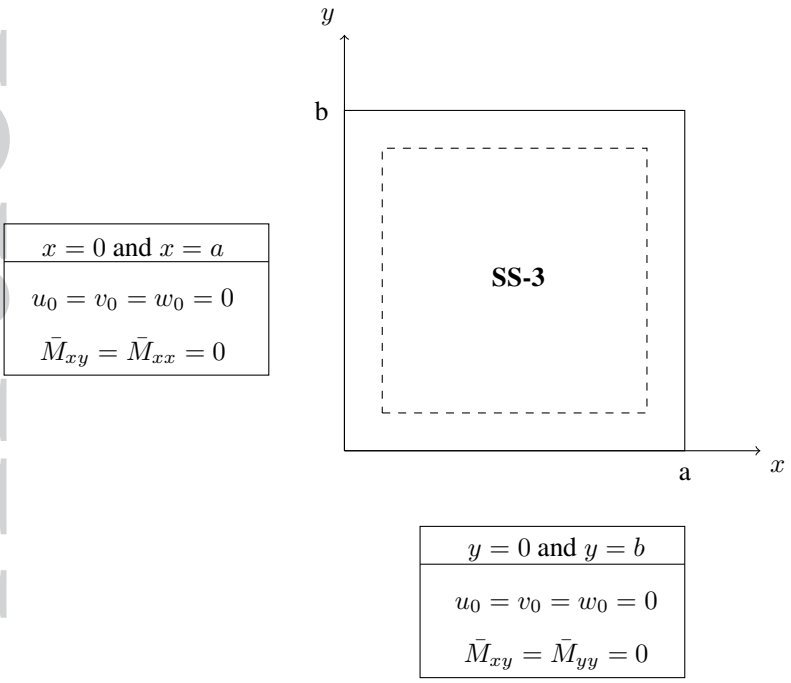

Figure 14. SS-3 Boundary conditions

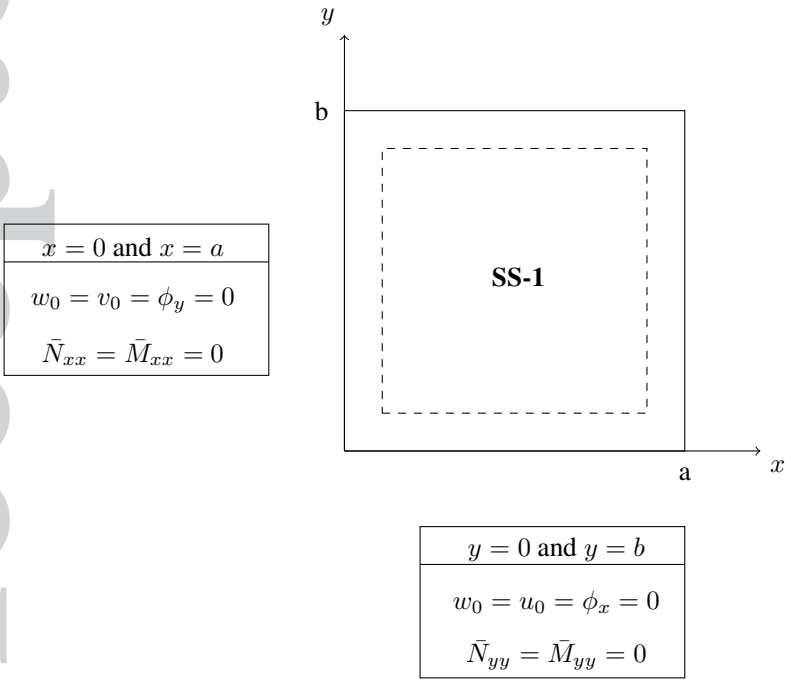

Figure 15. SS-1 Boundary conditions

Table I. Linear analysis for dimensionless central deflection ($\bar{w}$) of the laminated ($0^\circ/90^\circ/90^\circ/0^\circ$) plate under sinusoidal load.

$\frac{a}{h}$	Method	$\bar{w}$
10	Analytical [2]	0.6627
	FEM-HSDT [1]	0.7147
	FSM-HSDT [92]	0.7149
	RBF-PS [93]	0.7203
	Layerwise [94]	0.7309
	IGA-TSDT [95]	0.7359
	PRMn-PL[32]	0.7218
	4 noded- REC[90]	0.7150
	PolyFEM-Present work	0.6958
20	Analytical [2]	0.4912
	FEM-HSDT [1]	0.5060
	FSM-HSDT [92]	0.5061
	RBF-PS [93]	0.5113
	Layerwise [94]	0.5121
	IGA-TSDT [95]	0.5170
	PRMn-PL[[32]]	0.5096
	4 noded- REC[90]	0.5060
	PolyFEM-Present work	0.4953

Table II. Comparison of dimensionless central deflection of a laminated plate ($0^\circ/90^\circ/90^\circ/0^\circ$) plate for μ=0 and μ=1 under sinusoidal load. The comparison made with the standard FEM using 4-noded elements [90] for various load factor during nonlinear analysis.

Load value	$\mu = 0$		$\mu = 1$	
	FEM[90]	PolyFEM -Present	FEM[90]	Poly FEM- Present
0.005	0.00282	0.00237	0.00405	0.00362
0.01	0.00431	0.00389	0.00579	0.00549
0.02	0.00610	0.00583	0.00785	0.00779
0.03	0.00729	0.00716	0.00925	0.00936
0.04	0.00824	0.00820	0.01034	0.01059
0.05	0.00899	0.00907	0.01125	0.01162
0.10	0.01173	0.01216	0.01451	0.01530
0.25	0.01636	0.01738	0.02011	0.02157
0.50	0.02091	0.02247	0.02561	0.02769
0.75	0.02408	0.02600	0.02946	0.03195
1.00	0.02661	0.02880	0.03252	0.03533

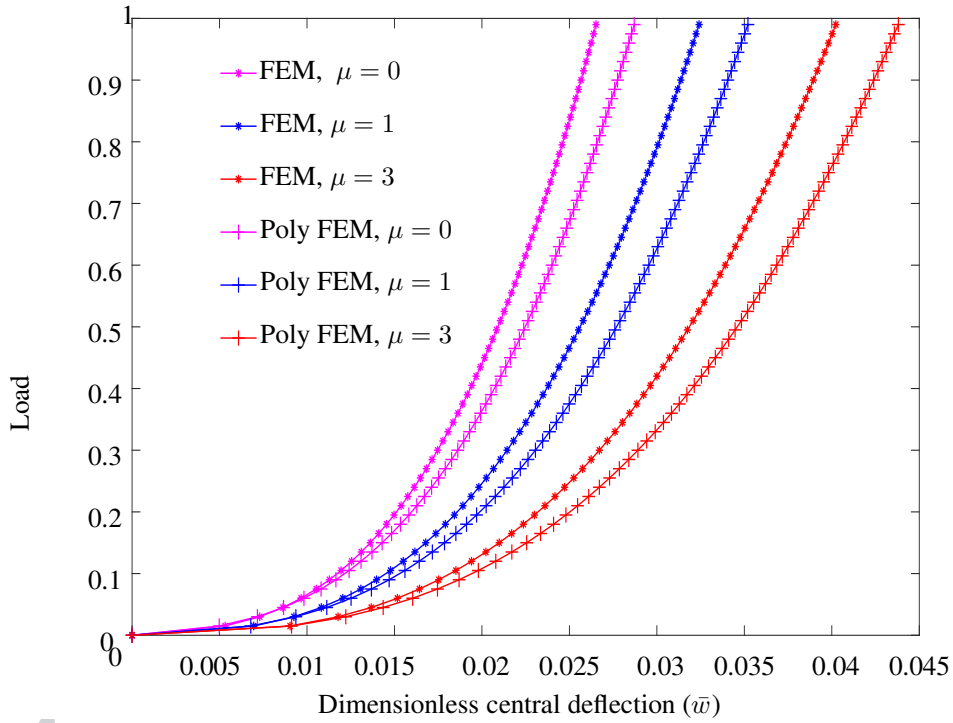

Figure 16. Comparison between standard finite element method and polygonal finite element method for the (0°/90°/90°/0) plate for various length scales with SS3 boundary condition.

Table I compares the dimensionless central deflection obtained by linear analysis with that of analytical solution [2] and other standard finite element solution [1]. The deflections are also compared against the values obtained using the standard finite element [92] with the selective integration and with other meshless methods[93]. A comparison is also made with layerwise theories [94] and isogeometric analysis [95]. It is clearly seen from Table I that the results obtained from the present work are closer to the analytical solution compared to the solution obtained from other methods.

Displacement patch test

Patch test is necessary and sufficient condition for ensuring the convergence of the proposed polygonal element. First, we check the ability of the element in reproducing linear field. For this purpose, we carry out displacement patch test for both inplane and out of plane deformations. The analysis is performed on sufficient discretization with 20, 40, 80 and 500 (see Figure 18) elements in the analysis. A displacement field of $u_x = X_i$ and $u_y = Y_i$ is applied on the boundary for inplane behavior. Convergence is first studied for the inplane degrees of freedom. L^2 and H^1 norms in the displacement are computed and given in Table III. The expression for L^2 and H^1 norm are given by

$$||\boldsymbol{u} - \boldsymbol{u^h}||_{L^2(\Omega)} = \sqrt{\int_\Omega [\boldsymbol{u} - \boldsymbol{u^h}]^T [\boldsymbol{u} - \boldsymbol{u^h}] d\Omega} \tag{36}$$

$$||\boldsymbol{u} - \boldsymbol{u^h}||_{H^1(\Omega)} = \sqrt{\int_\Omega [\boldsymbol{u} - \boldsymbol{u^h}]^T [\boldsymbol{u} - \boldsymbol{u^h}] d\Omega} + \sqrt{\int_\Omega [\nabla \boldsymbol{u} - \nabla \boldsymbol{u^h}]^T : [\nabla \boldsymbol{u} - \nabla \boldsymbol{u^h}] d\Omega} \tag{37}$$

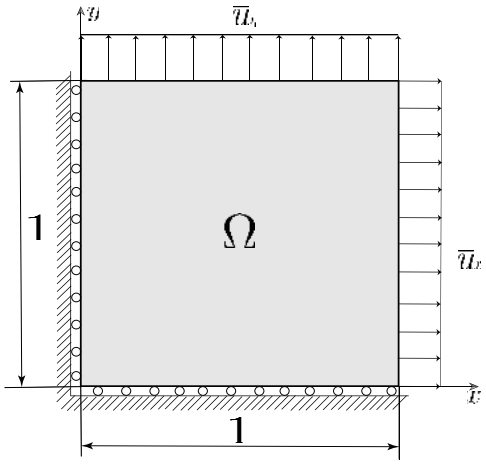

Figure 17. A square domain of unit length for displacement patch test.

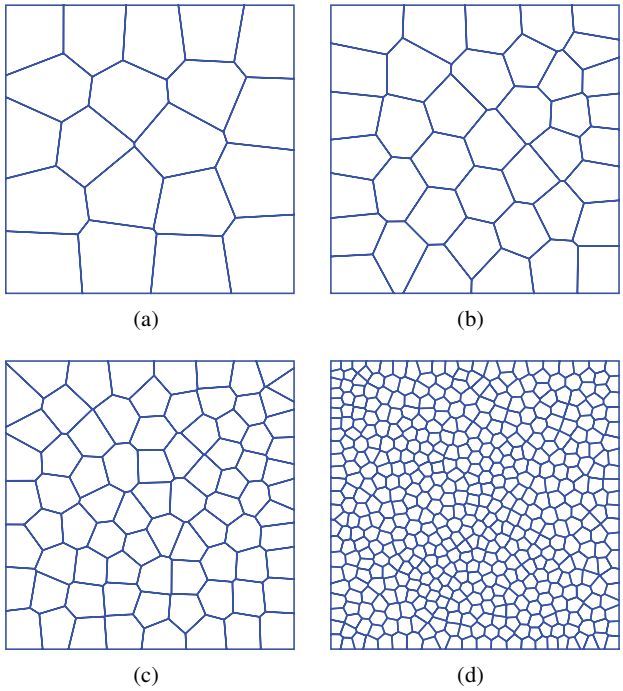

Figure 18. Different polygonal meshes used for displacement patch test. (a) 20 elements (b) 40 elements (c) 80 elements (d) 500 elements

It is observed from Table III that a quadratic convergence in inplane displacement values is obtained for both L^2 and H^1 norms of the solution. Convergence test for transverse deflection w and bending moment M are studied by taking different number of elements (See Figure.12). SS3 symmetric boundary condition is used and (0°/90°/90°/0°) laminate pattern is considered with a/h equal to 10. The results are compared with studies from standard triangular and quadrilateral elements reported in literature [91]. It is observed that the proposed polygonal element has better convergence characteristics than triangular and quadrilateral elements.

Table III. L_2 and H_1 error norms for different patches from displacement patch test.

Mesh	Elements	L_2 Norm	H_1 Norm
a	10	1.7884×10^{-3}	7.14×10^{-2}
b	20	4.4467×10^{-4}	4.48×10^{-4}
c	40	3.0629×10^{-6}	2.76×10^{-6}
d	80	1.6312×10^{-8}	2.92×10^{-8}
d	500	2.4912×10^{-12}	1.192×10^{-12}

Nonlinear analysis

Table II gives the values of dimensionless central deflection of the plate for nonlinear analysis. It is observed that the results obtained from polygonal FEM are higher than those obtained from standard finite element. This clearly is seen at higher nonlocal parameter values of μ=1, indicating the increase in flexibility obtained from polygonal finite element method. Figure 16 depicts effect of various nonlocal parameter on the deflection of plate. As the value of the nonlocal parameter is increased, the deflection becomes more as compared to standard finite element results. Figure 19 shows the effect of E_1/E_2 on the deflection values for various values of nonlocal parameter. It is observed that at lower E_1/E_2 ratio, the central deflection is higher and at larger values of E_1/E_2 ratio, the deflection values are lower. Comparison between Polygonal FEM and standard FEM is shown in Figure 16 for load-deflection behavior. Figure 20 shows the variation of central displacement with a/h ratio for various values of nonlocal parameter. At lower a/h values, the nonlocal parameter has a significant effect on the dimensionless central deflection. At higher values of a/h ratio, this effect is not much pronounced.

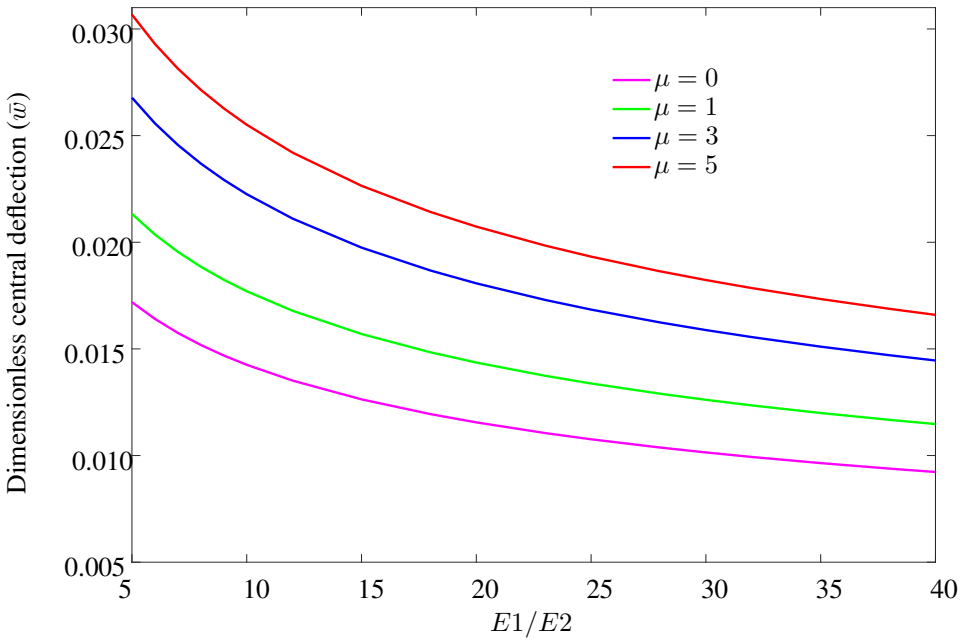

Figure 19. Deflection versus E_1/E_2 plots for (0°/90°/90°/0) plate with SS-3 boundary condition.

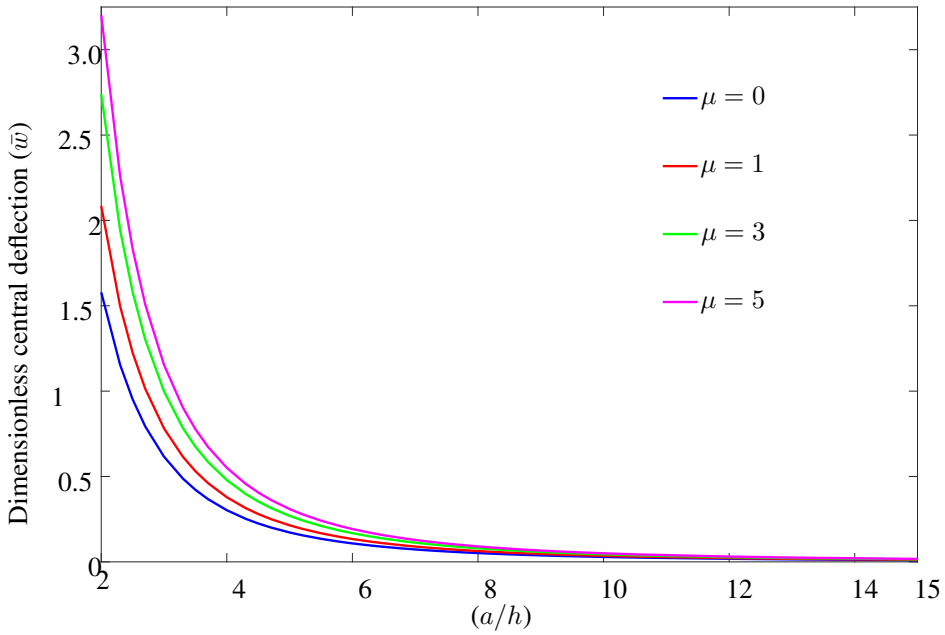

Figure 20. a/h ratio vs central deflection for various nonlocal parameter in the (0°/90°/90°/0)plate with SS-3 boundary condition.

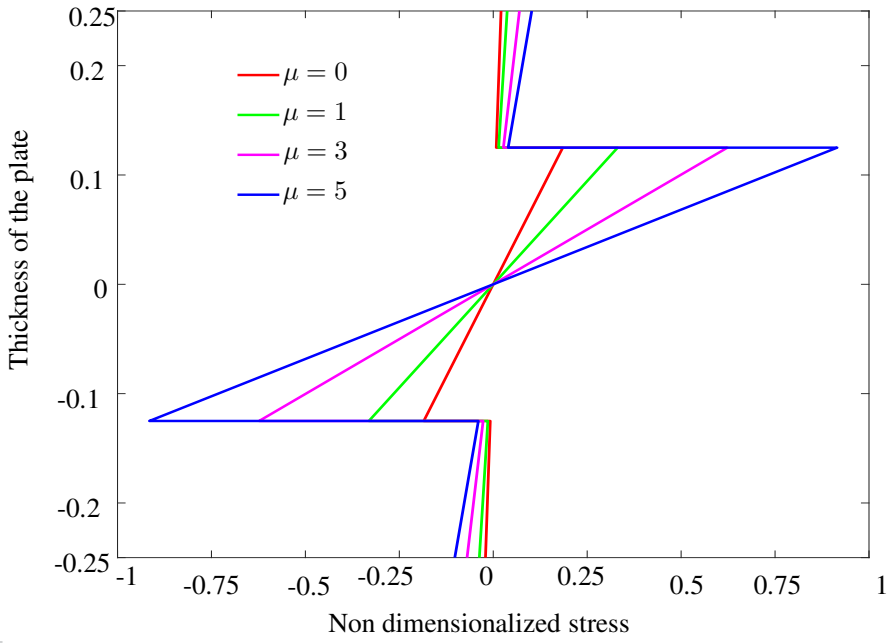

Figure 21. Variation of σ_{yy} at $x = a/2$, $y = a/2$ along the thickness of $(0^\circ/90^\circ/90^\circ/0^\circ)$ laminate for various nonlocal parameters (μ).

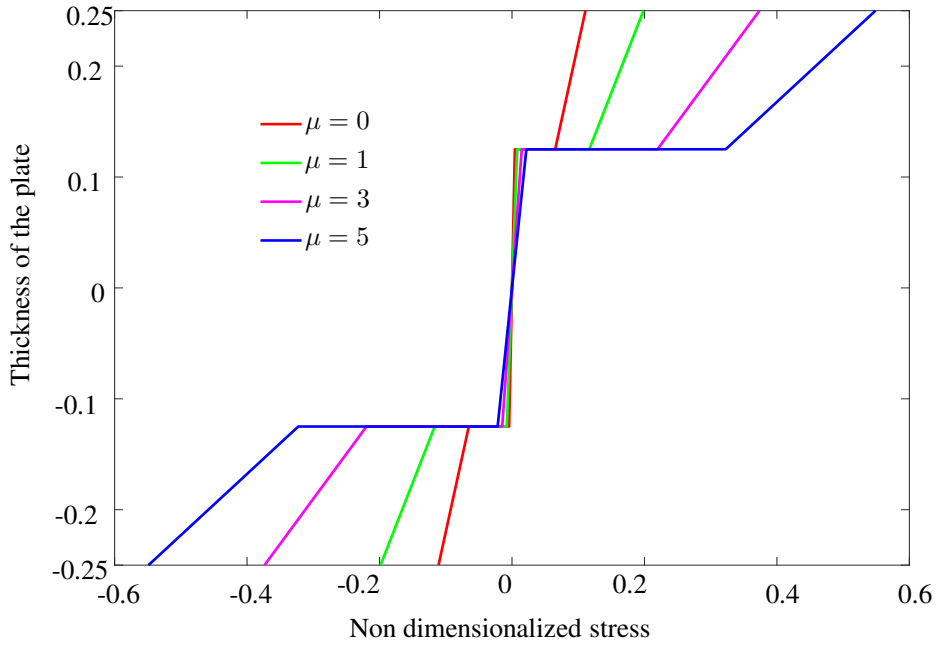

Figure 22. Variation of σ_{xx} at $x = a/2$, $y = a/2$ along the thickness of $(0^\circ/90^\circ/90^\circ/0\,)$ laminate for various nonlocal parameters (μ).

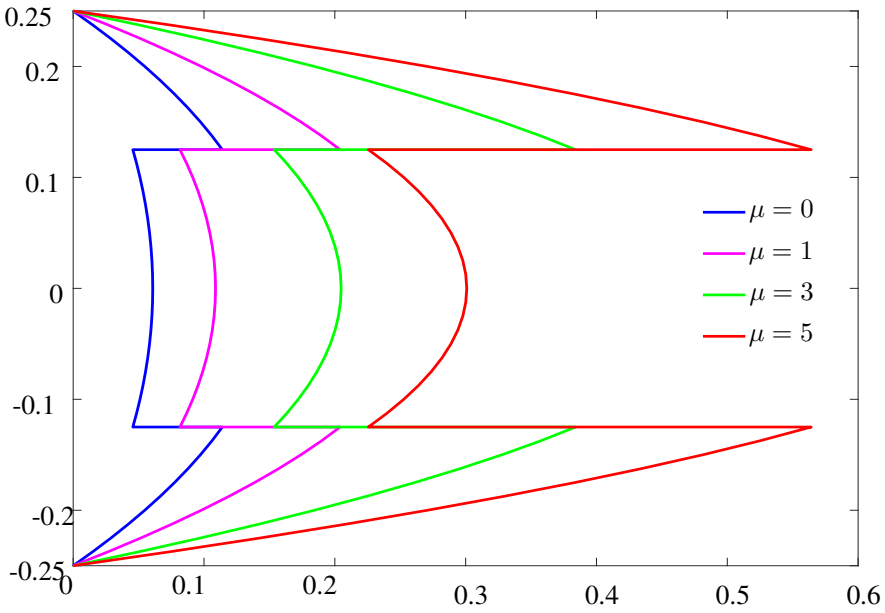

Figure 23. Variation of σ_{xz} through the thickness for $(0^\circ/90^\circ/90^\circ/0)$ laminate for various nonlocal parameters (μ).

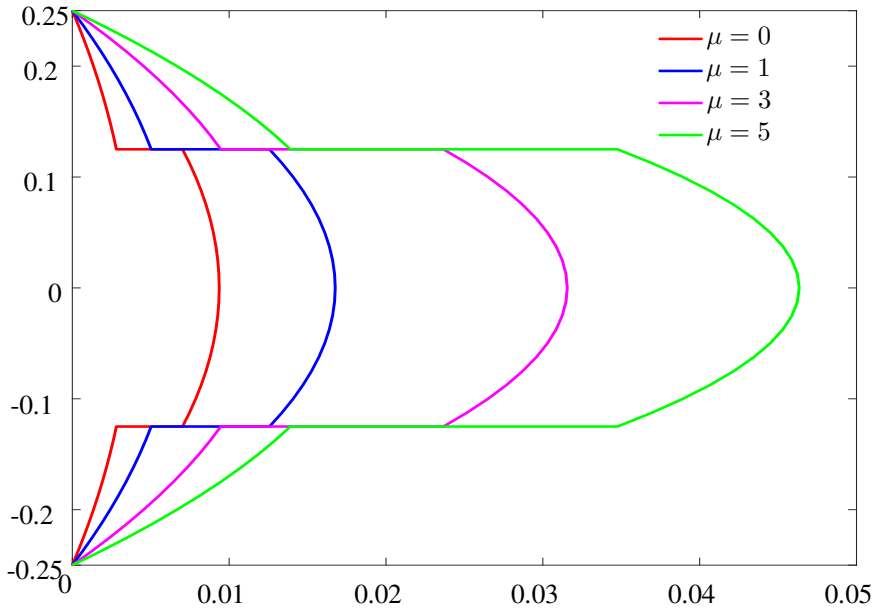

Figure 24. Variation of σ_{yz} through the thickness of a $(0^\circ/90^\circ/90^\circ/0)$ laminate for various nonlocal parameters (μ).

For analyzing stress at a given point in the plate, various points along the thickness direction of the laminate are considered and plotted for an unit value of applied load. The stresses are plotted at $x = a/2,\ y = a/2$ for various values of nonlocal parameter as shown in Figure 21. The plots clearly signify the importance of nonlocal parameter on the estimation of stress. Variation of (σ_{xz}) and (σ_{yz}) is also shown in Figure 23 and Figure 24 respectively.

Example 2: Shear locking behavior

Various methods to eliminate locking behavior has been discussed in section 7 . Two different discretized domain of 32 and 72 elements (see Figure 25) are taken to demonstrate the consistent interpolation and reduced integration technique. A square cross-ply symmetric $(0^\circ/90^\circ/90^\circ/0^\circ)$ laminated plate of length a=5 units is considered. The laminate is made up of equal thickness layers each of 0.125 units. The plate is subjected to sinusoidal load of unit intensity. The plate is analyzed for thin plate limits and simply supported boundary condition of SS-3 type is considered. Material properties of the plate considered are

$$E_1/E_2 = 25,\ G_{12}/E_2 = 0.5,\ G_{23}/E_2 = 0.2,\ G_{12} = G_{13},\ \nu_{12} = 0.25,\ \nu_{12} = \nu_{13}$$

. For reduced integration studies, the effect of various integration scheme by taking different number of Gauss points in the background triangular subdomain is considered. The position of different Gauss points is shown in Figure 10. Various combination of Gauss points are taken for full and reduced integration. The dimensionless central deflection of the plate are given in Table IV for various choices of integration schemes. It is observed that comparative values of central deflection are obtained in thin plate limits for different combination of Gauss points. The results are also compared with reference values from literature. Results for consistent interpolation procedure is presented in Table V where we have taken the same number of Gauss points to integrate the bending terms and the shear energy terms. It is observed that consistent interpolation gives the comparative central deflection value irrespective of the number of Gauss points used. Hence, the method of consistent interpolation proved to be efficient in eliminating shear locking in the proposed element.

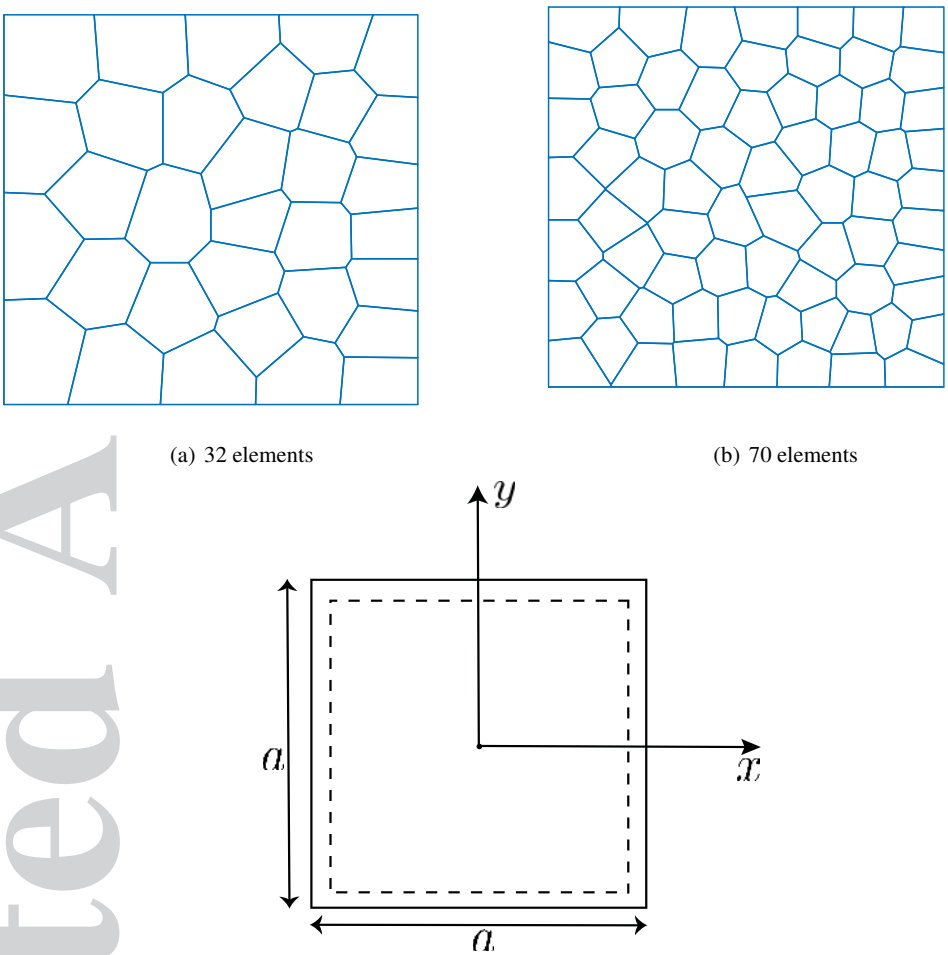

(a) 32 elements (b) 70 elements

(c) Boundary condition

Figure 25. Discretization considered to analyze plate for reduced integration and consistent interpolation technique.

Example 3

A four-layer square symmetric cross-ply laminated plate (-45°/45°/45°/-45°) is considered for the analysis. Dimension of the square plate is taken as a=5 units. Layers of equal thickness of 0.125 units is considered. The a/h ratio of the plate is taken as 10. The plate is subjected to sinusoidal load of unit intensity. Simply supported boundary condition of SS-1 and SS-3 type are considered. The domain is discretized using polygonal elements as shown in Figure 26(a). Orientation of an angle ply is shown in Figure 26(c). The nonlocal parameter is taken as 0,1,3 and 5. Material properties considered are given below:

$$E_1/E_2 = 25,\ G_{12}/E_2 = 0.5,\ G_{23}/E_2 = 0.2,\ G_{12} = G_{13},\ \nu_{12} = 0.25,\ \nu_{12} = \nu_{13}$$

Plots for dimensionless central deflection versus load are shown in Figure 27 and Figure 28 for various nonlocal parameter, considering SS-1 and SS-3 boundary condition respectively. It is observed that SS-3 boundary condition makes the plate stiffer compared to SS-1 boundary condition. Also the lamination scheme (-45°/45°/45°/-45°) has comparatively lesser deflection values than (0°/90°/90°/0°) lamination scheme when same SS-3 boundary condition is taken (see example-1) for various nonlocal parameter.

Table IV. Effect of reduced integration on the deflection of plate.

Mesh	B.C	Integration Type	Central deflection
32 elements	SS3	F(3)	1.6945
	SS3	F(3)R(1)	1.8466
	SS3	F(6)	1.6725
	SS3	F(6)R(3)	1.6701
	SS3	F(13)R(13)	1.6788
	SS3	F(13)R(6)	1.2145
70 elements	SS3	F(3)	1.7373
	SS3	F(3)R(1)	1.8578
	SS3	F(6)	1.7198
	SS3	F(6)R(3)	1.7094
	SS3	F(13)R(13)	1.4229
	SS3	F(13)R(6)	1.2309

F(M)R(N): 'M' number of Gauss points in full integration (bending terms) and 'N' Gauss point for reduced integration (shear terms) considered in each triangular subdomain of the parent polygonal element.
F(M): 'M' number of Gauss points for both shear and bending terms.

Table V. Effect of consistent interpolation on the deflection of plate.

Mesh	B.C	Integration Type	Central deflection
32 elements	SS3	F(3)	1.6945
	SS3	F(6)	1.6725
	SS3	F(13)	1.4193
70 elements	SS3	F(3)	1.6482
	SS3	F(6)	1.6416
	SS3	F(13)	1.6418

F(K): 'K' number of Gauss points are taken for full integration in each triangular subdomain of the parent polygonal element.

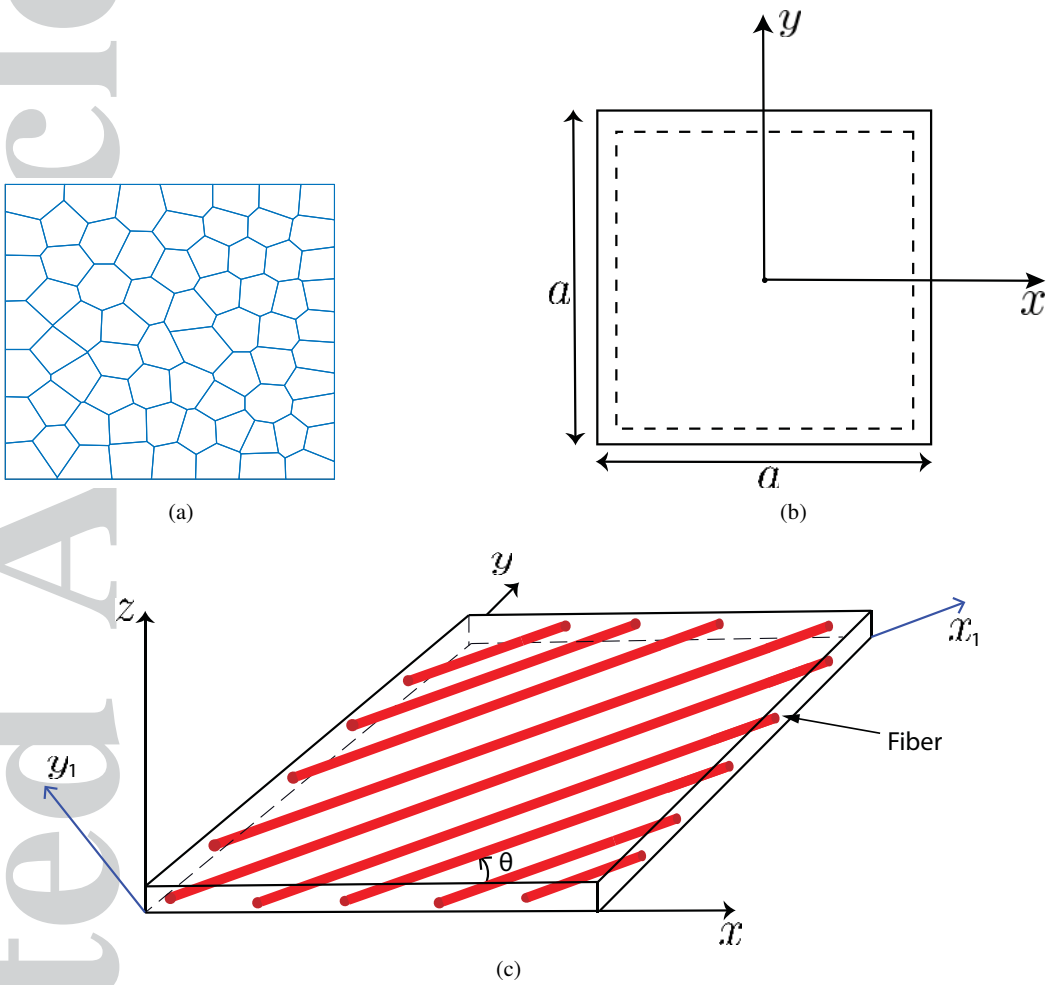

Figure 26. (a) Polygonal mesh discretization of square plate with 70 elements. (b) Boundary condition of the plate. (c) Geometry of an angle-ply oriented at angle θ.

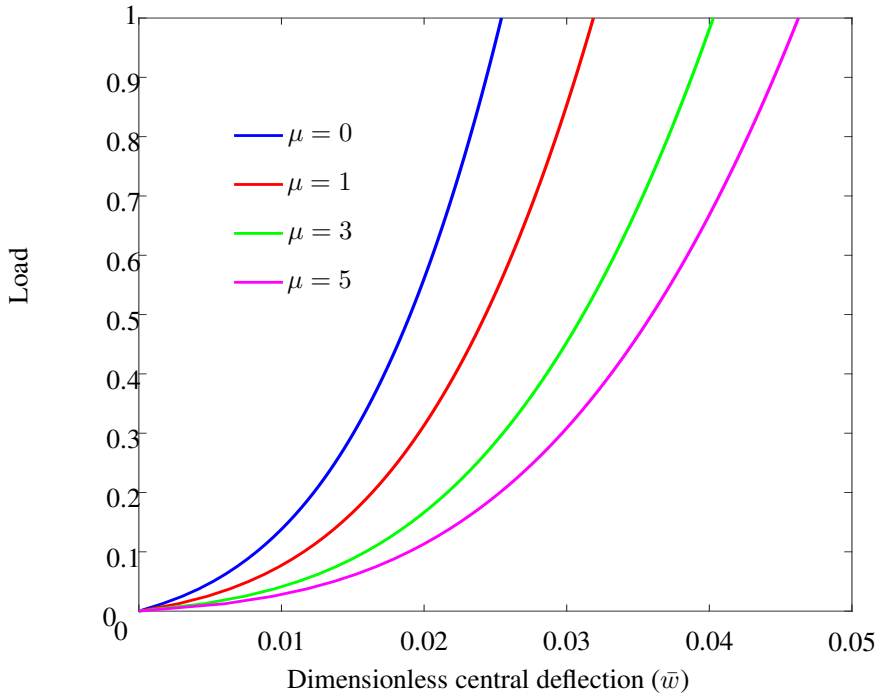

Figure 27. Load versus central deflection for (-45°/45°/45°/-45)plate with SS-1 boundary condition.

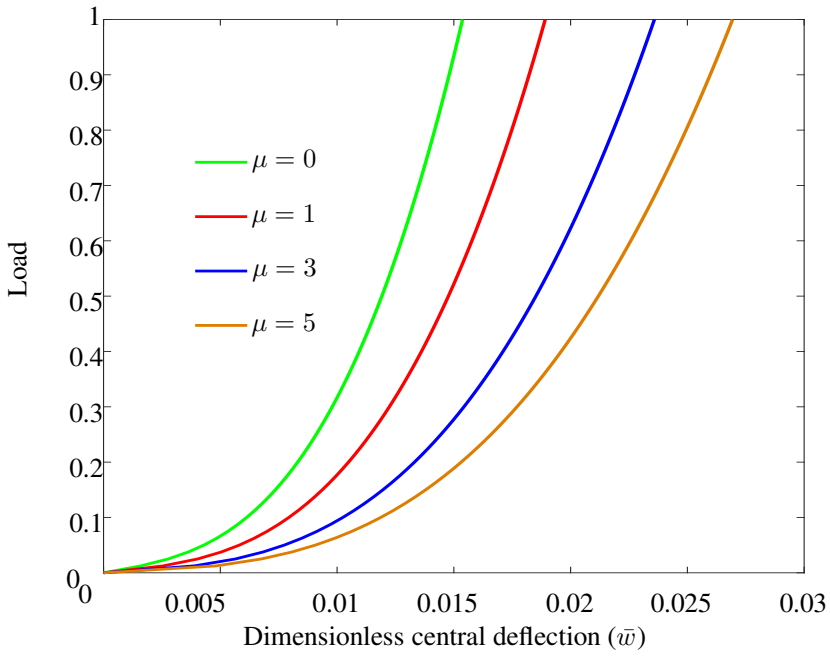

Figure 28. Load versus central deflection for (-45°/45°/45°/-45)plate with SS-3 boundary condition.

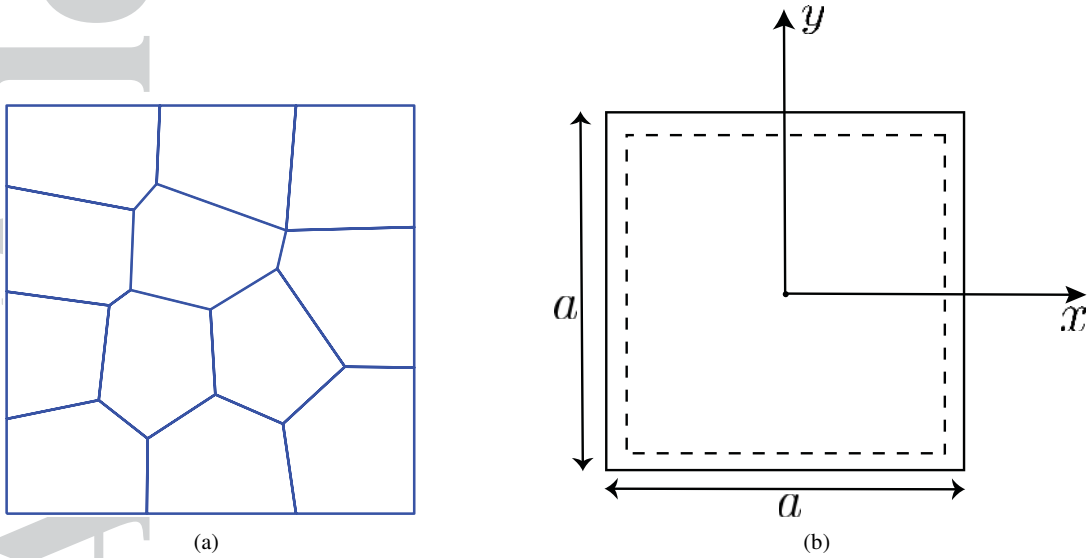

(a) (b)

Figure 29. (a) Polygonal mesh discretization of square plate with 70 elements. (b) Boundary condition. (c) Geometry of 4 layer cross-ply (0°/90°/90°/0°) laminate.

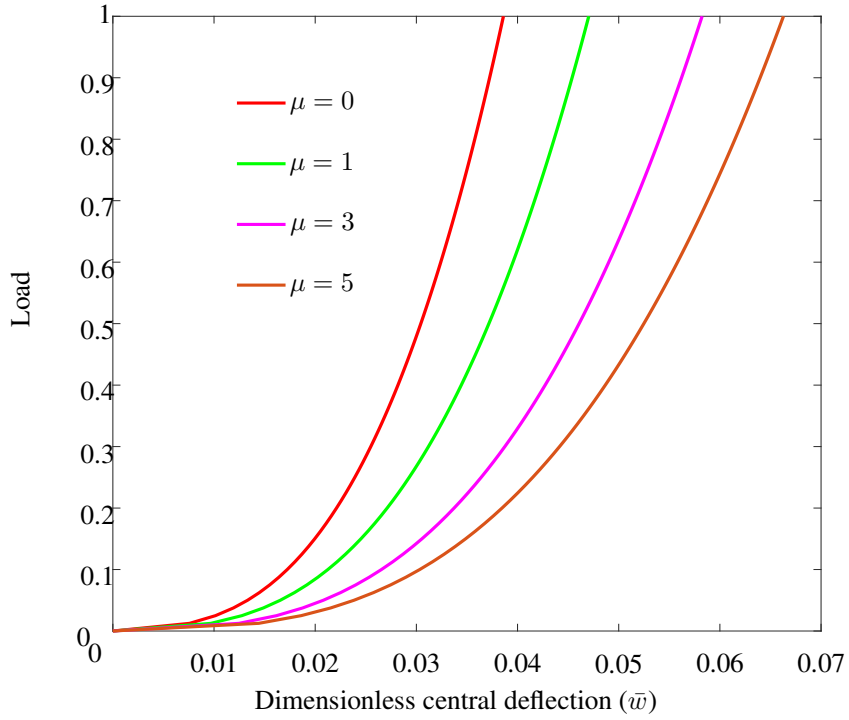

Figure 30. Load versus central deflection for (0°/90)plate with SS-1 boundary condition.

Example 4

A two-layer square symmetric cross-ply laminated plate (0°/90°) is considered with SS-1 type boundary condition. Dimension of the square plate is taken as a=5 units. Layers of equal thickness of 0.125 units is considered. The a/h ratio of the plate is taken as 10. Sinusoidal load of unit intensity

is applied. Mesh discretization given in the Figure 29(a) is used. The nonlocal parameter is taken as 0,1,3 and 5. Material properties considered are given below:

$$E_1/E_2 = 25,\ G_{12}/E_2 = 0.5,\ G_{23}/E_2 = 0.2,\ G_{12} = G_{13},\ \nu_{12} = 0.25,\ \nu_{12} = \nu_{13}$$

Figure 30 shows the plot for dimensionless central deflection versus load for various nonlocal parameters.

9. CONCLUSIONS

In this study, a locking-free n-sided C^1 polygonal finite element is presented for nonlinear analysis of laminated plates. The plate kinematics is based on Reddy's third-order shear deformation theory (TSDT) [1, 2]. The inplane displacements are approximated using barycentric form of Lagrange shape functions. The weak-form Galerkin formulation based on the kinematics of TSDT requires the C^1 approximation of the transverse displacement over the polygonal element. This is achieved by embedding the C^0 Lagrange interpolants over a cubic Bernstein–Bezier patch defined over the n-sided polygonal element. Such an approach ensures the continuity of the derivative field at the inter-element edges. In addition, Eringen's stress-gradient nonlocal [3] constitutive equations are used in the present formulation to account for nonlocality. The effect of geometric nonlinearity is taken by considering the von Kármán' geometric nonlinearity. Examples are presented to show the effect of nonlocality, geometric nonlinearity, and the lamination scheme on the bending behavior of laminated composite plates. In linear analysis it is observed that polygonal finite elements provide greater flexibility and better convergence. This is also confirmed from the patch test studies on inplane displacements and convergence stuides on out of plane displacements. The effect of reduced integration and consistent interpolation are found to improve the results of the polygonal element. Eringens nonlocality is able to capture the length scale effects. The nonlocal parameter (μ) has a greater effect in polygonal finite element framework than in finite element method. The dimensionless central deflection and stress values increase, as we increase the nonlocal parameter value. It has been shown from this study that n sided polygonal finite element method has more advantages in terms of discretization and accuracy which is C^1 continuous.

A. APPENDIX-1

Displacement field

In the third-order shear deformation theory, the displacement field is expanded up to third degree of the thickness coordinate:

$$\begin{aligned} u(x,y,z) &= u_0(x,y) + z\phi_x - \frac{4z^3}{3h^2}\left(\phi_x + \frac{\partial w_0}{\partial x}\right) \\ v(x,y,z) &= v_0(x,y) + z\phi_y - \frac{4z^3}{3h^2}\left(\phi_y + \frac{\partial w_0}{\partial y}\right) \\ w(x,y,z) &= w_0(x,y) \end{aligned} \tag{38}$$

where (u_0, v_0, w_0) displacements of the point on the mid plane in the in plane directions. (i.e., $z = 0$). ϕ_x and ϕ_y represent the rotations of a transverse normal line at the mid-plane ($\phi_x = \frac{\partial u}{\partial z}$ and $\phi_y = \frac{\partial v}{\partial z}$). h is the total thickness of the plate.

Strain–displacement relations

The Green–Lagrange strain components that account for the geometric nonlinearity in TSDT are

$$\begin{Bmatrix} \varepsilon_{xx} \\ \varepsilon_{yy} \\ \gamma_{xy} \end{Bmatrix} = \begin{Bmatrix} \varepsilon_{xx}^{(0)} \\ \varepsilon_{yy}^{(0)} \\ \gamma_{xy}^{(0)} \end{Bmatrix} + z \begin{Bmatrix} \varepsilon_{xx}^{(1)} \\ \varepsilon_{yy}^{(1)} \\ \gamma_{xy}^{(1)} \end{Bmatrix} + z^3 \begin{Bmatrix} \varepsilon_{xx}^{(3)} \\ \varepsilon_{yy}^{(3)} \\ \gamma_{xy}^{(3)} \end{Bmatrix} \tag{39}$$

$$\begin{Bmatrix} \gamma_{yz} \\ \gamma_{xz} \end{Bmatrix} = \begin{Bmatrix} \gamma_{yz}^{(0)} \\ \gamma_{xz}^{(0)} \end{Bmatrix} + z^2 \begin{Bmatrix} \gamma_{yz}^{(2)} \\ \gamma_{xz}^{(2)} \end{Bmatrix} \tag{40}$$

where

$$\begin{Bmatrix} \varepsilon_{xx}^{(0)} \\ \varepsilon_{yy}^{(0)} \\ \gamma_{xy}^{(0)} \end{Bmatrix} = \begin{Bmatrix} \dfrac{\partial u_0}{\partial x} + \dfrac{1}{2}(\dfrac{\partial w_0}{\partial x})^2 \\ \dfrac{\partial v_0}{\partial y} + \dfrac{1}{2}(\dfrac{\partial w_0}{\partial y})^2 \\ \dfrac{\partial u_0}{\partial y} + \dfrac{\partial v_0}{\partial x} + \dfrac{\partial w_0}{\partial x}\dfrac{\partial w_0}{\partial y} \end{Bmatrix}, \begin{Bmatrix} \varepsilon_{xx}^{(1)} \\ \varepsilon_{yy}^{(1)} \\ \gamma_{xy}^{(1)} \end{Bmatrix} = \begin{Bmatrix} \dfrac{\partial \phi_x}{\partial x} \\ \dfrac{\partial \phi_y}{\partial y} \\ \dfrac{\partial \phi_x}{\partial y} + \dfrac{\partial \phi_y}{\partial x} \end{Bmatrix} \tag{41}$$

$$\begin{Bmatrix} \varepsilon_{xx}^{(3)} \\ \varepsilon_{yy}^{(3)} \\ \gamma_{xy}^{(3)} \end{Bmatrix} = -c_1 \begin{Bmatrix} \dfrac{\partial \phi_x}{\partial x} + \dfrac{\partial^2 w_0}{\partial x^2} \\ \dfrac{\partial \phi_y}{\partial y} + \dfrac{\partial^2 w_0}{\partial y^2} \\ \dfrac{\partial \phi_x}{\partial y} + \dfrac{\partial \phi_y}{\partial x} + 2\dfrac{\partial^2 w_0}{\partial x \partial y} \end{Bmatrix} \tag{42}$$

$$\begin{Bmatrix} \gamma_{yz}^{(0)} \\ \gamma_{xz}^{(0)} \end{Bmatrix} = \begin{Bmatrix} \phi_y + \dfrac{\partial w_0}{\partial y} \\ \phi_x + \dfrac{\partial w_0}{\partial x} \end{Bmatrix}, \begin{Bmatrix} \gamma_{yz}^{(2)} \\ \gamma_{xz}^{(2)} \end{Bmatrix} = -c_2 \begin{Bmatrix} \phi_y + \dfrac{\partial w_0}{\partial y} \\ \phi_x + \dfrac{\partial w_0}{\partial x} \end{Bmatrix} \tag{43}$$

B. APPENDIX-2

Lamina constitutive relations

Since the laminate is made of several orthotropic layers, with their material axes oriented arbitrarily with respect to laminate coordinates, the constitutive equations of each layer must be transformed to the laminate coordinates (x, y, z). The transformed stress–strain relations in the laminate coordinates (x, y, z) are given by

$$\begin{Bmatrix} \sigma_{xx} \\ \sigma_{yy} \\ \sigma_{xy} \end{Bmatrix} = \begin{bmatrix} \bar{Q}_{11} & \bar{Q}_{12} & \bar{Q}_{16} \\ \bar{Q}_{12} & \bar{Q}_{22} & \bar{Q}_{26} \\ \bar{Q}_{16} & \bar{Q}_{26} & \bar{Q}_{66} \end{bmatrix} \begin{Bmatrix} \varepsilon_{xx} \\ \varepsilon_{yy} \\ \gamma_{xy} \end{Bmatrix}, \quad \begin{Bmatrix} \sigma_{yz} \\ \sigma_{xz} \end{Bmatrix} = \begin{bmatrix} \bar{Q}_{44} & \bar{Q}_{45} \\ \bar{Q}_{45} & \bar{Q}_{55} \end{bmatrix} \begin{Bmatrix} \gamma_{yz} \\ \gamma_{xz} \end{Bmatrix} \tag{44}$$

where

$$\begin{aligned}
\bar{Q}_{11} &= Q_{11}\cos^4\theta + 2\left(Q_{12}+2Q_{66}\right)\sin^2\theta\cos^2\theta + Q_{22}\sin^4\theta \\
\bar{Q}_{12} &= \left(Q_{11}+Q_{22}-4Q_{66}\right)\sin^2\theta\cos^2\theta + Q_{12}\left(\sin^4\theta+\cos^4\theta\right) \\
\bar{Q}_{16} &= \left(Q_{11}-Q_{12}-2Q_{66}\right)\sin\theta\cos^3\theta + \left(Q_{12}-Q_{22}+2Q_{66}\right)\sin^3\theta\cos\theta \\
\bar{Q}_{22} &= Q_{11}\sin^4\theta + 2\left(Q_{16}+2Q_{66}\right)\sin^2\theta\cos^2\theta + Q_{22}\cos^4\theta \\
\bar{Q}_{26} &= \left(Q_{11}-Q_{12}-2Q_{66}\right)\sin^3\theta\cos\theta + \left(Q_{12}-Q_{22}+2Q_{66}\right)\sin\theta\cos^3\theta \\
\bar{Q}_{66} &= \left(Q_{11}+Q_{22}-2Q_{12}-2Q_{66}\right)\sin^2\theta\cos^2\theta + Q_{66}(\sin^4\theta+\cos^4\theta)
\end{aligned} \tag{45}$$

$$\begin{aligned}
\bar{Q}_{44} &= Q_{44}\cos^2\theta + Q_{55}\sin^2\theta \\
\bar{Q}_{45} &= \left(Q_{55}-Q_{44}\right)\cos\theta\sin\theta \\
\bar{Q}_{55} &= Q_{44}\sin^2\theta + Q_{55}\cos^2\theta
\end{aligned} \tag{46}$$

where

$$Q_{11} = \frac{E_1}{1-\nu_{12}\nu_{21}}, \quad Q_{12} = \frac{\nu_{12}E_2}{1-\nu_{12}\nu_{21}}, \quad Q_{22} = \frac{E_2}{1-\nu_{12}\nu_{21}}, \quad Q_{66} = G_{12}, \tag{47}$$

$$Q_{16} = Q_{26} = 0, \quad Q_{44} = G_{23}, \quad Q_{55} = G_{13} \tag{48}$$

where θ is the orientation, measured in counterclockwise, from the fiber direction to the positive x-axis, E_1 and E_2 are elastic moduli, ν_{12} and ν_{21} are Poisson's ratios, and G_{12}, G_{13} and G_{23} are the shear moduli.

C. APPENDIX-3

The coefficients of the stiffness matrix in equation ((31)) are as follows:

$$K_{ij}^{11} = \int_{\Omega^e}\left(A_{11}\frac{\partial\psi_j^{(1)}}{\partial x}\frac{\partial\psi_i^{(1)}}{\partial x} + A_{66}\frac{\partial\psi_j^{(1)}}{\partial y}\frac{\partial\psi_i^{(1)}}{\partial y} + A_{16}\left(\frac{\partial\psi_j^{(1)}}{\partial y}\frac{\partial\psi_i^{(1)}}{\partial x} + \frac{\partial\psi_j^{(1)}}{\partial x}\frac{\partial\psi_i^{(1)}}{\partial y}\right)\right)dxdy \tag{49}$$

$$K_{ij}^{12} = \int_{\Omega^e}\left(A_{12}\frac{\partial\psi_j^{(1)}}{\partial y}\frac{\partial\psi_i^{(1)}}{\partial x} + A_{66}\frac{\partial\psi_j^{(1)}}{\partial x}\frac{\partial\psi_i^{(1)}}{\partial y} + A_{16}\frac{\partial\psi_j^{(1)}}{\partial x}\frac{\partial\psi_i^{(1)}}{\partial x} + A_{26}\frac{\partial\psi_j^{(1)}}{\partial y}\frac{\partial\psi_i^{(1)}}{\partial y}\right)dxdy \tag{50}$$

$$\begin{aligned}
K_{ij}^{13} = \int_{\Omega^e}\Bigg[&\frac{\partial\psi_i^{(1)}}{\partial x}\left(\frac{1}{2}A_{11}\frac{\partial w}{\partial x}\frac{\partial\varphi_j}{\partial x} + \frac{1}{2}A_{12}\frac{\partial w}{\partial y}\frac{\partial\varphi_j}{\partial y} + \frac{1}{2}A_{16}\left(\frac{\partial w}{\partial x}\frac{\partial\varphi_j}{\partial y} + \frac{\partial w}{\partial y}\frac{\partial\varphi_j}{\partial x}\right) - c_1E_{11}\frac{\partial^2\varphi_j}{\partial x^2}\right. \\
&\left. - c_1E_{12}\frac{\partial^2\varphi_j}{\partial y^2} - 2c_1E_{16}\frac{\partial^2\varphi_j}{\partial x\partial y}\right) \\
&+ \frac{\partial\psi_i^{(1)}}{\partial y}\left(\frac{1}{2}A_{16}\frac{\partial w}{\partial x}\frac{\partial\varphi_j}{\partial x} + \frac{1}{2}A_{26}\frac{\partial w}{\partial y}\frac{\partial\psi_j}{\partial y} + \frac{1}{2}A_{66}\left(\frac{\partial w}{\partial x}\frac{\partial\varphi_j}{\partial y} + \frac{\partial w}{\partial y}\frac{\partial\varphi_j}{\partial x}\right) - c_1E_{16}\frac{\partial^2\varphi_j}{\partial x^2}\right. \\
&\left. - c_1E_{26}\frac{\partial^2\varphi_j}{\partial y^2} - 2c_1E_{66}\frac{\partial^2\varphi_j}{\partial x\partial y}\right)\Bigg]dxdy
\end{aligned} \tag{51}$$

$$\begin{aligned}
K_{ij}^{14} = \int_{\Omega^e}\Bigg[&\frac{\partial\psi_i^{(1)}}{\partial x}\left(B_{11}\frac{\partial\psi_j^{(2)}}{\partial x} + B_{16}\frac{\partial\psi_j^{(2)}}{\partial y} - c_1E_{11}\frac{\partial\psi_j^{(2)}}{\partial x} - c_1E_{16}\frac{\partial\psi_j^{(2)}}{\partial y}\right) \\
&+ \frac{\partial\psi_i^{(1)}}{\partial y}\left(B_{16}\frac{\partial\psi_j^{(2)}}{\partial x} + B_{66}\frac{\partial\psi_j^{(2)}}{\partial y} - c_1E_{16}\frac{\partial\psi_j^{(2)}}{\partial x} - c_1E_{66}\frac{\partial\psi_j^{(2)}}{\partial y}\right)\Bigg]dxdy
\end{aligned} \tag{52}$$

$$K_{ij}^{15}=\int_{\Omega^e}\Bigg[\frac{\partial\psi_i^{(1)}}{\partial x}\left(B_{12}\frac{\partial\psi_j^{(2)}}{\partial y}+B_{16}\frac{\partial\psi_j^{(2)}}{\partial x}-c_1E_{22}\frac{\partial\psi_j^{(2)}}{\partial y}-c_1E_{26}\frac{\partial\psi_j^{(2)}}{\partial x}\right)$$
$$+\frac{\partial\psi_i^{(1)}}{\partial y}\left(B_{26}\frac{\partial\psi_j^{(2)}}{\partial y}+B_{66}\frac{\partial\psi_j^{(2)}}{\partial x}-c_1E_{26}\frac{\partial\psi_j^{(2)}}{\partial y}-c_1E_{66}\frac{\partial\psi_j^{(2)}}{\partial x}\right)\Bigg]dxdy \tag{53}$$

$$K_{ij}^{21}=\int_{\Omega^e}\left(A_{12}\frac{\partial\psi_j^{(1)}}{\partial x}\frac{\partial\psi_i^{(1)}}{\partial y}+A_{16}\frac{\partial\psi_j^{(1)}}{\partial x}\frac{\partial\psi_i^{(1)}}{\partial x}+A_{26}\frac{\partial\psi_j^{(1)}}{\partial y}\frac{\partial\psi_i^{(1)}}{\partial y}+A_{66}\frac{\partial\psi_j^{(1)}}{\partial y}\frac{\partial\psi_i^{(1)}}{\partial x}\right)dxdy \tag{54}$$

$$K_{ij}^{22}=\int_{\Omega^e}\left(A_{22}\frac{\partial\psi_j^{(1)}}{\partial y}\frac{\partial\psi_i^{(1)}}{\partial y}+A_{26}(\frac{\partial\psi_j^{(1)}}{\partial x}\frac{\partial\psi_i^{(1)}}{\partial y}+\frac{\partial\psi_j^{(1)}}{\partial y}\frac{\partial\psi_i^{(1)}}{\partial x})+A_{66}\frac{\partial\psi_j^{(1)}}{\partial x}\frac{\partial\psi_i^{(1)}}{\partial x}\right)dxdy \tag{55}$$

$$K_{ij}^{23}=\int_{\Omega^e}\Bigg[\frac{\partial\psi_i^{(1)}}{\partial y}\left(\frac{1}{2}A_{12}\frac{\partial w}{\partial x}\frac{\partial\varphi_j}{\partial x}+\frac{1}{2}A_{22}\frac{\partial w}{\partial y}\frac{\partial\varphi_j}{\partial y}+\frac{1}{2}A_{26}(\frac{\partial w}{\partial x}\frac{\partial\varphi_j}{\partial y}+\frac{\partial w}{\partial y}\frac{\partial\varphi_j}{\partial y})-c_1E_{12}\frac{\partial^2\varphi_j}{\partial x^2}\right.$$
$$\left.-c_1E_{22}\frac{\partial^2\varphi_j}{\partial y^2}-2c_1E_{26}\frac{\partial^2\varphi_j}{\partial x\partial y}\right)$$
$$+\frac{\partial\psi_i^{(1)}}{\partial x}\left(\frac{1}{2}A_{16}\frac{\partial w}{\partial x}\frac{\partial\varphi_j}{\partial x}+\frac{1}{2}A_{26}\frac{\partial w}{\partial y}\frac{\partial\varphi_j}{\partial y}+\frac{1}{2}A_{66}(\frac{\partial w}{\partial x}\frac{\partial\varphi_j}{\partial y}\frac{\partial w}{\partial y}\frac{\partial\varphi_j}{\partial y})-c_1E_{16}\frac{\partial^2\psi_j}{\partial x^2}\right.$$
$$\left.-c_1E_{26}\frac{\partial^2\varphi_j}{\partial y^2}-2c_1E_{66}\frac{\partial^2\varphi_j}{\partial x\partial y}\right)\Bigg]dxdy \tag{56}$$

$$K_{ij}^{24}=\int_{\Omega^e}\Bigg[\frac{\partial\psi_i^{(1)}}{\partial y}\left(B_{21}\frac{\partial\psi_j^{(2)}}{\partial x}+B_{26}\frac{\partial\psi_j^{(2)}}{\partial y}-c_1E_{12}\frac{\partial\psi_j^{(2)}}{\partial x}-c_1E_{26}\frac{\partial\psi_j^{(2)}}{\partial y}\right)$$
$$+\frac{\partial\psi_i^{(1)}}{\partial x}\left(B_{16}\frac{\partial\psi_j^{(2)}}{\partial x}+B_{66}\frac{\partial\psi_j^{(2)}}{\partial y}-c_1E_{16}\frac{\partial\psi_j^{(2)}}{\partial x}-c_1E_{66}\frac{\partial\psi_j^{(2)}}{\partial y}\right)\Bigg]dxdy \tag{57}$$

$$K_{ij}^{25}=\int_{\Omega^e}\Bigg[\frac{\partial\psi_i^{(1)}}{\partial y}\left(B_{22}\frac{\partial\psi_j^{(2)}}{\partial y}+B_{26}\frac{\partial\psi_j^{(2)}}{\partial x}-c_1E_{22}\frac{\partial\psi_j^{(2)}}{\partial y}-c_1E_{26}\frac{\partial\psi_j^{(2)}}{\partial x}\right)$$
$$+\frac{\partial\psi_i^{(1)}}{\partial x}\left(B_{26}\frac{\partial\psi_j^{(2)}}{\partial y}+B_{66}\frac{\partial\psi_j^{(2)}}{\partial x}-c_1E_{26}\frac{\partial\psi_j^{(2)}}{\partial y}-c_1E_{66}\frac{\partial\psi_j^{(2)}}{\partial x}\right)\Bigg]dxdy \tag{58}$$

$$K_{ij}^{31}=\int_{\Omega^e}\Bigg[\frac{\partial\varphi_i}{\partial x}\left(A_{11}\frac{\partial w}{\partial x}\frac{\partial\psi_j^{(1)}}{\partial x}+A_{16}\frac{\partial w}{\partial x}\frac{\partial\psi_j^{(1)}}{\partial y}+A_{16}\frac{\partial w}{\partial y}\frac{\partial\psi_j^{(1)}}{\partial x}+A_{66}\frac{\partial w}{\partial y}\frac{\partial\psi_j^{(1)}}{\partial y}\right)$$
$$+\frac{\partial\varphi_i}{\partial y}\left(A_{12}\frac{\partial w}{\partial y}\frac{\partial\psi_j^{(1)}}{\partial x}+A_{16}\frac{\partial w}{\partial x}\frac{\partial\psi_j^{(1)}}{\partial x}+A_{26}\frac{\partial w}{\partial y}\frac{\partial\psi_j^{(1)}}{\partial y}+A_{66}\frac{\partial w}{\partial x}\frac{\partial\psi_j^{(1)}}{\partial y}\right)$$
$$+\frac{\partial^2\varphi_i}{\partial x^2}\left(-c_1E_{11}\frac{\partial\psi_j^{(1)}}{\partial x}-c_1E_{16}\frac{\partial\psi_j^{(1)}}{\partial y}\right)+\frac{\partial^2\varphi_i}{\partial y^2}\left(-c_1E_{12}\frac{\partial\psi_j^{(1)}}{\partial x}-c_1E_{26}\frac{\partial\psi_j^{(1)}}{\partial y}\right)$$
$$+\frac{\partial^2\varphi_i}{\partial x\partial y}\left(-2c_1E_{16}\frac{\partial\psi_j^{(1)}}{\partial x}-2c_1E_{66}\frac{\partial\psi_j^{(1)}}{\partial y}\right)\Bigg]dxdy \tag{59}$$

$$K_{ij}^{32}=\int_{\Omega^e}\Bigg[\frac{\partial\varphi_i}{\partial x}\left(A_{12}\frac{\partial w}{\partial x}\frac{\partial\psi_j^{(1)}}{\partial y}+A_{16}\frac{\partial w}{\partial x}\frac{\partial\psi_j^{(1)}}{\partial x}+A_{26}\frac{\partial w}{\partial y}\frac{\partial\psi_j^{(1)}}{\partial y}+A_{66}\frac{\partial w}{\partial y}\frac{\partial\psi_j^{(1)}}{\partial x}\right)$$
$$+\frac{\partial\varphi_i}{\partial y}\left(A_{22}\frac{\partial w}{\partial y}\frac{\partial\psi_j^{(1)}}{\partial y}+A_{66}\frac{\partial w}{\partial x}\frac{\partial\psi_j^{(1)}}{\partial x}+A_{26}\frac{\partial w}{\partial x}\frac{\partial\psi_j^{(1)}}{\partial y}+A_{26}\frac{\partial w}{\partial x}\frac{\partial\psi_j^{(1)}}{\partial x}\right)$$
$$+\frac{\partial^2\varphi_i}{\partial x^2}\left(-c_1E_{12}\frac{\partial\psi_j^{(1)}}{\partial y}-c_1E_{16}\frac{\partial\psi_j^{(1)}}{\partial x}\right)+\frac{\partial^2\varphi_i}{\partial y^2}\left(-c_1E_{22}\frac{\partial\psi_j^{(1)}}{\partial y}-c_1E_{26}\frac{\partial\psi_j^{(1)}}{\partial x}\right)$$
$$+\frac{\partial^2\varphi_i}{\partial x\partial y}\left(-2c_1E_{26}\frac{\partial\psi_j^{(1)}}{\partial y}-2c_1E_{66}\frac{\partial\psi_j^{(1)}}{\partial x}\right)\Bigg]dxdy \tag{60}$$

$$K_{ij}^{33}=\int_{\Omega^e}\Bigg[\frac{\partial\varphi_i}{\partial x}\left(\frac{1}{2}A_{11}(\frac{\partial w}{\partial x})^2\frac{\partial\varphi_j}{\partial x}+\frac{1}{2}A_{12}(\frac{\partial w}{\partial y})^2\frac{\partial\varphi_j}{\partial y}+\frac{1}{2}A_{16}\frac{\partial w}{\partial x}(\frac{\partial w}{\partial x}\frac{\partial\varphi_j}{\partial y}+\frac{\partial w}{\partial x}\frac{\partial\varphi_j}{\partial y})\right.$$
$$+\frac{1}{2}A_{16}\frac{\partial w}{\partial x}\frac{\partial w}{\partial y}\frac{\partial\varphi_j}{\partial x}+\frac{1}{2}A_{26}(\frac{\partial w}{\partial y})^2\frac{\partial\varphi_j}{\partial y}+\frac{1}{2}A_{66}\frac{\partial w}{\partial y}(\frac{\partial w}{\partial x}\frac{\partial\varphi_j}{\partial y}+\frac{\partial w}{\partial y}\frac{\partial\varphi_j}{\partial x})+A_{45}\frac{\partial\varphi_j}{\partial y}$$
$$+A_{55}\frac{\partial\varphi_j}{\partial x}-2c_2D_{45}\frac{\partial\varphi_j}{\partial y}-2c_2D_{55}\frac{\partial\varphi_j}{\partial x}+c_2^2F_{45}\frac{\partial\varphi_j}{\partial y}+c_2^2F_{55}\frac{\partial\varphi_j}{\partial x}-c_1E_{11}\frac{\partial^2\varphi_j}{\partial x^2}\frac{\partial w}{\partial x}$$
$$-c_1E_{12}\frac{\partial^2\varphi_j}{\partial y^2}\frac{\partial w}{\partial x}-2c_1E_{16}\frac{\partial^2\varphi_j}{\partial x\partial y}\frac{\partial w}{\partial x}-c_1E_{16}\frac{\partial^2\varphi_j}{\partial x^2}\frac{\partial w}{\partial y}-c_1E_{26}\frac{\partial^2\varphi_j}{\partial y^2}\frac{\partial w}{\partial y}$$
$$\left.-2c_1E_{66}\frac{\partial^2\varphi_j}{\partial x\partial y}\frac{\partial w}{\partial y}\right)+\frac{\partial\varphi_i}{\partial y}\left(\frac{1}{2}A_{16}(\frac{\partial w}{\partial x})^2\frac{\partial\varphi_j}{\partial x}+\frac{1}{2}A_{26}\frac{\partial w}{\partial y}\frac{\partial w}{\partial x}\frac{\partial\varphi_j}{\partial y}\right.$$
$$+\frac{1}{2}A_{66}\frac{\partial w}{\partial x}(\frac{\partial w}{\partial y}\frac{\partial\varphi_j}{\partial x}+\frac{\partial w}{\partial y}\frac{\partial\varphi_j}{\partial x})+\frac{1}{2}A_{12}(\frac{\partial w}{\partial x})^2\frac{\partial\varphi_j}{\partial x}+\frac{1}{2}A_{22}(\frac{\partial w}{\partial y})^2\frac{\partial\varphi_j}{\partial y}$$
$$+\frac{1}{2}A_{26}\frac{\partial w}{\partial y}(\frac{\partial w}{\partial x}\frac{\partial\varphi_j}{\partial y}+\frac{\partial w}{\partial y}\frac{\partial\varphi_j}{\partial x})+A_{44}\frac{\partial\varphi_j}{\partial y}+A_{45}\frac{\partial\varphi_j}{\partial x}-2c_2D_{44}\frac{\partial\varphi_j}{\partial y}-2c_2D_{45}\frac{\partial\varphi_j}{\partial x}$$
$$+c_2^2F_{44}\frac{\partial\varphi_j}{\partial y}+c_2^2F_{45}\frac{\partial\varphi_j}{\partial x}-c_1E_{12}\frac{\partial^2\varphi_j}{\partial y^2}\frac{\partial w}{\partial x}-c_1E_{12}\frac{\partial^2\varphi_j}{\partial x^2}\frac{\partial w}{\partial y}-2c_1E_{26}\frac{\partial^2\varphi_j}{\partial x\partial y}\frac{\partial w}{\partial y}$$
$$\left.-c_1E_{16}\frac{\partial^2\varphi_j}{\partial x^2}\frac{\partial w}{\partial x}-c_1E_{26}\frac{\partial^2\varphi_j}{\partial y^2}\frac{\partial w}{\partial x}-2c_1E_{66}\frac{\partial^2\varphi_j}{\partial x\partial y}\frac{\partial w}{\partial x}\right)+\frac{\partial^2\varphi_i}{\partial x^2}\left(-\frac{1}{2}c_1E_{11}\frac{\partial w}{\partial x}\frac{\partial\varphi_j}{\partial x}\right.$$
$$-\frac{1}{2}c_1E_{12}\frac{\partial w}{\partial y}\frac{\partial\varphi_j}{\partial y}-\frac{1}{2}c_1E_{16}(\frac{\partial w}{\partial x}\frac{\partial\varphi_j}{\partial y}+\frac{\partial w}{\partial y}\frac{\partial\varphi_j}{\partial x})+c_1^2H_{11}\frac{\partial^2\varphi_j}{\partial x^2}+c_1^2H_{12}\frac{\partial^2\varphi_j}{\partial y^2}$$
$$\left.+2c_1^2H_{16}\frac{\partial^2\varphi_j}{\partial x\partial y}\right)+\frac{\partial^2\varphi_i}{\partial y^2}\left(-\frac{1}{2}c_1E_{12}\frac{\partial w}{\partial x}\frac{\partial\varphi_j}{\partial x}-\frac{1}{2}c_1E_{22}\frac{\partial w}{\partial y}\frac{\partial\varphi_j}{\partial y}\right.$$
$$\left.\left.-\frac{1}{2}c_1E_{26}(\frac{\partial w}{\partial x}\frac{\partial\varphi_j}{\partial y}+\frac{\partial w}{\partial y}\frac{\partial\varphi_j}{\partial x})+c_1^2H_{12}\frac{\partial^2\varphi_j}{\partial x^2}+c_1^2H_{22}\frac{\partial^2\varphi_j}{\partial y^2}+2c_1^2H_{26}\frac{\partial^2\varphi_j}{\partial x\partial y}\right)\right. \tag{61}$$

$$K_{ij}^{34}=\int_{\Omega^e}\Bigg[\frac{\partial\varphi_i}{\partial x}\left(A_{55}\psi_j^{(2)}-2c_2D_{55}\psi_j^{(2)}+c_2^2F_{55}\psi_j^{(2)}+(B_{11}-c_1E_{11})\frac{\partial w}{\partial x}\frac{\partial\psi_j^{(2)}}{\partial x}\right.$$
$$\left.+(B_{16}-c_1E_{16})\frac{\partial w}{\partial x}\frac{\partial\psi_j^{(2)}}{\partial y}+(B_{16}-c_1E_{16})\frac{\partial w}{\partial y}\frac{\partial\psi_j^{(2)}}{\partial x}+(B_{66}-c_1E_{66})\frac{\partial w}{\partial y}\frac{\partial\psi_j^{(2)}}{\partial y}\right)$$
$$+\frac{\partial\varphi_i}{\partial y}\left(A_{45}\psi_j^{(2)}-2c_2D_{45}\psi_j^{(2)}+c_2^2F_{45}\psi_j^{(2)}+(B_{12}-c_1E_{12})\frac{\partial w}{\partial y}\frac{\partial\psi_j^{(2)}}{\partial x}\right.$$

$$+(B_{26}-c_1E_{26})\frac{\partial w}{\partial y}\frac{\partial \psi_j^{(2)}}{\partial y}+(B_{16}-c_1E_{16})\frac{\partial w}{\partial x}\frac{\partial \psi_j^{(2)}}{\partial x}+(B_{66}-c_1E_{66})\frac{\partial w}{\partial x}\frac{\partial \psi_j^{(2)}}{\partial y}\Bigg)$$
$$+\frac{\partial^2\varphi_i}{\partial x^2}\Bigg(-c_1F_{11}\frac{\partial \psi_j^{(2)}}{\partial x}-c_1F_{16}\frac{\partial \psi_j^{(2)}}{\partial y}+c_1^2H_{11}\frac{\partial \psi_j^{(2)}}{\partial x}+c_1^2H_{16}\frac{\partial \psi_j^{(2)}}{\partial y}\Bigg)$$
$$+\frac{\partial^2\varphi_i}{\partial y^2}\Bigg(-c_1F_{12}\frac{\partial \psi_j^{(2)}}{\partial x}-c_1F_{26}\frac{\partial \psi_j^{(2)}}{\partial y}+c_1^2H_{12}\frac{\partial \psi_j^{(2)}}{\partial x}+c_1^2H_{26}\frac{\partial \psi_j^{(2)}}{\partial y}\Bigg)$$
$$+\frac{\partial^2\varphi_i}{\partial x\partial y}\Bigg(-2c_1F_{16}\frac{\partial \psi_j^{(2)}}{\partial x}-2c_1F_{66}\frac{\partial \psi_j^{(2)}}{\partial y}+2c_1^2H_{16}\frac{\partial \psi_j^{(2)}}{\partial x}+2c_1^2H_{66}\frac{\partial \psi_j^{(2)}}{\partial y}\Bigg)\Bigg]dxdy \tag{62}$$

$$K_{ij}^{35}=\int_{\Omega^e}\Bigg[\frac{\partial\varphi_i}{\partial x}\Bigg(A_{45}\psi_j^{(2)}-2c_2D_{45}\psi_j^{(2)}+c_2^2F_{45}\psi_j^{(2)}+(B_{12}-c_1E_{12})\frac{\partial w}{\partial x}\frac{\partial \psi_j^{(2)}}{\partial y}$$
$$+(B_{16}-c_1E_{16})\frac{\partial w}{\partial x}\frac{\partial \psi_j^{(2)}}{\partial x}+(B_{26}-c_1E_{26})\frac{\partial w}{\partial y}\frac{\partial \psi_j^{(2)}}{\partial y}+(B_{66}-c_1E_{66})\frac{\partial w}{\partial y}\frac{\partial \psi_j^{(2)}}{\partial x}\Bigg)$$
$$+\frac{\partial\varphi_i}{\partial y}\Bigg(A_{44}\psi_j^{(2)}-2c_2D_{44}\psi_j^{(2)}+c_2^2F_{44}\psi_j^{(2)}+(B_{22}-c_1E_{22})\frac{\partial w}{\partial y}\frac{\partial \psi_j^{(2)}}{\partial y}$$
$$+(B_{26}-c_1E_{26})\frac{\partial w}{\partial y}\frac{\partial \psi_j^{(2)}}{\partial x}+(B_{26}-c_1E_{26})\frac{\partial w}{\partial x}\frac{\partial \psi_j^{(2)}}{\partial y}+(B_{66}-c_1E_{66})\frac{\partial w}{\partial x}\frac{\partial \psi_j^{(2)}}{\partial x}\Bigg)$$
$$+\frac{\partial^2\varphi_i}{\partial x^2}\Bigg(-c_1F_{12}\frac{\partial \psi_j^{(2)}}{\partial y}-c_1F_{16}\frac{\partial \psi_j^{(2)}}{\partial x}+c_1^2H_{12}\frac{\partial \psi_j^{(2)}}{\partial y}+c_1^2H_{16}\frac{\partial \psi_j^{(2)}}{\partial x}\Bigg)$$
$$+\frac{\partial^2\varphi_i}{\partial y^2}\Bigg(-c_1F_{22}\frac{\partial \psi_j^{(2)}}{\partial y}-c_1F_{26}\frac{\partial \psi_j^{(2)}}{\partial x}+c_1^2H_{22}\frac{\partial \psi_j^{(2)}}{\partial y}+c_1^2H_{26}\frac{\partial \psi_j^{(2)}}{\partial x}\Bigg)$$
$$+\frac{\partial^2\varphi_i}{\partial x\partial y}\Bigg(-2c_1F_{26}\frac{\partial \psi_j^{(2)}}{\partial y}-2c_1F_{66}\frac{\partial \psi_j^{(2)}}{\partial x}+2c_1^2H_{26}\frac{\partial \psi_j^{(2)}}{\partial y}+2c_1^2H_{66}\frac{\partial \psi_j^{(2)}}{\partial x}\Bigg)\Bigg]dxdy \tag{63}$$

$$K_{ij}^{41}=\int_{\Omega^e}\Bigg[\frac{\partial\psi_i^{(2)}}{\partial x}\Bigg(B_{11}\frac{\partial \psi_j^{(1)}}{\partial x}+B_{16}\frac{\partial \psi_j^{(1)}}{\partial y}-c_1E_{11}\frac{\partial \psi_j^{(1)}}{\partial x}-c_1E_{16}\frac{\partial \psi_j^{(1)}}{\partial y}\Bigg)$$
$$+\frac{\partial\psi_i^{(2)}}{\partial y}\Bigg(B_{16}\frac{\partial \psi_j^{(1)}}{\partial x}+B_{66}\frac{\partial \psi_j^{(1)}}{\partial y}-c_1E_{16}\frac{\partial \psi_j^{(1)}}{\partial x}-c_1E_{66}\frac{\partial \psi_j^{(1)}}{\partial y}\Bigg)\Bigg]dxdy \tag{64}$$

$$K_{ij}^{42}=\int_{\Omega^e}\Bigg[\frac{\partial\psi_i^{(2)}}{\partial x}\Bigg(B_{12}\frac{\partial \psi_j^{(1)}}{\partial y}+B_{16}\frac{\partial \psi_j^{(1)}}{\partial x}-c_1E_{12}\frac{\partial \psi_j^{(1)}}{\partial y}-c_1E_{16}\frac{\partial \psi_j^{(1)}}{\partial x}\Bigg)$$
$$+\frac{\partial\psi_i^{(2)}}{\partial y}\Bigg(B_{26}\frac{\partial \psi_j^{(1)}}{\partial y}+B_{66}\frac{\partial \psi_j^{(1)}}{\partial x}-c_1E_{26}\frac{\partial \psi_j^{(1)}}{\partial y}-c_1E_{66}\frac{\partial \psi_j^{(1)}}{\partial x}\Bigg)\Bigg]dxdy \tag{65}$$

$$K_{ij}^{43}=\int_{\Omega^e}\Bigg[\frac{\partial\psi_i^{(2)}}{\partial x}\Bigg(\frac{1}{2}B_{11}\frac{\partial w}{\partial x}\frac{\partial\varphi_j}{\partial x}+\frac{1}{2}B_{12}\frac{\partial w}{\partial y}\frac{\partial\varphi_j}{\partial y}+\frac{1}{2}B_{16}(\frac{\partial w}{\partial x}\frac{\partial\varphi_j}{\partial y}+\frac{\partial w}{\partial y}\frac{\partial\varphi_j}{\partial x})-c_1\frac{1}{2}E_{11}\frac{\partial w}{\partial x}\frac{\partial\varphi_j}{\partial x}$$
$$-c_1\frac{1}{2}E_{12}\frac{\partial w}{\partial y}\frac{\partial\varphi_j}{\partial y}-\frac{1}{2}c_1E_{16}(\frac{\partial w}{\partial x}\frac{\partial\varphi_j}{\partial y}+\frac{\partial w}{\partial y}\frac{\partial\varphi_j}{\partial x})-c_1F_{11}\frac{\partial^2\varphi_j}{\partial x^2}-c_1F_{12}\frac{\partial^2\varphi_j}{\partial y^2}$$
$$-2c_1F_{16}\frac{\partial^2\varphi_j}{\partial x\partial y}+c_1^2H_{11}\frac{\partial^2\varphi_j}{\partial x^2}+c_1^2H_{12}\frac{\partial^2\varphi_j}{\partial y^2}+2c_1^2H_{16}\frac{\partial^2\varphi_j}{\partial x\partial y}\Bigg)+\frac{\partial\psi_i^{(2)}}{\partial y}\Bigg(\frac{1}{2}B_{16}\frac{\partial w}{\partial x}\frac{\partial\varphi_j}{\partial x}$$
$$+\frac{1}{2}B_{26}\frac{\partial w}{\partial y}\frac{\partial\varphi_j}{\partial y}+\frac{1}{2}B_{66}(\frac{\partial w}{\partial x}\frac{\partial\varphi_j}{\partial y}+\frac{\partial w}{\partial y}\frac{\partial\varphi_j}{\partial x})-c_1\frac{1}{2}E_{16}\frac{\partial w}{\partial x}\frac{\partial\varphi_j}{\partial x}-c_1\frac{1}{2}E_{26}\frac{\partial w}{\partial y}\frac{\partial\varphi_j}{\partial y}$$
$$-\frac{1}{2}c_1E_{66}(\frac{\partial w}{\partial x}\frac{\partial\varphi_j}{\partial y}+\frac{\partial w}{\partial y}\frac{\partial\varphi_j}{\partial x})-c_1F_{16}\frac{\partial^2\varphi_j}{\partial x^2}-c_1F_{26}\frac{\partial^2\varphi_j}{\partial y^2}-2c_1F_{66}\frac{\partial^2\varphi_j}{\partial x\partial y}+c_1^2H_{16}\frac{\partial^2\varphi_j}{\partial x^2}$$
$$+c_1^2H_{26}\frac{\partial^2\varphi_j}{\partial y^2}+2c_1^2H_{66}\frac{\partial^2\varphi_j}{\partial x\partial y}\Bigg)+\psi_i^{(2)}\Bigg(A_{45}\frac{\partial\varphi_j}{\partial y}+A_{55}\frac{\partial\varphi_j}{\partial x}-2c_2D_{45}\frac{\partial\varphi_j}{\partial y}-2c_2D_{55}\frac{\partial\varphi_j}{\partial x}$$
$$+c_2^2F_{45}\frac{\partial\varphi_j}{\partial y}+c_2^2F_{55}\frac{\partial\varphi_j}{\partial x}\Bigg)\Bigg]dxdy \tag{66}$$

$$K_{ij}^{44}=\int_{\Omega^e}\Bigg[\frac{\partial\psi_i^{(2)}}{\partial x}\Bigg(D_{11}\frac{\partial\psi_j^{(2)}}{\partial x}+D_{16}\frac{\partial\psi_j^{(2)}}{\partial y}-2c_1F_{11}\frac{\partial\psi_j^{(2)}}{\partial x}-2c_1F_{16}\frac{\partial\psi_j^{(2)}}{\partial y}+c_1^2H_{11}\frac{\partial\psi_j^{(2)}}{\partial x}$$
$$+c_1^2H_{16}\frac{\partial\psi_j^{(2)}}{\partial y}\Bigg)+\frac{\partial\psi_i^{(2)}}{\partial y}\Bigg(D_{16}\frac{\partial\psi_j^{(2)}}{\partial x}+D_{66}\frac{\partial\psi_j^{(2)}}{\partial y}-2c_1F_{16}\frac{\partial\psi_j^{(2)}}{\partial x}-2c_1F_{66}\frac{\partial\psi_j^{(2)}}{\partial y}$$
$$+c_1^2H_{16}\frac{\partial\psi_j^{(2)}}{\partial x}+c_1^2H_{66}\frac{\partial\psi_j^{(2)}}{\partial y}\Bigg)+\psi_i^{(2)}\Bigg(A_{55}\psi_j^{(2)}-2c_2D_{55}\psi_j^{(2)}+c_2^2F_{55}\psi_j^{(2)}\Bigg)\Bigg]dxdy \tag{67}$$

$$K_{ij}^{45}=\int_{\Omega^e}\Bigg[\frac{\partial\psi_i^{(2)}}{\partial x}\Bigg(D_{12}\frac{\partial\psi_j^{(2)}}{\partial y}+D_{16}\frac{\partial\psi_j^{(2)}}{\partial x}-2c_1F_{12}\frac{\partial\psi_j^{(2)}}{\partial y}-2c_1F_{16}\frac{\partial\psi_j^{(2)}}{\partial x}+c_1^2H_{12}\frac{\partial\psi_j^{(2)}}{\partial y}$$
$$+c_1^2H_{16}\frac{\partial\psi_j^{(2)}}{\partial x}\Bigg)+\frac{\partial\psi_i^{(2)}}{\partial y}\Bigg(D_{26}\frac{\partial\psi_j^{(2)}}{\partial y}+D_{66}\frac{\partial\psi_j^{(2)}}{\partial x}-2c_1F_{26}\frac{\partial\psi_j^{(2)}}{\partial y}-2c_1F_{66}\frac{\partial\psi_j^{(2)}}{\partial x}$$
$$+c_1^2H_{26}\frac{\partial\psi_j^{(2)}}{\partial y}+c_1^2H_{66}\frac{\partial\psi_j^{(2)}}{\partial x}\Bigg)+\psi_i^{(2)}(A_{45}\psi_j^{(2)}-2c_2D_{45}\psi_j^{(2)}+c_2^2F_{45}\psi_j^{(2)})\Bigg]dxdy \tag{68}$$

$$K_{ij}^{51}=\int_{\Omega^e}\Bigg[\frac{\partial\psi_i^{(2)}}{\partial y}\Bigg(B_{12}\frac{\partial\psi_j^{(1)}}{\partial x}+B_{26}\frac{\partial\psi_j^{(1)}}{\partial y}-c_1E_{12}\frac{\partial\psi_j^{(1)}}{\partial x}-c_1E_{26}\frac{\partial\psi_j^{(1)}}{\partial y}\Bigg)$$
$$+\frac{\partial\psi_i^{(2)}}{\partial x}\Bigg(B_{16}\frac{\partial\psi_j^{(1)}}{\partial x}+B_{66}\frac{\partial\psi_j^{(1)}}{\partial y}-c_1E_{16}\frac{\partial\psi_j^{(1)}}{\partial x}-c_1E_{66}\frac{\partial\psi_j^{(1)}}{\partial y}\Bigg)\Bigg]dxdy \tag{69}$$

$$K_{ij}^{52}=\int_{\Omega^e}\Bigg[\frac{\partial\psi_i^{(2)}}{\partial y}\Bigg(B_{22}\frac{\partial\psi_j^{(1)}}{\partial y}+B_{26}\frac{\partial\psi_j^{(1)}}{\partial x}-c_1E_{22}\frac{\partial\psi_j^{(1)}}{\partial y}-c_1E_{26}\frac{\partial\psi_j^{(1)}}{\partial x}\Bigg)$$
$$+\frac{\partial\psi_i^{(2)}}{\partial x}\Bigg(B_{26}\frac{\partial\psi_j^{(1)}}{\partial y}+B_{66}\frac{\partial\psi_j^{(1)}}{\partial x}-c_1E_{26}\frac{\partial\psi_j^{(1)}}{\partial y}-c_1E_{66}\frac{\partial\psi_j^{(1)}}{\partial x}\Bigg)\Bigg]dxdy \tag{70}$$

$$K_{ij}^{53} = \int_{\Omega^e} \Bigg[\frac{\partial \psi_i^{(2)}}{\partial x} \Bigg(\frac{1}{2} B_{16} \frac{\partial w}{\partial x} \frac{\partial \varphi_j}{\partial x} + \frac{1}{2} B_{26} \frac{\partial w}{\partial y} \frac{\partial \varphi_j}{\partial y} + B_{66} \Big(\frac{\partial w}{\partial x} \frac{\partial \varphi_j}{\partial y} + \frac{\partial w}{\partial y} \frac{\partial \varphi_j}{\partial x} \Big) - c_1 \frac{1}{2} E_{16} \frac{\partial w}{\partial x} \frac{\partial \varphi_j}{\partial x} - c_1 \frac{1}{2} E_{26} \frac{\partial w}{\partial y} \frac{\partial \varphi_j}{\partial y} - c_1 E_{66} \Big(\frac{\partial w}{\partial x} \frac{\partial \varphi_j}{\partial y} + \frac{\partial w}{\partial y} \frac{\partial \varphi_j}{\partial x} \Big) - c_1 F_{16} \frac{\partial^2 \varphi_j}{\partial x^2} - c_1 F_{26} \frac{\partial^2 \varphi_j}{\partial y^2} - 2 c_1 F_{66} \frac{\partial^2 \varphi_j}{\partial x \partial y} + c_1^2 H_{16} \frac{\partial^2 \varphi_j}{\partial x^2} + c_1^2 H_{26} \frac{\partial^2 \varphi_j}{\partial y^2} + 2 c_1^2 H_{66} \frac{\partial^2 \varphi_j}{\partial x \partial y} \Bigg) + \frac{\partial \psi_i^{(2)}}{\partial y} \Bigg(\frac{1}{2} B_{12} \frac{\partial w}{\partial x} \frac{\partial \varphi_j}{\partial x} + \frac{1}{2} B_{22} \frac{\partial w}{\partial y} \frac{\partial \varphi_j}{\partial y} + B_{26} \Big(\frac{\partial w}{\partial x} \frac{\partial \varphi_j}{\partial y} + \frac{\partial w}{\partial y} \frac{\partial \varphi_j}{\partial x} \Big) - c_1 \frac{1}{2} E_{12} \frac{\partial w}{\partial x} \frac{\partial \varphi_j}{\partial x} - c_1 \frac{1}{2} E_{22} \frac{\partial w}{\partial y} \frac{\partial \varphi_j}{\partial y} - c_1 E_{26} \Big(\frac{\partial w}{\partial x} \frac{\partial \varphi_j}{\partial y} + \frac{\partial w}{\partial y} \frac{\partial \varphi_j}{\partial x} \Big) - c_1 F_{12} \frac{\partial^2 \varphi_j}{\partial x^2} - c_1 F_{22} \frac{\partial^2 \varphi_j}{\partial y^2} - 2 c_1 F_{26} \frac{\partial^2 \varphi_j}{\partial x \partial y} + c_1^2 H_{12} \frac{\partial^2 \varphi_j}{\partial x^2} + c_1^2 H_{22} \frac{\partial^2 \varphi_j}{\partial y^2} + 2 c_1^2 H_{26} \frac{\partial^2 \varphi_j}{\partial x \partial y} \Bigg) + \psi_i^{(2)} \Big(A_{44} \frac{\partial \varphi_j}{\partial y} + A_{45} \frac{\partial \varphi_j}{\partial x} - 2 c_2 D_{44} \frac{\partial \varphi_j}{\partial y} - 2 c_2 D_{45} \frac{\partial \varphi_j}{\partial x} + c_2^2 F_{44} \frac{\partial \varphi_j}{\partial y} + c_2^2 F_{45} \frac{\partial \varphi_j}{\partial x} \Big) \Bigg] dx dy \tag{71}$$

$$K_{ij}^{54} = \int_{\Omega^e} \Bigg[\frac{\partial \psi_i^{(2)}}{\partial y} \Bigg(D_{12} \frac{\partial \psi_j^{(2)}}{\partial x} + D_{26} \frac{\partial \psi_j^{(2)}}{\partial y} - 2 c_1 F_{12} \frac{\partial \psi_j^{(2)}}{\partial x} - 2 c_1 F_{26} \frac{\partial \psi_j^{(2)}}{\partial y} + c_1^2 H_{12} \frac{\partial \psi_j^{(2)}}{\partial x} + c_1^2 H_{26} \frac{\partial \psi_j^{(2)}}{\partial y} \Bigg) + \frac{\partial \psi_i^{(2)}}{\partial x} \Bigg(D_{16} \frac{\partial \psi_j^{(2)}}{\partial x} + D_{66} \frac{\partial \psi_j^{(2)}}{\partial y} - 2 c_1 F_{16} \frac{\partial \psi_j^{(2)}}{\partial x} - 2 c_1 F_{66} \frac{\partial \psi_j^{(2)}}{\partial y} + c_1^2 H_{16} \frac{\partial \psi_j^{(2)}}{\partial x} + c_1^2 H_{66} \frac{\partial \psi_j^{(2)}}{\partial y} \Bigg) + \psi_i^{(2)} \Bigg(A_{45} \psi_j^{(2)} - 2 c_2 D_{45} \psi_j^{(2)} + c_2^2 F_{45} \psi_j^{(2)} \Bigg) \Bigg] dx dy \tag{72}$$

$$K_{ij}^{55} = \int_{\Omega^e} \Bigg[\frac{\partial \psi_i^{(2)}}{\partial y} \Bigg(D_{22} \frac{\partial \psi_j^{(2)}}{\partial y} + D_{26} \frac{\partial \psi_j^{(2)}}{\partial x} - 2 c_1 F_{22} \frac{\partial \psi_j^{(2)}}{\partial y} - 2 c_1 F_{26} \frac{\partial \psi_j^{(2)}}{\partial x} + c_1^2 H_{22} \frac{\partial \psi_j^{(2)}}{\partial y} + c_1^2 H_{26} \frac{\partial \psi_j^{(2)}}{\partial x} \Bigg) + \frac{\partial \psi_i^{(2)}}{\partial x} \Bigg(D_{26} \frac{\partial \psi_j^{(2)}}{\partial y} + D_{66} \frac{\partial \psi_j^{(2)}}{\partial x} - 2 c_1 F_{26} \frac{\partial \psi_j^{(2)}}{\partial y} - 2 c_1 F_{66} \frac{\partial \psi_j^{(2)}}{\partial x} + c_1^2 H_{26} \frac{\partial \psi_j^{(2)}}{\partial y} + c_1^2 H_{66} \frac{\partial \psi_j^{(2)}}{\partial x} \Bigg) + \psi_i^{(2)} \Big(A_{44} \psi_j^{(2)} - 2 c_2 D_{44} \psi_j^{(2)} + c_2^2 F_{44} \psi_j^{(2)} \Big) \Bigg] dx dy \tag{73}$$

The elements of the force vector are given by

$$F_i^1 = \oint_{\Gamma^e} (N_{xx} \hat{n}_x + N_{xy} \hat{n}_y) ds \tag{74}$$

$$F_i^2 = \oint_{\Gamma^e} (N_{xy} \hat{n}_x + N_{yy} \hat{n}_y) ds \tag{75}$$

$$F_i^3 = \int_{\Omega^e} (1 - \mu \nabla^2) q \varphi_i dx dy + \oint_{\Gamma^e} \Bigg\{ (\bar{Q}_x \hat{n}_x + \bar{Q}_y \hat{n}_y) + (N_{xx} \frac{\partial w_0}{\partial x} + N_{xy} \frac{\partial w_0}{\partial y}) \hat{n}_x + (N_{xy} \frac{\partial w_0}{\partial x} + N_{yy} \frac{\partial w_0}{\partial y}) \hat{n}_y + c_1 \Bigg[(\frac{\partial P_{xx}}{\partial x} + \frac{\partial P_{xy}}{\partial y}) \hat{n}_x + (\frac{\partial P_{yy}}{\partial y} + \frac{\partial P_{xy}}{\partial x}) \hat{n}_y \Bigg] - c_1 \Bigg[(P_{xx} + P_{xy}) \hat{n}_x + (P_{yy} + P_{xy}) \hat{n}_y \Bigg] \Bigg\} ds \tag{76}$$

$$F_i^4 = \oint_{\Gamma^e} (M_{xx}\hat{n}_x + M_{xy}\hat{n}_y)\psi^{(2)} ds \tag{77}$$

$$F_i^5 = \oint_{\Gamma^e} (M_{xy}\hat{n}_x + M_{yy}\hat{n}_y)\psi^{(2)} ds \tag{78}$$

Solution of nonlinear equations

Newton-Raphson method is employed for solving the nonlinear finite element equations. The linearized equations for the incremental solution at the $(r+1)$st iteration are written as:

$$\delta\boldsymbol{\Delta} = -(\hat{\mathbf{T}}(\boldsymbol{\Delta}_{s+1}^r))^{-1}\mathbf{R}_{s+1}^r \tag{79}$$

$$\hat{\mathbf{T}}(\boldsymbol{\Delta}_{s+1}^r)\left[\frac{\partial \mathbf{R}}{\partial \boldsymbol{\Delta}}\right]_{s+1}^r, \quad \mathbf{R}_{s+1}^r = \hat{\mathbf{K}}(\boldsymbol{\Delta}_{s+1}^r)\boldsymbol{\Delta}_{s+1}^r - \hat{\mathbf{F}} \tag{80}$$

The total solution is obtained from

$$\boldsymbol{\Delta}_{s+1}^{r+1} = \boldsymbol{\Delta}_{s+1}^r + \delta\boldsymbol{\Delta}$$

The tangent stiffness coefficients can be computed as (see [96])

$$T_{ij}^{\alpha\beta} \equiv \frac{\partial R_i^\alpha}{\partial \Delta_j^\beta} = K_{ij}^{\alpha\beta} + \sum_{k=1}^{n_\gamma} \frac{\partial K_{ik}^{\alpha\gamma}}{\partial \Delta_j^\beta}\Delta_k^\gamma - \frac{\partial F_i^\alpha}{\partial \Delta_j^\beta} \tag{81}$$

Using the above equation the tangent stiffness coeffcients are derived as follows,

$$T_{ij}^{11} = K_{ij}^{11}, \quad T_{ij}^{12} = K_{ij}^{12} \tag{82}$$

$$\begin{aligned} T_{ij}^{13} = K_{ij}^{13} + \int_{\Omega^e} \Bigg[& \frac{\partial \psi_i^{(1)}}{\partial x}\left(\frac{1}{2}A_{11}\frac{\partial w}{\partial x}\frac{\partial \varphi_j}{\partial x} + \frac{1}{2}A_{12}\frac{\partial w}{\partial y}\frac{\partial \varphi_j}{\partial y} + \frac{1}{2}A_{16}\left(\frac{\partial w}{\partial x}\frac{\partial \varphi_j}{\partial y} + \frac{\partial w}{\partial y}\frac{\partial \varphi_j}{\partial x}\right)\right) \\ & + \frac{\partial \psi_i^{(1)}}{\partial y}\left(\frac{1}{2}A_{16}\frac{\partial w}{\partial x}\frac{\partial \varphi_j}{\partial x} + \frac{1}{2}A_{26}\frac{\partial w}{\partial y}\frac{\partial \psi_j}{\partial y} + \frac{1}{2}A_{66}\left(\frac{\partial w}{\partial x}\frac{\partial \varphi_j}{\partial y} + \frac{\partial w}{\partial y}\frac{\partial \varphi_j}{\partial x}\right)\right)\Bigg] dxdy \end{aligned} \tag{83}$$

$$T_{ij}^{14} = K_{ij}^{14}, \quad T_{ij}^{15} = K_{ij}^{15} \tag{84}$$

$$T_{ij}^{21} = K_{ij}^{21}, \quad T_{ij}^{22} = K_{ij}^{22} \tag{85}$$

$$\begin{aligned} T_{ij}^{23} = K_{ij}^{23} + \int_{\Omega^e} \Bigg[& \frac{\partial \psi_i^{(1)}}{\partial y}\left(\frac{1}{2}A_{12}\frac{\partial w}{\partial x}\frac{\partial \varphi_j}{\partial x} + \frac{1}{2}A_{22}\frac{\partial w}{\partial y}\frac{\partial \varphi_j}{\partial y} + \frac{1}{2}A_{26}\left(\frac{\partial w}{\partial x}\frac{\partial \varphi_j}{\partial y} + \frac{\partial w}{\partial y}\frac{\partial \varphi_j}{\partial y}\right)\right) \\ & + \frac{\partial \psi_i^{(1)}}{\partial x}\left(\frac{1}{2}A_{16}\frac{\partial w}{\partial x}\frac{\partial \varphi_j}{\partial x} + \frac{1}{2}A_{26}\frac{\partial w}{\partial y}\frac{\partial \varphi_j}{\partial y} + \frac{1}{2}A_{66}\left(\frac{\partial w}{\partial x}\frac{\partial \varphi_j}{\partial y}\frac{\partial w}{\partial y}\frac{\partial \varphi_j}{\partial y}\right)\right)\Bigg] dxdy \end{aligned} \tag{86}$$

$$T_{ij}^{24} = K_{ij}^{24}, \quad T_{ij}^{25} = K_{ij}^{25} \tag{87}$$

$$T_{ij}^{31} = K_{ij}^{31}, T_{ij}^{32} = K_{ij}^{32} \tag{88}$$

$$\begin{aligned} T_{ij}^{33} = K_{ij}^{33} + \int_{\Omega^e} \Bigg\{ & \frac{\partial \varphi_i}{\partial x}\frac{\partial \varphi_j}{\partial y}(A_{11}\frac{\partial u}{\partial x} + A_{16}\frac{\partial u}{\partial y}) + \frac{\partial \varphi_i}{\partial y}\frac{\partial \varphi_j}{\partial y}(A_{12}\frac{\partial u}{\partial x} + A_{26}\frac{\partial u}{\partial y}) + \Bigg(\frac{\partial \varphi_i}{\partial x}\frac{\partial \varphi_j}{\partial y} + \\ & \frac{\partial \varphi_i}{\partial y}\frac{\partial \varphi_j}{\partial x}\Bigg)\Bigg(A_{11}\frac{\partial u}{\partial x} + A_{16}\frac{\partial u}{\partial y}\Bigg) + \frac{\partial \varphi_i}{\partial x}\frac{\partial \varphi_j}{\partial x}(A_{16}\frac{\partial v}{\partial x} + A_{12}\frac{\partial v}{\partial y}) + \frac{\partial \varphi_i}{\partial y}\frac{\partial \varphi_j}{\partial y}(A_{26}\frac{\partial v}{\partial x} \\ & + A_{22}\frac{\partial v}{\partial y}) + \Bigg(\frac{\partial \varphi_i}{\partial x}\frac{\partial \varphi_j}{\partial y} + \frac{\partial \varphi_i}{\partial y}\frac{\partial \varphi_j}{\partial x}\Bigg)\Bigg(A_{66}\frac{\partial v}{\partial x} + A_{26}\frac{\partial v}{\partial y}\Bigg) + \frac{\partial \varphi_i}{\partial x}\frac{\partial \varphi_j}{\partial x}\Bigg(A_{11}(\frac{\partial w}{\partial x})^2 \\ & + A_{66}(\frac{\partial w}{\partial y})^2 + 2A_{16}\frac{\partial w}{\partial x}\frac{\partial w}{\partial y}\Bigg) + \frac{\partial \varphi_i}{\partial y}\frac{\partial \varphi_j}{\partial y}\Bigg(A_{66}(\frac{\partial w}{\partial x})^2 + A_{22}(\frac{\partial w}{\partial y})^2 + 2A_{26}\frac{\partial w}{\partial x}\frac{\partial w}{\partial y}\Bigg) \\ & + \Bigg(\frac{\partial \varphi_i}{\partial x}\frac{\partial \varphi_j}{\partial y} + \frac{\partial \varphi_i}{\partial y}\frac{\partial \varphi_j}{\partial x}\Bigg)\Bigg(A_{16}(\frac{\partial w}{\partial x})^2 + A_{26}(\frac{\partial w}{\partial y})^2 + (A_{16} + A_{66})\frac{\partial w}{\partial x}\frac{\partial w}{\partial y}\Bigg) \\ & - c_1\Bigg[\frac{\partial \varphi_i}{\partial x}\frac{\partial \varphi_j}{\partial y}\Bigg(E_{11}\frac{\partial^2 w}{\partial x^2} + E_{12}\frac{\partial^2 w}{\partial y^2} + 2E_{16}\frac{\partial^2 w}{\partial x \partial y}\Bigg) + \frac{\partial \varphi_i}{\partial y}\frac{\partial \varphi_j}{\partial y}\Bigg(E_{12}\frac{\partial^2 w}{\partial x^2} + E_{22}\frac{\partial^2 w}{\partial y^2} \\ & + 2E_{23}\frac{\partial^2 w}{\partial x \partial y}\Bigg) + \Bigg(\frac{\partial \varphi_i}{\partial x}\frac{\partial \varphi_j}{\partial y} + \frac{\partial \varphi_i}{\partial y}\frac{\partial \varphi_j}{\partial x}\Bigg)\Bigg(E_{16}\frac{\partial^2 w}{\partial x^2} + E_{26}\frac{\partial^2 w}{\partial y^2} + 2E_{66}\frac{\partial^2 w}{\partial x \partial y}\Bigg)\Bigg] \\ & - \frac{c_1}{2}\Bigg[\frac{\partial w}{\partial x}\Bigg(E_{11}\frac{\partial^2 \varphi_i}{\partial x^2}\frac{\partial \varphi_j}{\partial x} + E_{16}\frac{\partial^2 \varphi_i}{\partial x^2}\frac{\partial \varphi_j}{\partial y} + E_{12}\frac{\partial^2 \varphi_i}{\partial y^2}\frac{\partial \varphi_j}{\partial x} + E_{26}\frac{\partial^2 \varphi_i}{\partial y^2}\frac{\partial \varphi_j}{\partial y} + 2E_{16}\frac{\partial^2 \varphi_i}{\partial x \partial y}\frac{\partial \varphi_j}{\partial x} \\ & + 2E_{66}\frac{\partial^2 \varphi_j}{\partial x \partial y}\frac{\partial \varphi_j}{\partial y}\Bigg) + \frac{\partial w}{\partial y}\Bigg(E_{12}\frac{\partial^2 \varphi_i}{\partial x^2}\frac{\partial \varphi_j}{\partial y} + E_{16}\frac{\partial^2 \varphi_i}{\partial x^2}\frac{\partial \varphi_j}{\partial x} + E_{22}\frac{\partial^2 \varphi_i}{\partial y^2}\frac{\partial \varphi_j}{\partial y} + E_{26}\frac{\partial^2 \varphi_i}{\partial y^2}\frac{\partial \varphi_j}{\partial x} \\ & + 2E_{26}\frac{\partial^2 \varphi_i}{\partial x \partial y}\frac{\partial \varphi_j}{\partial y} + 2E_{66}\frac{\partial^2 \varphi_i}{\partial x \partial y}\frac{\partial \varphi_j}{\partial x}\Bigg)\Bigg]\Bigg\} dxdy \end{aligned} \tag{89}$$

$$T_{ij}^{34} = K_{ij}^{34}, \quad T_{ij}^{35} = K_{ij}^{35} \tag{90}$$

$$T_{ij}^{41} = K_{ij}^{41}, \quad T_{ij}^{42} = K_{ij}^{42} \tag{91}$$

$$\begin{aligned} T_{ij}^{43} = K_{ij}^{43} + \int_{\Omega^e} \Bigg[& \frac{\partial \psi_i^{(2)}}{\partial x}\Bigg(\frac{1}{2}B_{11}\frac{\partial w}{\partial x}\frac{\partial \varphi_j}{\partial x} + \frac{1}{2}B_{12}\frac{\partial w}{\partial y}\frac{\partial \varphi_j}{\partial y} + B_{16}(\frac{\partial w}{\partial x}\frac{\partial \varphi_j}{\partial y} + \frac{\partial w}{\partial y}\frac{\partial \varphi_j}{\partial x}) \\ & - c_1\frac{1}{2}E_{11}\frac{\partial w}{\partial x}\frac{\partial \varphi_j}{\partial x} - c_1\frac{1}{2}E_{12}\frac{\partial w}{\partial y}\frac{\partial \varphi_j}{\partial y} - c_1E_{16}(\frac{\partial w}{\partial x}\frac{\partial \varphi_j}{\partial y} + \frac{\partial w}{\partial y}\frac{\partial \varphi_j}{\partial x})\Bigg) \\ & + \frac{\partial \psi_i^{(2)}}{\partial y}\Bigg(\frac{1}{2}B_{16}\frac{\partial w}{\partial x}\frac{\partial \varphi_j}{\partial x} + \frac{1}{2}B_{26}\frac{\partial w}{\partial y}\frac{\partial \varphi_j}{\partial y} + B_{66}(\frac{\partial w}{\partial x}\frac{\partial \varphi_j}{\partial y} + \frac{\partial w}{\partial y}\frac{\partial \varphi_j}{\partial x}) - c_1\frac{1}{2}E_{16}\frac{\partial w}{\partial x}\frac{\partial \varphi_j}{\partial x} \\ & - c_1\frac{1}{2}E_{26}\frac{\partial w}{\partial y}\frac{\partial \varphi_j}{\partial y} - c_1E_{66}(\frac{\partial w}{\partial x}\frac{\partial \varphi_j}{\partial y} + \frac{\partial w}{\partial y}\frac{\partial \varphi_j}{\partial x})\Bigg)\Bigg] dxdy \end{aligned} \tag{92}$$

$$T_{ij}^{44} = K_{ij}^{44}, \quad T_{ij}^{45} = K_{ij}^{45} \tag{93}$$

$$T_{ij}^{51} = K_{ij}^{51}, \quad T_{ij}^{52} = K_{ij}^{52} \tag{94}$$

$$T_{ij}^{53} = K_{ij}^{53} + \int_{\Omega^e} \Bigg[\frac{\partial \psi_i^{(2)}}{\partial x} \Bigg(\frac{1}{2} B_{16} \frac{\partial w}{\partial x} \frac{\partial \varphi_j}{\partial x} + \frac{1}{2} B_{26} \frac{\partial w}{\partial y} \frac{\partial \varphi_j}{\partial y} + B_{66} \Big(\frac{\partial w}{\partial x} \frac{\partial \varphi_j}{\partial y} + \frac{\partial w}{\partial y} \frac{\partial \varphi_j}{\partial x} \Big) - c_1 \frac{1}{2} E_{16} \frac{\partial w}{\partial x} \frac{\partial \varphi_j}{\partial x} - c_1 \frac{1}{2} E_{26} \frac{\partial w}{\partial y} \frac{\partial \varphi_j}{\partial y} - c_1 E_{66} \Big(\frac{\partial w}{\partial x} \frac{\partial \varphi_j}{\partial y} + \frac{\partial w}{\partial y} \frac{\partial \varphi_j}{\partial x} \Big) \Bigg) + \frac{\partial \psi_i^{(2)}}{\partial y} \Bigg(\frac{1}{2} B_{12} \frac{\partial w}{\partial x} \frac{\partial \varphi_j}{\partial x} + \frac{1}{2} B_{22} \frac{\partial w}{\partial y} \frac{\partial \varphi_j}{\partial y} + B_{26} \Big(\frac{\partial w}{\partial x} \frac{\partial \varphi_j}{\partial y} + \frac{\partial w}{\partial y} \frac{\partial \varphi_j}{\partial x} \Big) - c_1 \frac{1}{2} E_{12} \frac{\partial w}{\partial x} \frac{\partial \varphi_j}{\partial x} - c_1 \frac{1}{2} E_{22} \frac{\partial w}{\partial y} \frac{\partial \varphi_j}{\partial y} - c_1 E_{26} \Big(\frac{\partial w}{\partial x} \frac{\partial \varphi_j}{\partial y} + \frac{\partial w}{\partial y} \frac{\partial \varphi_j}{\partial x} \Big) \Bigg) \Bigg] dxdy \tag{95}$$

$$T_{ij}^{54} = K_{ij}^{54}, \quad T_{ij}^{55} = K_{ij}^{55} \tag{96}$$

D. APPENDIX-4

The stress resultants in (20) are given as follows where x and y values are replaced with α and β respectively.

$$\begin{Bmatrix} N_{xx} \\ N_{yy} \\ N_{xy} \end{Bmatrix} = \begin{bmatrix} A_{11} & A_{12} & A_{16} \\ A_{12} & A_{22} & A_{26} \\ A_{16} & A_{26} & A_{66} \end{bmatrix} \begin{Bmatrix} \varepsilon_{xx}^{(0)} \\ \varepsilon_{yy}^{(0)} \\ \gamma_{xy}^{(0)} \end{Bmatrix} + \begin{bmatrix} B_{11} & B_{12} & B_{16} \\ B_{12} & B_{22} & B_{26} \\ B_{16} & B_{26} & B_{66} \end{bmatrix} \begin{Bmatrix} \varepsilon_{xx}^{(1)} \\ \varepsilon_{yy}^{(1)} \\ \gamma_{xy}^{(1)} \end{Bmatrix} + \begin{bmatrix} E_{11} & E_{12} & E_{16} \\ E_{12} & E_{22} & E_{26} \\ E_{16} & E_{26} & E_{66} \end{bmatrix} \begin{Bmatrix} \varepsilon_{xx}^{(3)} \\ \varepsilon_{yy}^{(3)} \\ \gamma_{xy}^{(3)} \end{Bmatrix} \tag{97}$$

$$\begin{Bmatrix} M_{xx} \\ M_{yy} \\ M_{xy} \end{Bmatrix} = \begin{bmatrix} B_{11} & B_{12} & B_{16} \\ B_{12} & B_{22} & B_{26} \\ B_{16} & B_{26} & B_{66} \end{bmatrix} \begin{bmatrix} \varepsilon_{xx}^{(0)} \\ \varepsilon_{yy}^{(0)} \\ \gamma_{xy}^{(0)} \end{bmatrix} + \begin{bmatrix} D_{11} & D_{12} & D_{16} \\ D_{12} & D_{22} & D_{26} \\ D_{16} & D_{26} & D_{66} \end{bmatrix} \begin{Bmatrix} \varepsilon_{xx}^{(1)} \\ \varepsilon_{yy}^{(1)} \\ \gamma_{xy}^{(1)} \end{Bmatrix} + \begin{bmatrix} F_{11} & F_{12} & F_{16} \\ F_{12} & F_{22} & F_{26} \\ F_{16} & F_{26} & F_{66} \end{bmatrix} \begin{Bmatrix} \varepsilon_{xx}^{(3)} \\ \varepsilon_{yy}^{(3)} \\ \gamma_{xy}^{(3)} \end{Bmatrix} \tag{98}$$

$$\begin{Bmatrix} P_{xx} \\ P_{yy} \\ P_{xy} \end{Bmatrix} = \begin{bmatrix} E_{11} & E_{12} & E_{16} \\ E_{12} & E_{22} & E_{26} \\ E_{16} & E_{26} & E_{66} \end{bmatrix} \begin{Bmatrix} \varepsilon_{xx}^{(0)} \\ \varepsilon_{yy}^{(0)} \\ \gamma_{xy}^{(0)} \end{Bmatrix} + \begin{bmatrix} F_{11} & F_{12} & F_{16} \\ F_{12} & F_{22} & F_{26} \\ F_{16} & F_{26} & F_{66} \end{bmatrix} \begin{Bmatrix} \varepsilon_{xx}^{(1)} \\ \varepsilon_{yy}^{(1)} \\ \gamma_{xy}^{(1)} \end{Bmatrix} + \begin{bmatrix} H_{11} & H_{12} & H_{16} \\ H_{12} & H_{22} & H_{26} \\ H_{16} & H_{26} & H_{66} \end{bmatrix} \begin{bmatrix} \varepsilon_{xx}^{(3)} \\ \varepsilon_{yy}^{(3)} \\ \gamma_{xy}^{(3)} \end{bmatrix} \tag{99}$$

$$\begin{Bmatrix} Q_{yz} \\ Q_{xz} \end{Bmatrix} = \begin{bmatrix} A_{44} & A_{45} \\ A_{45} & A_{55} \end{bmatrix} \begin{Bmatrix} \gamma_{yz}^{(0)} \\ \gamma_{xz}^{(0)} \end{Bmatrix} + \begin{bmatrix} D_{44} & D_{45} \\ D_{45} & D_{55} \end{bmatrix} \begin{Bmatrix} \gamma_{yz}^{(2)} \\ \gamma_{xz}^{(2)} \end{Bmatrix} \tag{100}$$

$$\begin{Bmatrix} R_{yz} \\ R_{xz} \end{Bmatrix} = \begin{bmatrix} D_{44} & D_{45} \\ D_{45} & D_{55} \end{bmatrix} \begin{Bmatrix} \gamma_{yz}^{(0)} \\ \gamma_{xz}^{(0)} \end{Bmatrix} + \begin{bmatrix} F_{44} & F_{45} \\ F_{45} & F_{55} \end{bmatrix} \begin{Bmatrix} \gamma_{yz}^{(2)} \\ \gamma_{xz}^{(2)} \end{Bmatrix} \tag{101}$$

$$\{A_{ij}, B_{ij}, D_{ij}, E_{ij}, F_{ij}, H_{ij}\} = \sum_{k=1}^{N} \int_{z_k}^{z_{k+1}} \bar{Q}_{ij}^{(k)} \left(1, z, z^2, z^3, z^4, z^6\right) \, dz \quad (i,j = 1,2,6) \tag{102}$$

$$\{A_{ij}, D_{ij}, F_{ij}\} = \sum_{k=1}^{N} \int_{z_k}^{z_{k+1}} \bar{Q}_{ij}^{(k)} \left(1, z^2, z^4\right) \, dz \quad (i,j = 4,5) \tag{103}$$

The nonlocal governing equations in terms of local stress resultants can be obtained by applying the operator $\mathcal{L}$ on both sides of the equations (14) - (18). Making use of the relations in equation (19), we obtain:

$$\frac{\partial N_{xx}}{\partial x} + \frac{\partial N_{xy}}{\partial y} = 0 \tag{104}$$

$$\frac{\partial N_{xy}}{\partial x} + \frac{\partial N_{yy}}{\partial y} = 0 \tag{105}$$

$$\begin{aligned} &\frac{\partial \bar{Q}_x}{\partial x} + \frac{\partial \bar{Q}_y}{\partial y} + \frac{\partial}{\partial x}\left(N_{xx}\frac{\partial w_0}{\partial x} + N_{xy}\frac{\partial w_0}{\partial y}\right) + \frac{\partial}{\partial y}\left(N_{xy}\frac{\partial w_0}{\partial x} + N_{yy}\frac{\partial w_0}{\partial y}\right) \\ &+c_1\left(\frac{\partial^2 P_{xx}}{\partial x^2} + 2\frac{\partial^2 P_{xy}}{\partial x\,\partial y} + \frac{\partial^2 P_{yy}}{\partial y^2}\right) = -q\left(1 - \mu\nabla^2\right) \end{aligned} \tag{106}$$

$$\frac{\partial \bar{M}_{xx}}{\partial x} + \frac{\partial \bar{M}_{xy}}{\partial y} - \bar{Q}_x = 0 \tag{107}$$

$$\frac{\partial \bar{M}_{xy}}{\partial x} + \frac{\partial \bar{M}_{yy}}{\partial y} - \bar{Q}_y = 0 \tag{108}$$

REFERENCES

1. Reddy J.N. A simple higher-order theory for laminated plates. *Journal of Applied Mechanics*, 51:745–752, 1984.
2. Reddy J.N. *Mechanics of Laminated Composite Plates and Shells*. CRC Press, 2004.
3. Eringen A.C and Edelen D.G.B. On nonlocal elasticity. *International Journal of Engineering Science*, 10:233–248, 1972.
4. Chi H, Talischi C, Pamies O.L, and Paulino G.H. Polygonal finite element for finite elasticity. *International Journal for Numerical Methods in Engineering*, 101(4):305–328, 2015.
5. Lv J, Zhang H.W, and Yang D.S. Multiscale method for mechanical analysis of heterogeneous materials with polygonal microstructures. *Mechanics of Materials*, 56:38–52, 2013.
6. Simone A, Duarte C, and Van der Giessen E. A generalized finite element method for polycrystals with discontinuous grain boundaries. *Internantional Journal for Numerical Methods in Engineering*, 67(8):1122–45, 2006.
7. Sze K.Y and Sheng N. Polygonal finite element method for nonlinear constitutive modeling of polycrystalline ferroelectrics. *Finite Elements in Analysis and Design*, 42(2):107–129, 2005.
8. Menk A and Bordas S.P.A. Numerically determined enrichment functions for the extended finite element method and application to bi-material anisotropy fracture and polycrystals. *Internantional Journal for Numerical Methods in Engineering*, 83(7):805–28, 2010.
9. Tabarraei A and Sukumar N. Application of polygonal finite elements in linear elasticity. *International Journal of Computational Methods*, 03:503–520, 2006.

10. Nguyen-Xuan H, Nguyen-Hoang S, Rabczuk T, and Hackl K. A polytree-based adaptive approach to limit analysis of cracked structures. *Computer Methods in Applied Mechanics and Engineering*, 313:1006–1039, 2017.
11. Nguyen-Thoi T, Phung-Van P, Rabczuk T, Nguyen-Xuan H, and Le-Van C. Free and forced vibration analysis using n-sided polygonal cell-based smoothed finite method $nCS - FEM$. *International Journal of Computational Methods*, 10(1), 2013.
12. Khoei A.R, Yasbolaghi R, and Biabanaki S.O.R. A polygonal finite element method for modeling crack propagation with minimum remeshing. *International Journal of Fracture*, 194(2):123–48, 2015.
13. Thanh V.M.N, Zhuang X, Xuan H.N, Rabczuk T, and Wriggers P. A virtual element method for 2d linear elastic fracture analysis. *Computer Methods in Applied Mechanics and Engineering*, 13:129–163, 2018.
14. Hoang S.N, Sohn D, and Kim H.G. A new polyhedral element for the analysis of hexahedral-dominant finite element models and its application to nonlinear solid mechanics problems. *Computer Methods in Applied Mechanics and Engineering*, 324:248–277, 2017.
15. Nguyen-Thoi T, Liu G.R, and Nguyen-Xuan H. An n?sided polygonal edge?based smoothed finite element method (nES?FEM) for solid mechanics. *International Journal for Numerical Methods in Biomedical Engineering*, 10, 2011.
16. Biabanaki S.O.R and Khoei A.R. A polygonal finite element method for modeling arbitrary interfaces in large deformation problems. *Computational Mechanics*, 50:19–33, 2012.
17. Talischi C, Paulino G.H, Pereira A, and Menzes I.F.M. Polygonal finite element for topology optimization:a unifying paradigm. *Internantional Journal for Numerical Methods in Engineering*, 82(6):671–98, 2010.
18. Nguyen K.C, Tran P, and Xuan Nguyen H. Multi-material topology optimization for additive manufacturing using polytree-based adaptive polygonal finite elements. *Automation in Construction*, 99:79–90, 2019.
19. Rajagopal A, Kraus M, and Steinmann P. Hyperelastic analysis based on a polygonal finite element method. *Mechanics of Advanced Materials and Structures*, 25(11):930–942, 2018.
20. Biabanaki S.O.R, Khoei A.R, and Wriggers P. Polygonal finite element method for contact impact problems on non conformal meshes. *Computer Methods in Applied Mechanics and Engineering*, 269:198–221, 2014.
21. Ding S, Shao G, Li A, Su J, and Shi H. Numerical simulation of holes and inclusions using adaptive polygonal finite element method. *Journal of Mechanical Science and Technology*, 31(9):4305–4317, 2017.
22. Brezzi F and Marini L.D. Virtual element method for plate bending problem. *Computer Methods in Applied Mechanics and Engineering*, 253:455–462, 2013.
23. Sellam M, Natarajan S, and Kannan K. Smoothed polygonal finite element method for generalized elastic solids subjected to torsion. *Computers and Structures*, 188(9):32–44, 2017.
24. Chau K.N, Khanh N.C, Ngo T, Hackl K, and Nguyen-Xuan H. A polytree-based adaptive polygonal finite element method for multi material topology optimization. *Computer Methods in Applied Mechanics and Engineering.*, 332:712–39, 2018.
25. Nguyen-Xuan H. A polytree-based adaptive polygonal finite element method for topology optimization. *International Journal for Numerical Methods in Engineering*, 110:972–1000, 2016.
26. Hui W, Qing-Hua Q, and Cheuk-Yu L. A n-sided polygonal hybrid finite element with unified fundamental solution kernels for topology optimization. *Applied Mathematical Modelling*, 66:97–117, 2019.
27. Nguyen K.C, Tran P, and Nguyen H.X. Multi-material topology optimization for additive manufacturing using polytree-based adaptive polygonal finite elements. *Automation in Construction*, 99:79–90, 2019.
28. Nguyen N.V, Nguyen H.X, Lee S, and Nguyen-Xuan H. Geometrically nonlinear polygonal finite element analysis of functionally graded porous plates. *Advances in Engineering Software*, 126:110–126, 2018.
29. Chen X, Luo T, Ooi E.T, Ooi E.H, and Song C. A quadtree-polygon-based scaled boundary finite element method for crack propagation modelling in functionally graded materials. *Theoretical and Applied Fracture Mechanics*, 94:120–133, 2018.
30. Huynh H.D, Tran P, Zhuang X, and Nguyen-Xuan H. An extended polygonal finite element method for large deformation fracture analysis. *Engineering Fracture Mechanics*, 209:344–368, 2019.
31. Nguyen-Xuan H. A polygonal finite element method for plate analysis. *Computers and Structures*, 188:45–62, 2017.
32. Nguyen N.V, Nguyen H.X, Phan D.H, and Nguyen-Xuan H. A polygonal finite element method for laminated composite plates. *International journal for mechanical sciences*, 133:863–882, 2017.
33. Thai C.H, Wahab M.A, and Xuan H.N. A layerwise C^0 type higher order shear deformation theory for laminated composite and sandwich plates. *Comptes Rendus Mecanique*, 346:57–76, 2018.
34. Wachspress E.L. *A rational finite element basis*. Elsevier, 1975.
35. Dasgupta G. Interpolants within convex polygons: Wachspress' shape functions. *Journal of Aerospace Engineering*, 16:1–8, 2003.
36. Floater M.S. Mean value coordinates. *Computer aided geometric design*, 20(1):19–27, 2003.
37. Hormann K and Sukumar N. Maximum entropy coordinates for arbitrary polytopes. *Eurographics Symposium on Geometry Processing*, 27, 2008.
38. Floater M.S, Hormann K, and Kos G. A general construction of barycentric coordinates over convex polygons. *Advances in Computational Mathematics*, 24(1-4):311–331, 2006.
39. Floater M.S, Gillette A, and Sukumar N. Gradient bounds for wachspress coordinates on polytopes. *SIAM Jornal on Numerical Analysis*, 52(1):515–532, 2014.
40. Floater M.S. Generalized barycentric coordinates and applications. *Acta Numerica*, 24:161–214, 2015.
41. Malsch E.A and Dasgupta G. Interpolation for temperature distributions: a method for all non-concave polygons. *International Journal of Solids and Structures*, 41(8):2165–88, 2004.
42. Hiyoshi H and Sugihara K. Two generalizations of an interpolant based on voronoi diagrams. *International Journal of Shape Modeling*, 5(2):219–231, 1999.
43. Sukumar N and Tabarraei A. Conforming polygonal finite elements. *International Journal for Numerical Methods in Engineering*, 61(12):2045–66, 2004.

44. Belikov VV, Ivanov VD, Kontorovich VK, and Korytnik SA. The non-sibsonian interpolation:a new method of interpolation of the values of a function on an arbitrary set of points. *Computational Mathematics and Mathematical Physics*, 37(1):9–15, 1997.
45. Manson J and Schaefer S. Moving least squares coordinates. *Computer Graphics Forum*, 29:1517–1524, 2010.
46. Warren J. Barycentric coordinates for convex polytopes. *Advances in Computational Mathematics*, 6(1):97–108, 1996.
47. Dikshit H.P and Ojha A. On C^1 continuity of wachspress quadrilateral patches. *Computer Aided Geometric Design*, 19:207–222, 2002.
48. Mousavi S.E, Xiao H, and Sukumar N. Generalized gaussian quadrature rules on arbitrary polygons. *International Journal for Numerical Methods in Engineering*, 00:1–26, 2009.
49. Xiao H and Gimbutas Z. A numerical algorithm for the construction of efficient quadrature in two and higher dimensions. *Computers and Mathematics with Applications*, 59:663–676, 2010.
50. Mousavi S.E and Sukumar N. Numerical integration of polynomials and discontinuous functions on irregular convex polygon and polyhedrons. *Computational Mechanics*, 47:535–54, 2011.
51. Lasserre J.B. Integration on a convex polytope. *Proceedings of the American Mathematical Society*, 126(8):2433–2441, 1998.
52. Lasserre J.B. Integration and homogeneous functions. *Proceedings of the American Mathematical Society*, 127(3):813–818, 1999.
53. Chin E.B, Lasserre J.B, and Sukumar N. Numerical integration of homogeneous functions on convex and nonconvex polygons and polyhedra. *Computational Mechanics*, 56(6):967–81, 2015.
54. Suvranu D and Bathe K.J. The method of finite spheres with improved numerical integration. *Computer and Structures*, 79:2183–2196, 2001.
55. Chakraborty S, Natarajan S, Singh S, Mahapatra D.R, and Bordas S.P.A. Optimal numerical integration schemes for a family of polygonal finite elements with schwarz-christoffel conformal mapping. *International Journal for Numerical Methods in Engineering Science and Mechanics*, 0:1–22, 2018.
56. Jun Li C, Lamberti P, and Dagnino C. Numerical integration over polygons using an eight-node quadrilateral spline finite element. *Journal of Computational and Applied Mathematics*, 233:279–292, 2009.
57. Chen J.S, Wu C.T, Yoon S, and You Y. A stabilized conforming nodal integration for Galerkin mesh free methods. *International Journal for Numerical Methods in Engineering*, 50:435–466, 2001.
58. Puso M.A, Chen J.S, Zywicz E, and Elmer W. Meshfree and finite element nodal integration methods. *International Journal For Numerical Methods in Engineering*, 74:416–446, 2007.
59. Talischi C and Paulino G.H. Addressing integration error for polygonal finite elements through polynomial projections: A patch test connection. *Mathematical Models and Methods in Applied Sciences*, 8:1701–1727, 2014.
60. Antonietti P.F, Houston P, and Pennesi G. Fast numerical integration on polytopic meshes with applications to discontinuous Galerkin finite element methods. *Journal of Scientific Computing*, 77:1339–1370, 2018.
61. Thai C.H, Ferreira A.J.M, and Xuan H.N. Naturally stabilized nodal integration meshfree formulations for analysis of laminated composite and sandwich plates. *Composite Structures*, 178:260–276, 2017.
62. Belytschko T, Tay C, and Liu W. A stabilization matrix for the bilinear Mindlin plate element. *Computer Methods in Applied Mechanics and Engineering*, 29:313–27, 1981.
63. Bletzinger K.U, Bischoff M, and Ramm E. A unified approach for shear-locking-free triangular and rectangular shell elements. *Computers and Structures*, 75:321–334, 2000.
64. Spilker R and Munir N. The hybrid-stress model for thin plates. *International Journal for Numerical Methods in Engineering*, 15:1239–60, 1980.
65. Katili I. A new discrete Krichoff-Mindlin element based on Mindlin-Reissner plate theory and assumed shear strain fields-Part-II: An extended DKQ element for thick-plate bending analysis. *International Journal for Numerical Methods in Engineering*, 36:1285–1908, 1993.
66. Balaji K, Rajagopal A, and Steinmann P. Adaptive poly-fem for the analysis of plane elasticity problems. *International Journal for Computational Methods in Engineering Science and Mechanics*, 18(2-3):146–165, 2017.
67. Talischi C and Paulino G.H. Addressing integration error for polygonal finite elements through polynomial projections: A patch test connection. *Mathematical Models and Methods in Applied Sciences*, 24:1701–1727, 2014.
68. Talischi C, Pereira A, Menezes I.F.M, and Paulino G.H. Gradient correction for polygonal and polyhedral finite elements. *International Journal for Numerical Methods in Engineering*, 102:728–747, 2015.
69. Chi H, Talischi C, Pamies O.L, and Paulino G.H. A paradigm for higher-order polygonal elements in finite elasticity using a gradient correction scheme. *Computer Methods in Applied Mechanics and Engineering*, 306:216–251, 2016.
70. Meiche N. EI, Touns A, Ziane N, Mechab I, Abbes EI, and Bedia A. A new hyperbolic shear deformation theory for buckling and vibration of functionally graded sandwich plate. *International Journal of Mechanical Sciences*, 53(4):237–247, 2011.
71. Mantari J.L and Soares C.G. Four unknown quasi-3d shear deformation theory for advanced composite plates. *Composite Structures*, 109:231–239, 2014.
72. Arya H, Shimpi R.P, and Naik N.K. A zigzag model for laminated composite beams. *Composite structures*, 56(1):21–24, 2002.
73. Jinseok K and Reddy J.N. A general third order theory of functionally graded plates with modified couple stress effect and the Von kármán' nonlinearity: theory and finite element analysis. *Acta Mechanica*, 226:2973–2998, 2015.
74. Phan N.D and Reddy J.N. Analysis of laminated composite plates using a higher-order shear deformation theory. *International Journal for Numerical Methods in Engineering*, 21:2201–2219, 1985.
75. Farin G. Curves and surfaces for computer aided geometric design. *Computer Aided Geometric Design: A Practical Guide*, 3, 1993.
76. J.N Reddy. *An Introduction to the Finite Element Method*. McGraw-Hill, 4th edition, 2019.

77. de Boor C. B-form basics, geometric modeling, edited by G. Farin. *SIAM, Philadelphia*, pages 131–148, 1987.
78. Kraus M, Rajagopal A, and Steinmann P. Investigation on the polygonal finite element method: Constrained adaptive delaunay tessellation and conformal interpolants. *Computers and Structures*, 120:33–46, 2013.
79. Talischi C, Paulino G.H, Pereira A, and Menezes I.F.M. Polymesher: a general purpose mesh generator for polygonal elements in matlab. *Structural and Multidisciplinary Optimization*, 45:309–328, 2012.
80. Eringen A.C. A unified theory of thermomechanical materials. *International Journal of Engineering Science*, 4:179–202, 1966.
81. Kröner E. Elasticity theory of materials with long range cohesive forces. *International Journal of Solids and Structures*, 3:731–742, 1967.
82. Eringen A.C. *Microcontinuum filed theories- I: Foundations and Solids*. Springer-Verlag, 1998.
83. Reddy J.N. A penalty plate bending element for the analysis of laminated anisotropic composite plate. *International Journal for Numerical Methods in Engineering*, 15(8):1187–1206, 1980.
84. Averill R.C and Reddy J.N. On the behavior of plate element based on the first-order shear deformation theory. *Engineering Computations*, 7(1):57–74, 1990.
85. Senjanović I, Vladimir N, and Neven H. Modified Mindlin plate theory and shear locking-free finite element formulation. *Mechanics Research Communications*, 55:95–104, 2014.
86. Khezri M, Gharib M, and Rasmussen K.J.R. A unified approach to meshless analysis of thin to moderately thick plates based on a shear-locking-free Mindlin theory formulation. *Thin-Walled Structures*, 124:161–179, 2018.
87. Luong-Van H, Nguyen-Thoi T, Liu G.R, and Phung-Van P. A cell-based smoothed finite element method using three-node shear-locking free Mindlin plate element CS-FEM-MIN3 for dynamic response of laminated composite plates on viscoelastic foundation. *Engineering Analysis with Boundary Elements*, 42:8–19, 2014.
88. Katili I, Maknun I.J, Batoz J.L, and Ibrahimbegovic A. Shear deformable shell element DKMQ24 for composite structures. *Composite Structures*, 202:182–200, 2018.
89. Zhu H, Zhang G, and Cai Y. Locking-free triangular plate element using polynomial incompatible approximation for analysis of cracked thick-thin plates. *International Journal of Fracture*, 211:1–12, 2018.
90. Piska R, Rajagopal A, and Reddy J.N. Nonlocal nonlinear finite element analysis of composite plate using TSDT. *Composite Structures*, 185:38–50, 2018.
91. Soh A.K, Long Z.F, and Cen S. A new nine dof triangular element for analysis of thick and thin plates. *Computational Mechanics*, 24(5):408–417, 1999.
92. Akhras G, Cheung M.S, and Li W. Finite strip analysis of anisotropic laminated composite plates using higher-order shear deformation theory. *Computers and Structures*, 52(3):471–477, 1994.
93. Ferreira A.J.M, Fasshauer G.E, Batra R.C, and Rodrigues J.D. Static deformations and vibration analysis of composite and sandwich plates using a layerwise theory and RBF-PS discretizations with optimal shape parameter. *Composite Structures*, 86(3):328–343, 2008.
94. Ferreira A.J.M. Analysis of composite plates using a layerwise theory and multiquadrics discretization. *Mechanics of Advanced Materials and Structures*, 12(2):99–112, 2005.
95. Thai C.H, Ferreira A.J.M, Wahab M.A, and Nguyen-Xuan H. A generalized layerwise higher order shear deformation theory for laminated composite and sandwich plates based on isogeometric analysis. *Acta Mechanica*, 227(5):1225–1250, 2016.
96. Reddy J.N. *An Introduction to nonlinear finite element analysis*. Oxford university Press, Oxford, UK., 2015.